SOME THEORETICAL PROBLEMS IN LOW TEMPERATURE OPTICAL PROPERTIES OF SEMICONDUCTORS

Thesis by

Dee-Son Pan

In Partial Fulfillment of the Requirements

for the Degree of

Doctor of Philosophy

California Institute of Technology

Pasadena, California

1978

(Submitted September 1, 1977)

To My Father and Mother

ACKNOWLEDGEMENTS

I would like to express my sincere gratitude to Dr. Thomas C. McGill and Dr. Darryl L. Smith, who gave me excellent guidance to avoid serious mistakes and yet reasonable freedom to develop myself throughout the course of this work. I wish to continue this valuable interaction with them in the future.

I enjoyed various fruitful discussions with Dr. M. Chen, K.R. Elliot, Dr. R.B. Hammond, S.A. Lyon, Dr. V. Marrello, G.C. Osbourn and J.N. Schulman. Thanks also go to Dr. James W. Mayer and Dr. Barry C. Barish for their encouragements. I am indebted to Mrs. Vere Snell for her kind assistance in typing the manuscript.

Financial supports received from Anthony Fellowship, the Office of Naval Research and the California Institute of Technology are much appreciated.

Above all, I am deeply grateful to my dear family and parents in-law. The love and faith in Christ I share with them and especially with my wife Tse-Hwei, have helped me at every turn and enabled me to complete my study at Caltech.

ABSTRACT

This thesis contains 5 topics investigating some theoretical problems in the low temperature behavior of electrons and holes in semiconductors.

Motivated by many recent experiments, the phonon damping of the motion of the electron hole droplet in pure Ge was investigated in chapter 1. The screening effect of the carrier phonon interaction inside the droplet was studied in the random phase approximation. This effect was found to be small for the deformation potential coupling in Ge; reducing the phonon damping by about a factor of two. The calculated damping coefficient in the low velocity case (less than sound velocity of the crystal) is in agreement with the ultrasonic absorption measurements. When the droplet velocity exceeds the sound velocity, we found that spontaneous phonon emission dominates the damping; and the damping is found to be sufficiently large to make it unlikely that velocities greater than the sound velocity will be observed experimentally.

Motivated by the recent interests of droplets in doped material and polar material, in chapter 3, we extend our investigation of damping in chapter 2 to two other damping mechanisms: impurity scatterings in doped material and piezoelectric phonon scatterings in pure polar material . The screening effect is very important for those two scattering mechanisms, since they are electrostatic in nature. The damping coefficient due to impurity scattering is calculated for Ge and GaP. The damping coefficient due to piezoelectric scattering is calculated by taking GaP as an example. We found that the piezoelectric damping is very weak in the low temperature limit (less than 10°K in GaP)

due to strong screening effect when compared with the deformation potential damping. (This is an interesting contrast to the fact that the mobility of pure polar semiconductor is known to be determined by piezoelectric scattering at low temperatures, less than 100°K.)

Motivated by Haynes' rule from experiments, a study of the structure of an exciton bound to a neutral acceptor is reported in chapter 4. We chose a central-field model to calculate the ground-state energy. We found that there are no stable bound states of the system in the Hartree-Fock approximation when the electron to hole mass ratio is close to one. We include the correlation energy by using the core polarization potential method and the correlation energies for the "two electron ions". The calculated dissociation energy is then in agreement with the Haynes' rule.

A theoretical investigation of the banding of the bound excitons in doped semiconductors is presented in chapter 5. As the impurity concentration increases, one could expect, in analogy with the impurity band, banding of the bound exciton states. We estimate various matrix elements for the interactions between a bound exciton complex and a neutral impurity to first and second orders. We found that the hopping of a bound exciton between impurities is not readily feasible. (The hopping matrix element is smaller than that of a bound carrier between two ionized impurities, despite the fact that the bound exciton complex has a larger radius.) Numerical estimates of the banding of bound excitons are consistent with recent experimental observations of the smallness of the concentration broadenings of the bound exciton states.

An investigation of the phenomenon of impact ionization of excitons in Ge and Si is reported in chapter 6. The charged free carrier in an applied electric field can pick up enough energy from the field to allow

it to impact ionize an exciton. For this to occur, the carrier must have an energy greater than the exciton binding energy. At low temperatures ($T \leq 10°K$ in Ge and $T \leq 30°K$ in Si), the energy of a significant number of carriers exceeds this threshold energy. Calculations of exciton concentration (for fixed carrier concentration) as a function of temperature and applied field strength show that a sudden drop in exciton concentration occurs when electric fields exceed a temperature dependent critical field.

Parts of this thesis either have been or will be published under the following titles:

Chapter 2: Phonon Damping of the Electron-Hole Droplet Motion, D. S. Pan, D. L. Smith and T. C. McGill, Solid State Comm._____, _____, 1977. The Damping of the EHD Motion, I. Deformation potential Coupling, D. S. Pan, D. L. Smith, and T. C. McGill, (to be published).

Chapter 3: The Damping of the EHD Motion, II. Impurity and Piezoelectric Scattering, D. S. Pan, D. L. Smith, and T. C. McGill, (to be published).

Chapter 4: Binding of an Exciton to a Neutral Acceptor, D. S. Pan, D. L. Smith, and T. C. McGill, Solid State Comm. 18, 1557, 1976.

Chapter 5: Banding of Bound Exciton States, D. S. Pan, D. L. Smith, and T. C. McGill (to be published).

Chapter 6: Impact Ionization of Excitons in Ge and Si, D. L. Smith, D. S. Pan, and T. C. McGill, Phys. Rev. 12, 4360, 1975.

TABLE OF CONTENTS

		Page
ACKNOWLEDGEMENTS		iii
ABSTRACT		iv
CHAPTER 1:	INTRODUCTION	1
	I. Scope of the Thesis	2
	II. Background	2
	III. Outline of Thesis and Summary of Main Results	8
	REFERENCES	16
CHAPTER 2:	DAMPING OF THE DROPLET MOTION: I. DEFORMATION POTENTIAL SCATTERING	18
	I. Introduction	19
	II. Screening of Carrier-Phonon Interaction in EHD	23
	III. Damping of Low Velocity Droplets	30
	IV. The Phonon Damping of Low Velocity Droplet Motion in Ge	34
	V. Damping of High Velocity Droplets	42
	VI. Results and Discussion	46
	APPENDIX: Evaluation of Integrals for the Momentum Loss Rate	54
	REFERENCES	60
CHAPTER 3:	DAMPING OF THE DROPLET MOTION: II. IMPURITY AND PIEZOELECTRIC SCATTERING	63
	I. Introduction	64
	II. Impurity Damping	66
	III. Piezoelectric Damping	68
	IV. Results and Discussions	74

		Page
CHAPTER 4:	BINDING OF AN EXCITON TO A NEUTRAL ACCEPTOR	81
	I. Introduction	82
	II. Calculation of Ground State Energy	84
	III. Results and Discussion	90
	REFERENCES	94
CHAPTER 5:	IMPURITY BANDING OF BOUND EXCITON STATES	95
	I. Introduction	96
	II. Calculation of Matrix Elements	98
	III. Second Order Interactions	106
	IV. Results and Discussion	110
	REFERENCES	118
CHAPTER 6:	IMPACT IONIZATION OF EXCITONS IN Ge AND Si	119
	I. Introduction	120
	II. Qualitative Physics	122
	III. Calculation of Exciton Concentration	128
	IV. Summary and Discussion	141
	REFERENCES	144
APPENDIX:	EFFECTIVE MASS APPROXIMATION	146
	REFERENCES	155

CHAPTER 1

INTRODUCTION

I. Scope of the Thesis

Some theoretical problems in the low temperature behavior of electrons and holes in semiconductors are investigated in this thesis.

The problems of the damping of electron-hole droplet motion in Ge are investigated in Chapter 2. The dampings of electron-hole droplet motion due to impurity scattering, piezoelectric phonon coupling, are studied in Chapter 3. The structures of a bound exciton binding to shallow neutral impurity are investigated in Chapter 4. The banding of the bound excitons due to interactions with more than one impurity is studied in Chapter 5. The impact ionization of free excitons by field excited free carriers is investigated in Chapter 6.

The quantum description of carriers is based on the effective mass approximation of the simple band theory throughout this work.

II. Background

In this section, some backgrounds relevant to the works in this thesis are briefly reviewed.

Experimentally, the generation of electrons and holes in a semiconductor at low temperature is readily feasible. In Ge, for example, high density of electrons and holes can be generated by lasers. Those carriers are usually created somewhere in the k-space remote from the extrema of the conduction and valence bands. However, they thermalize to the bottom of the conduction band and top of the valence band in about nanoseconds[1] through carrier phonon coupling. The carrier recombination time in Ge is about five microseconds[2]. One, therefore, has

several microseconds to go to investigate the system of electrons and holes in quasi thermal equilibrium. Various experimental techniques can be applied to study the properties of the system[3].

For a theoretical description of carriers in semiconductors, it is well known that one can obtain considerable information, frequently sufficient to interpret experiments, by considering only one band and treating the electrons (or holes) in this band by methods similar to those applicable to free electrons. This is the so-called effective mass approximation. In the appendix of this thesis, a simple outline of it is given.

We know[4] that electron and hole can, though their mutual coulomb interaction, form a bound state called excitons, or free excitons (FE). We also know[5,6] now that an exciton can bind to a neutral impurity to form a complex called bound exciton complex (BE). It was established in the period between 1967 to 1970 that electrons and holes in semiconductors may condensate into drops of liquid state, called electron-hole droplets (EHD). Those are some of the various states that can be formed by electrons and holes in quasi-thermal equilibrium at low temperatures. The relative probabilities of finding those states in semiconductors may depend on many factors. Among them are carrier injection density, temperature, and impurity doping concentration. A few physical properties of these states are outlined in the following:

A. Excitons

Excitons are the simplest collective excitation in solids which we can discuss either according to the Frenkel[7] or Wannier[8] models. It is

well known the Wannier model applies to semiconductors: one "electron" and "hole" are attracted according to the weak potential $e^2/\kappa R$ to form a bound state and travel through the crystal together. It is similar to the binding of an electron and a proton into an atom of hydrogen or an electron and positron into positronium by coulomb force. In semiconductors the exciton binding energy and their effective radii may be estimated from Bohr's well-known formulas, taking into account the fact that the effective mass of the electrons and holes differ from the free electron mass, and that the Coulomb interaction is weakened by the dielectric constant. The binding energy of excitons is less than the characteristic energy of atoms by 2-3 orders, and their radii are much greater than the inter-atomic distances in the crystal. The distortion of the crystal's structure by the presence of an exciton or even a large quantity of excitons is negligible. The usual Bohr formulas are only good for a rough estimate. They do not take into account a number of the complications in real crystals. For example, the effective masses of electrons and holes are as a rule anisotropic; in a crystal several different types of electrons and holes may exist; and the screening of the coulomb interaction due to dielectric constant disappears at distances on the order of interatomic distances.

Although excitons in semiconductors have been studied intensively for a long time[4], there are many problems related to excitons which are still of great interest at the present time. One of the problems is about the dynamics of excitons, i.e., the interaction of excitons with other particles or fields. In Chapter 6, we present an investigation of

one consequence of the interaction of excitons with free carriers in Si and Ge, namely, the impact ionization of excitons by field accelerated free carriers.

B. The Bound Exciton-Neutral Impurity Complex

Lampert[5] first suggested that stable complex of electron-hole pair bound to neutral impurity in semiconductors was possible. Experimental proof of the existence of such complex was first provided by Haynes[6]. He found that the low temperature photoluminescence spectra of silicon doped with Group III and V impurities were characterized by sharp lines which were shifted to a lower energy than the broad free exciton line. The structure of the complex is analogous to a bound state of a system composed of one proton, one positron and two electrons. In semiconductors, the electrons and holes may have different effective masses. If the hole effective mass is much heavier than that of electron, the structure of a bound exciton-neutral donor complex is very close to a hydrogen molecular and the structure of the bound exciton-neutral acceptor complex is close to a positive charged particle loosely bound to a negative hydrogen ion. The dissociation energy of a bound exciton is defined to be the energy required to release the bound exciton. Experimentally it is found that the dissociation energy of a bound exciton is about 10% of the ionization energy of the neutral impurity. There has recently been considerable experimental interest in bound excitons, partly due to their use in identifying impurities in semiconductors at very low concentration. The study of the bound exciton luminescence also allows one to obtain a variety of information both on the energy

levels of impurities in the crystal and the intrinsic properties of the crystal. We investigated the structure of a bound exciton-neutral acceptor complex in Chapter 4 and the banding of bound exciton states in Chapter 5.

C. The Electron-Hole Liquid

At low temperature, and high carrier injection level, the electrons and holes in semiconductors may condensate into a liquid state due to their mutual interactions. Such a liquid phase was first suggested by Keldysh[9], who said that metallized droplets of electrons and holes could form as the density of carriers is increased. The first evidence for the existence of such metallic droplets was given by the photoconductivity experiments of Asnin and Rogachev[10] and the observation of shifted recombination radiation attributed to the droplet state by Pokrovsky and Svistunova[11].

The phenomenon is roughly analogous to the condensation of water vapor into fog droplets. From divers experiments with germanium[3], these characteristics are emerging: the droplet medium itself is a two component cold dense plasma, of density $n=2\times10^{17}$ electron-hole pairs per cubic centimeter. They are usually a few micrometers in size and have a liquid metallic character and a lifetime of about 40 microseconds, decaying by emission of infrared light. The droplets have a definite surface energy. They can move in a pure crystal lattice. They can be accelerated by the crystal deformation gradients as well as by dynamic deformation from, e.g., ultrasound[12,13]. The motions usually are heavily damped.

Theoretical calculations including the details of the band structure have established the stability of such a liquid phase with respect to the exciton gas for a number of materials, including Ge, Si[14], GaP, CdS, ZnS, and AgBr[15]. Recently experimental evidence of the existence of an electron-hole liquid in some III-V[16] and II-VI compounds have been reported[17].

The behavior of the electron-hole droplets is of high intrinsic interest. It represents the first example of a quantum liquid of constant density in a periodic crystal lattice. Since 1970, its properties have received an extensive study in Si and Ge, especially in Ge. The properties investigated included: the thermodynamic properties, the formation mechanism, the impurity effect, and the motion of the droplets.

The motion of the droplet has been recently investigated using various experimental methods[18]. All the observed motions indicate features of damping. However, the observed dampings showed large discrepancies between the results in different experimental conditions. To understand the motion of the droplet, one has to first have a clear understanding of the damping of the droplet motion. In Chapter 2, we report our investigation of the damping of droplet, in both low velocity and high velocity cases, due to the deformation potential coupling to phonons. In Chapter 3, the damping of droplets due to two other mechanisms, namely, impurity and piezoelectric scattering, is investigated in the low velocity case.

III. Outline of Thesis and Summary of Main Results

In Chapter 2, we investigated the phonon damping of the electron-hole droplets (EHD) motion in Ge due to deformation potential coupling of carriers and phonons. Several experiments have recently been performed which demonstrate that EHD can move and that the motion shows damping[18]. As first pointed out by Keldysh, the motion of EHD in crystal should be damped by the interaction of the carriers in the EHD with acoustic phonons. Using deformation potential coupling, he calculated the damping rate as a function of temperature for droplet velocities much less than the sound velocity. The results of the calculations were in reasonable qualitative agreement with the damping rates deduced from some experiments. However, if the results from other experiments which are thought to measure EHD motion directly are interpreted in terms of droplet motion, either the phonon damping of the droplet motion must be much smaller than calculated by Keldysh or the droplets observed in these experiments were pushed along by some external force (e.g., a phonon wind). In deriving his results, Keldysh did not consider any modification of the free carrier-phonon interaction by carriers in EHD. Such screening significantly reduces the "bare" electron-phonon interaction in a metal, and one might expect a similar "large" reduction in the damping of the EHD motion due to screening. Because EHD is a two-component system, the screening is more complicated than in a metal. The deformation of the lattice produced by acoustic phonon is a non-coulombic perturbation and the polarization of the electrons and holes in the EHD produced by this perturbation may have

either the same or opposite phase. We examine the effect of screening in the random phase approximation. We find that the screening effect does not change the damping qualitatively for the deformation potential coupling. The damping rate is reduced by screening in the low velocity case by a factor of two in Ge. The damping coefficient in the low velocity case is calculated by evaluating the entropy production rate, as is used in the resistivity theory of metals. The anistropies in the crystal are simplified by taking a simple model motivated from mobility calculations in Ge. The calculated damping coefficient is found to be in reasonable agreement with results from ultrasonic absorption experiments[13]. We believe droplets in experiments designed to measure EHD motion directly showing much smaller damping are in fact being pushed by a phonon wind. Motivated by some experimental results[19], we also have investigated the damping of drops motion in high velocity limit; higher than sound velocity. The linear theory used in the metal resistivity is not valid in this case. We estimate the momentum loss rates from electrons and phonons directly due to coupling to phonons. We find in this high velocity case, the damping rate is very large and increases with velocity faster than linear. This rapid increase is due to the fact that spontaneous phonon emission process first becomes kinematically possible for the zero temperature Fermi distribution at the sound velocity. We conclude that the high initial velocities reported by the experiment should be reinterpreted[19]. The subsequent motion of droplets in that experiment can be understood by including the driving force produced by the phonon wind.

In Chapter 3, we investigate the damping of droplet motion due to two other scattering mechanisms: the impurity scattering and phonon scattering due to piezoelectric coupling. This work is motivated by the recent interests of investigations of electron-hole droplets in doped Ge[20] and Si and in polar semiconductors GaP[16]. We find the screening effect is very important here due to the electrostatic nature of these two interactions. This screening effect is treated in a random phase approximation. The impurity damping of the droplet motion is calculated for Ge and GaP. It is independent of temperature. The damping of droplets due to piezoelectric scattering is calculated for GaP. The piezoelectric damping coefficient has a T^7 temperature dependence in the low temperature limit. (If we neglect screening effect, it would have T^3 dependence). Since the deformation potential damping usually has a T^5 dependence, we expect deformation potential scattering will dominate the damping of droplets at low enough temperature for pure polar semiconductors. (The mobility of the pure dislocation free polar semiconductors is known to be determined by piezoelectric scattering at low temperature, $T < 100^{o}K$).

In Chapter 4, a study of the structure of an exciton bound to a neutral acceptor in semiconductors is reported. The optical spectrum due to the recombination of excitons bound to impurity centers in semiconductors has been extensively studied by experiments. Hopfield[21] made a theoretical estimate of the bound exciton dissociation energy by interpolating the dissociation energy of the hydrogen molecule and the negative hydrogen atom. Sharma and Rodriguez[22] have calculated the binding energies of excitons to neutral donors. Their method is

not valid for the exciton-neutral acceptor complex as pointed out by Sharma and Rodriguez.[22] We chose a central-field model to calculate the structure of the bound exciton-neutral acceptor complex. We found that there are no stable bound states of the system in the Hartree-Fock approximation when the electron to hole mass ratio is close to one. The correlation corrections are found to be necessary for stable bound states. We included the correlation energy by using the core polarization potential method and the correlation energies for the "two electron" ions. The dissociation energy, E_d, of an exciton bound to a neutral acceptor is calculated as a function of the electron to hole mass ratio. For a variation of the electron to hole mass ratio of between 0.1 and 1.0, the calculated ratio of E_d to the acceptor ionization energy, E_i, is found to vary between 0.075 and 0.13. This variation of E_d is in agreement with the experimental values of the ratio found for a number of different acceptors in Si, Ge, GaAs and various II-VI compounds.

In Chapter 5 we study theoretically the banding of the bound excitons in doped semiconductors. As the impurity concentration increases in the semiconductors, a single bound exciton may interact with more than one impurity. One could expect, in analogy with the impurity band, banding of the bound exciton states. The question arises then as to how fast the banding occurs when one increases the impurity concentration. We assume the bound exciton concentration is much smaller than the impurity concentration. We calculate the diagonal and off diagonal matrix elements for the interaction between a bound exciton-neutral acceptor complex and a neutral acceptor. The off diagonal matrix element in this case is the amplitude for the hopping of

the bound exciton between neutral impurities. The bandwidth of the banding of the bound excitons is proportional to the hopping matrix element of the bound exciton between two neutral impurities if the impurities are assumed to form a regular lattice. We find that because the hopping involves the simultaneous changing of two orbitals for two oppositely charged particles, the hopping matrix element is small. (It is smaller than that of one bound carrier between two ionized impurities, despite the fact that the bound exciton complex has a larger radius.) To determine qualitatively the effect of random distribution of impurities, one has to know the diagonal matrix element. We have estimated the diagonal matrix element of the interaction between a bound exciton complex and a neutral impurity. We also estimated the Van Der Waals interaction between a bound exciton and a neutral impurity. We find they are both of comparable size as the hopping matrix element. Our model gives a qualitative estimate of the banding of the bound exciton states. Numerical estimates of the banding are consistent with recent experimental observations of the smallness of the concentration broadenings of the bound exciton states.

In Chapter 6, an investigation of the phenomenon of impact ionization of excitons in Ge and Si is reported. An exciton in a semiconductor can be ionized by a number of processes: phonon absorption, collision with a free carrier etc. In pure materials with relatively low carrier concentrations in thermal equilibrium, phonon absorption is the dominant ionization process. In thermal equilibrium each ionization process is balanced by a corresponding recombination process, and corresponding ionization and recombination rates are related by the principle of de-

tailed balance. The application of an external electric field will change the balance between ionization and recombination processes and can, therefore, modify the relative concentration of excitons and free carriers. Impact ionization by free carriers is especially sensitive to electric fields; even quite small fields can greatly increase the rate of this process. The charged free carrier in an applied electric field can pick up enough energy from the field to allow it to impact-ionize an exciton. For this to occur, the carrier must have an energy greater than the exciton binding energy. At low temperatures ($T \leq 10^{o}K$ in Ge and $T \leq 30^{o}K$ in Si) and modest electric fields ($E \sim 2$ V/cm in pure Ge and $E \sim 20$ V/cm in pure Si), the energy of a significant number of carriers exceeds this threshold energy. Once this happens, the impact ionization process can change the relative concentration of excitons and free carriers, the equilibrium law of mass action is no longer satisfied. Calculations of exciton concentration (for fixed carrier concentration) as a function of temperature and applied field strength show that a sudden drop in exciton concentration occurs when electric fields exceed a temperature dependent critical field.

SUMMARY OF MAIN RESULTS

Chapter 2:

1. The screening effect of the carrier-phonon interaction by carriers inside droplets is small for the deformation potential coupling; reducing the damping by about a factor of two.
2. The calculated damping coefficient in the low velocity case is in agreement with the ultrasonic absorption measurements.
3. When the droplet velocity exceeds the sound velocity in the crystal, the spontaneous phonon emission dominates the damping. The damping is very large in this case.
4. The droplets generated by high intensity focused laser pulse are pushed by the phonon wind.

Chapter 3:

1. The screening effect is very important for the damping of the droplet motion by impurity scattering and piezoelectric phonon scattering.
2. The damping coefficient due to impurity scattering is calculated for Ge and GaP.
3. The damping coefficient due to piezoelectric scattering is calculated by taking GaP as an example.

Chapter 4:

1. The correlation correction is very important for the existence of a stable bound exciton-neutral acceptor complex.

2. The calculation of the dissociation energy of the bound exciton-neutral acceptor complex in a simple model is in agreement with the experimentally observed Haynes' rule.
3. The quantum structure of the bound exciton-neutral acceptor complex is more analogous to atoms than molecules.

Chapter 5

1. The hopping of a bound exciton between neutral acceptors is more difficult than that of holes between ionized acceptors, despite the fact that the bound exciton complex has a larger radius.
2. The banding of the bound exciton states is small.

Chapter 6

1. Impact ionization of excitons by free carriers is very sensitive to electric field.
2. Calculations of exciton concentration (for fixed carrier concentrations) as a function of temperature and applied field strength show that a sudden drop in exciton concentration occurs when electric fields exceed a temperature dependent critical field, in reasonable agreement with experiments.

REFERENCES

1. J. C. Hensel and K. Suzuki, Phys. Rev. B9, 4219 (1974).

2. See, for example, R. M. Westervelt, T. K. Lo, J. L. Staehli, and C. D. Jeffries, Phys. Rev. Lett. 32, 1051, (1974).

3. See, for example, C. D. Jeffries, Science 189, 955 (1975), and references contained therein.

4. See, for example, R. S. Knox, Theory of Excitons, (Academic Press, New York, 1963).

5. M. A. Lampert, Phys. Rev. Lett. 1, 450 (1958).

6. J. R. Haynes, Phys. Rev. Lett. 4, 361 (1960).

7. J. Frenkel, Phys. Rev. 37, 1276 (1931).

8. G. H. Wannier, Phys. Rev. 52, 191 (1937).

9. L. V. Keldysh, in Proceedings of the Ninth International Conference on the Physics of Semiconductors, Moscow, 1968, edited by S. M. Ryokin and V. V. Shmastsev (Nauka Leningrad, 1968), p. 1303.

10. V. M. Asnin and A. A. Rogachev, Zh. Eksp. Teor. Fiz. Pis'ma Red. 9, 415 (1969) [JETP Lett. 9, 248 (1969)].

11. Y. E. Pokrovsky and K. I. Svistunova, Zh. Eksp. Teor. Fiz. Pis'ma Red. 9, 453 (1969) [JETP Lett. 9, 261 (1969)].

12. L. V. Keldysh, and S. G. Tikhodeev, Pis'ma Zh. Eksp. Teor. Fiz. 21, 582 (1975) [JETP Lett. 21, 273 (1975)].

13. A. S. Alekseev, T. I. Galkina, V. M. Maslennikov, R. G. Khakomov, and E. E. Shchebnev, Pis'ma Zh. Eksp. Teor. Fiz. 21, 578 (1975) [JETP Lett. 21, 271 (1975)].

14. P. Vashista, S. G. Das and K. S. Singwi, Phys. Rev. Lett. 33, 911

(1974) and references contained therein.

15. G. Beni and T. M. Rice, Phys. Rev. Lett. 37, 874 (1976).

16. Jagdeep Shah, R. F. Laheny, W. R. Harding, and D. R. Wight, Phys. Rev. Lett. 38, 1164 (1977).

17. R. F. Leheny and Jagdeep Shah, Phys. Rev. Lett. 37, 871 (1976).

18. See, for example, references contained in Chapter 1.

19. T. C. Damen, and J. M. Worlock, in the Proceedings of the Third International Conference on Light Scattering in Solids, edited by M. Balkaniki, R. C. Leute, and S. P. Porto (Flammarion, 1976), p. 183-188.

20. M. Chen, D. L. Smith, and T. C. McGill, Phys. Rev. B15, 4983, (1977).

21. J. J. Hopfield, in Proc. 7th Int. Conf. Phys. Semicond. (Edited by M. Hulin) p. 725ff., Dumod, Paris (1964).

22. R. R. Sharma and S. Rodriguez, Phys. Rev. 159, 649 (1967).

CHAPTER 2

DAMPING OF THE DROPLET MOTION: I.

DEFORMATION POTENTIAL SCATTERING

I. INTRODUCTION

The condensation of excitons into electron-hole droplets (EHD) in Ge and Si have been studied extensively. Recently, there have been a number of experimental investigations [2-10] which give information on the interaction between acoustic phonons and EHD. These experiments may be divided into two classes.

The first class of experiments measures the damping of the drops by applying a known driving force.[2-7] The ultrasonic absorption experiments have been interpreted in terms of drops being accelerated by the dynamic deformation from ultrasound and dissipating energy because of interaction with thermal lattice phonons. From the temperature dependence of the absorption of ultrasound at 160 MHz, the deduced momentum relaxation time is about 1 nsec at 2.4°K [2,3]. Ultrasound in the gigahertz range couples with the capillary wave oscillations of drops. In this case, the deduced momentum relaxation time is about 7 nsec at 1.8°K [4]. Static nonuniform stress on the crystal also accelerates the drops. Experiments measuring the mobility of the EHD by setting up a static inhomogeneous deformation field give a relaxation time of roughly 6 nsec at 1.8°K [5]. Droplets have also been shown to be driven by a wind of phonons [6], and to be carried along by a current of free electrons and holes in an electric field [7]. However, for both the phonon wind and current drag, the forces were not accurately known.

The second class of experiments measures the arrival time of the EHD at some point in the crystal remote from the site of droplet generation [8-10]. The drops start with an initial drift velocity and their velocity decreases as a function of time or distance. Junction noise experiments [8] suggest

that EHD can move a distance of about 0.3 mm. Assuming no external force, the observed motion indicates a momentum relaxation time of about 1 μsec [8]. Doppler shifted light scattering experiments [9] have shown droplet motion in a direct fashion; the observed relaxation time is roughly 100 μsec (assuming no external force). In both experiments, the initial velocities of EHD are less than sound velocity. However, time and spatially resolved light scattering experiments suggest that the initial droplet velocities can even exceed the sound velocity [10] in the crystal when the drops are formed by a short, high intensity laser pulse; droplets are observed at a distance of about 5 mm from the excitation point and the damping is reported to be nonlinear [10].

Theoretically, Keldysh [11,12] has pointed out that the motion of EHD in pure Ge should be damped by the interaction of the carriers in the EHD with acoustic phonons.

Using deformation potential coupling, Keldysh calculated the damping rate (time derivative of the droplet drift velocity) in Ge as a function of temperature for droplet velocities much less than sound velocity [11,12]. In this low velocity regime, the damping rate is linear with velocity. The results of these calculations were in reasonable qualitative agreement with damping rates deduced from ultrasonic absorption measurements [2,3] and from droplet motion in an inhomogeneous deformation field [5]. However, if the junction noise experiments and the light scattering experiments are interpreted in terms of droplet motion, either the phonon damping of the droplet motion must be much smaller than calculated by Keldysh or the droplets observed in these experiments were pushed along by some external force (e.g., a phonon wind). In other words, with the large damping rate computed

by Keldysh, droplets could not move the distances observed in the junction noise and time and spatially resolved light scattering experiments unless they were pushed.

In deriving his results, Keldysh did not consider any modification of the free carrier electron-phonon interaction for the carriers inside the EHD. However, one might expect that this interaction is screened by the carriers in the EHD. Such screening significantly reduces the "bare" electron phonon interactions in a metal [13], and one might expect a similar large reduction in the damping of EHD motion due to screening. Because EHD is a two-component system, the screening is more complicated than in a metal. The deformation of the lattice produced by an acoustic phonon is not an electrostatic perturbation and the polarizations of the electrons and holes in the EHD produced by this perturbation may have either the same or opposite phase.

The main purposes of this paper are twofold: first, to examine the effect that screening by the carriers in the EHD has on the damping of EHD motion; second, to investigate the damping of the droplet motion in Ge for velocities greater than the sound velocity.

We adopt the approach that the screening of bare perturbation by the carriers in EHD is calculated in the random phase approximation (RPA). General results are derived for the low velocity damping rate from the entropy production rate [14], similar to those used in the theory of metal resistivity. This general result is evaluated making use of some simplifying approximations to the details conduction and valence band anistropies. The result is equivalent to Keldysh's damping formula for spherical band structure and a single effective deformation potential constant.

In the high velocity limit, the approximations to the distribution function used in the low velocity limit are not valid. The distribution function for electrons and holes is assumed to be a shifted Fermi distribution function for zero temperature and the damping rate is calculated from a momentum balance equation.

We find that screening does not change qualitatively the damping of the EHD motion. The magnitude of the damping is changed by within a factor of two from a similar unscreened calculation. Our results are in semi-quantitative agreement with the results of the ultrasonic attenuation experiments[2-4] and, hence, are in disagreement with the dynamical measurements[8,9] of EHD motion when interpreted without a driving force. Therefore, we conclude that droplets observed in junction noise and light scattering experiments are being pushed.

Our calculation of the damping rate in the high velocity limit is some three orders magnitude larger than that obtained by interpreting the results of experiments in which EHD motion was observed following a strong pulse excitation[10]. Thus, droplets moving at velocities greater than the sound velocity would be very rapidly damped. We believe the very high initial velocities reported in Ref. 10 should not be interpreted in terms of droplet motion. Subsequent motion, at lower velocities, may be interpreted as due to a phonon wind pushing the droplets.

This paper is divided into five major sections as follows: In Sec. II, we consider the screening by the two components EHD on the bare electron-phonon interactions. Sec. III outlines the calculations of the damping coefficient for low velocity droplet motion in cubic semiconductors. Sec. IV contains the calculation of the phonon damping coefficients of EHD in

Ge in the low velocity limit. Sec. V treats the phonon damping of droplets motion in Ge when the droplet velocity exceeds the velocity of sound. In Sec. VI, we give results, conclusion and summarization.

II. SCREENING OF CARRIER-PHONON INTERACTION IN EHD

In most transport problems in semiconductors the low density of carriers means that we can neglect the screening of the carrier-phonon interaction [14]. However, in the EHD the density of carriers ($2\times10^{17}cm^{-3}$ in Ge) is sufficiently high that screening may play an important role. A simple estimate shows that the Thomas Fermi screening wavevector q_{FT} is about $5\times10^{6}cm^{-1}$ for the EHD in Ge. This value of q_{FT} is actually larger than the characteristic wavevector of the phonons which play a role in the scattering in the EHD; the Fermi wavevector for EHD is about $2\times10^{6}cm^{-1}$ in Ge. Hence, we must consider the role of screening in the effective carrier phonon interaction in EHD.

This problem is further complicated by the fact that EHD is a two-component quantum plasma. Therefore, we must consider the screening response from both carrier types each responding to the perturbation produced by their respective deformation potential coupling. Since the deformation potential coupling is not electrostatic, the electrons and holes may respond with different magnitudes and phases which are not simply given by signs of these charges. Thus, the screening response cannot be gauged by a single dielectric function.

In this section, we calculate the response of the electrons and holes

to general carrier-phonon interaction. The responses are calculated in random-phase approximation.

A. Derivation of Screened Interaction in RPA

The electrons and holes in the EHD are treated on the basis of effective mass approximation. The band structure is taken to be that in the elemental semiconductors, Si and Ge, and the III-V semiconductors with indirect gaps. The conduction band is assumed to have a number of equivalent valleys ν; the valence bands are assumed to consist of four degenerate bands at the zone center. The conduction band valleys are assumed to be ellipsoidal with an energy for the n^{th} valley given by $E_n^e(\vec{k})$. The four hole valence bands are assumed to have energies given by $E_n^h(\vec{k})$ where n labels the different valence bands. For this case the single particle Hamiltonian is given by

$$H_o = \sum_{n=1}^{\nu} \sum_{\vec{k}} E_n^e(k)\, a_{\vec{k}n}^{+} a_{\vec{k}n} + \sum_{n=1}^{4} \sum_{\vec{k}} E_n^h(\vec{k})\, b_{\vec{k}n}^{+} b_{\vec{k}n} \quad , \tag{2.1}$$

where a_{kn}^{+} creates an electron in the state with wavevector $\vec{k}$ in the n^{th} valley and $b_{\vec{k}n}^{+}$ creates a hole in the n^{th} valence band in the state $\vec{k}$. The basic functions used in this second quantization are the Bloch functions from an appropriate band structure calculation. The interaction between carriers can be written as

$$V_{cc} = \sum_{\vec{q}} \frac{2\pi e^2}{\kappa q^2}\, \rho(\vec{q})\, \rho(-\vec{q}), \tag{2.2}$$

where κ is the static dielectric constant of the solid[15]. In Eq. (2.2) $\rho(\vec{q})$ is the charge density operator for the electrons and holes.

$$\rho(\vec{q}) = \sum_{\vec{k},nn'} O_{\vec{k}+\vec{q}n,\vec{k}n'} b^{+}_{\vec{k}+\vec{q}n} b_{\vec{k}n'} - \sum P_{\vec{k}+\vec{q}n,\vec{k}n'} a^{+}_{k+qn} a_{\vec{k}n'} \qquad (2.3)$$

where

$$O_{\vec{k}+\vec{q}n,\vec{k}n'} = \langle \psi^{h}_{\vec{k}+\vec{q}n} | e^{i\vec{q}\cdot\vec{r}} | \psi^{h}_{\vec{k}n'} \rangle \qquad (2.4)$$

and

$$P_{\vec{k}+\vec{q}n,\vec{k}n'} = \langle \psi^{e}_{\vec{k}+\vec{q}n} | e^{i\vec{q}\cdot\vec{r}} | \psi^{e}_{\vec{k}n'} \rangle . \qquad (2.5)$$

In Eq. (2.4) and Eq. (2.5) $\psi^{e}_{\vec{k},n}$ and $\psi^{h}_{\vec{k},n}$ are the appropriate Bloch functions for electrons and holes, respectively. In our treatment here we will neglect the large $\vec{q}$ components which arise from intervalley scattering. For single valley scattering, we can take

$$P_{\vec{k}+\vec{q}n,\vec{k}n'} \cong \delta_{nn'} \qquad (2.6)$$

neglecting terms of order $\vec{q}$. On the other hand for the valence band, no such simplification is possible.

The interactions of electrons and holes with phonons are of the general form:

$$V_{e\text{-}ph} = \sum_{\vec{k},\vec{q},n\lambda} D_n^e(\vec{k}+\vec{q},\vec{k},\lambda)\, a^+_{\vec{k}+\vec{q}n}\, a_{\vec{k}n}\, (A_{\vec{q}\lambda} + A^+_{-\vec{q}\lambda}) \quad , \tag{2.7}$$

and

$$V_{h\text{-}ph} = \sum_{\vec{k},\vec{q}nn'} D^h_{nn'}(\vec{k}+\vec{q},\vec{k},\lambda)\, b^+_{\vec{k}+\vec{q}n}\, b_{\vec{k}n'}\, (A_{\vec{q}\lambda} + A^+_{-\vec{q}\lambda}) \tag{2.8}$$

where $D^h_{nn'}(\vec{k}+q,\vec{k},\lambda)$, and $D^e_n(\vec{k}+\vec{q},\vec{k},\lambda)$ are the matrix elements of the interaction between phonons and a single carrier; and $A^+_{q\lambda}$ is the creation operators of a phonon with wave vector $\vec{q}$ and polarization λ. The intervalley phonon scattering is neglected in Eq. (2.7).

The total Hamiltonian is

$$H = H^o + V_{cc} + V_{e\text{-}ph} + V_{h\text{-}ph} \quad . \tag{2.9}$$

Using the well-known equation of motion techniques and RPA [16], we obtain the following expression for the induced charge density due to linear response to the phonon perturbation:

$$\rho(\vec{q}) = \sum_{\lambda} c_\lambda(\vec{q})\, (A_{\vec{q}\lambda} + A^+_{-\vec{q}\lambda}) \quad , \tag{2.10}$$

where $c_\lambda(q)$ is given by

$$c_\lambda(\vec{q}) = \frac{1}{\epsilon(\vec{q})}\left\{\sum_{\vec{k}nn'} \frac{D^h_{nn'}(\vec{k}+\vec{q},\vec{q},\lambda)\ O_{\vec{k}+\vec{q},n,\vec{k},n'}}{E^h_n(\vec{k}+\vec{q}) - E^h_{n'}(\vec{k})} - \sum_{\vec{k}n} \frac{D^e_n(\vec{k}+\vec{q},\vec{k},\lambda)}{E^e_n(\vec{k}+\vec{q}) - E^e_n(\vec{k})} + \text{complex conjugate}\right\} \qquad (2.11)$$

where $\epsilon(\vec{q})$ is the dielectric function of the two components EHD in the RPA.

$$\epsilon(\vec{q}) = 1 + \frac{8\pi e^2}{\kappa q^2}\left\{\sum_{kn} \frac{1}{E^e_n(\vec{k}) - E^e_n(\vec{k}+\vec{q})} + \sum_{\vec{k}nn'} \frac{\left|O_{\vec{k}+\vec{q},n,\vec{k},n'}\right|^2}{E^h_n(\vec{k}) - E^h_n(\vec{k}+\vec{q})}\right\} \qquad (2.12)$$

The summation in expressions for $c\lambda(\vec{q})$ and $\epsilon(\vec{q})$ are over the occupied single particle states.

Adding the response given by Eqns. (2.10-2.12), we obtain expressions for the screened carrier phonon interaction.

$$V^S_{e\text{-}ph} = \sum_{\vec{k}\vec{q}n\lambda} M^e_n(\vec{k}+\vec{q},\vec{k},\lambda)\ a^+_{\vec{k}+\vec{q}n} a_{\vec{k}n}\ (A_{\vec{q}\lambda} + A^+_{-\vec{q}\lambda}) \quad , \qquad (2.13)$$

$$V^{S}_{h\text{-}ph} = \sum_{\vec{k}\vec{q}nn'\lambda} M^{h}_{nn'}(\vec{k}+\vec{q},\vec{k},\lambda)\, b^{+}_{\vec{k}+\vec{q}n}\, b_{\vec{k}n'}\, (A_{\vec{q}\lambda} + A^{+}_{-\vec{q}\lambda}) \quad , \tag{2.14}$$

where M^{e} and M^{h} are given by

$$M^{e}_{n}(\vec{k}+\vec{q},\vec{k},\lambda) = D^{e}_{n}(\vec{k}+\vec{q},\vec{k},\lambda) + \frac{4\pi e^{2}}{\kappa q^{2}}\, c_{\lambda}(\vec{q}) \tag{2.15}$$

$$M^{h}_{nn'}(\vec{k}+\vec{q},\vec{k},\lambda) = D^{h}_{nn'}(\vec{k}+\vec{q},\vec{k},\lambda) - \frac{4\pi e^{2}}{\kappa q^{2}}\, O_{\vec{k}+\vec{q},n,\vec{k}n'}\, c_{\lambda}(\vec{q}) \tag{2.16}$$

B. Symmetry Considerations of Response

Symmetry arguments may be used to simplify the potential due to the screening charge $V_{\rho}(\vec{q},\lambda)$ for certain directions of $\vec{q}$ and polarization λ. Writing $V_{\rho}(\vec{q},\lambda)$ in terms of the local strain induced by a given phonon mode $\epsilon_{ij}(\vec{q},\lambda)$ we have

$$V_{\rho}(\vec{q},\lambda) = \sum_{ij} F_{ij}(\vec{q})\, \epsilon_{ij}(\vec{q},\lambda) \tag{2.18}$$

where $F_{ij}(\vec{q})$ is a second rank tensor characterizing the linear response.

In the long wave length limit, which means that the phonon wave vector $\vec{q}$ is much smaller in magnitude than the Thomas Fermi screening wave vector q_{FT}, the tensor $F_{ij}(\vec{q})$ is approximately independent of q and has the total cubic symmetry of the crystal. Thus, F_{ij} is a multiple of the unit

tensor, and we have

$$V_\rho(\vec{q},\lambda) = F \sum_i \varepsilon_{ii}(\vec{q},\lambda). \tag{2.19}$$

The sum on the diagonal components is called the dilation, $\Delta(\vec{q},\lambda)$. Hence, we have

$$V_\rho(\vec{q},\lambda) = F\Delta(\vec{q},\lambda). \tag{2.20}$$

For any phonon mode or wave vector in long wavelength limit only the dilational part of the local strain is screened.

However, in the range of the temperatures which are of interest around 2°K, phonons with wavelengths of the order of the Fermi wavevector for the EHD make the primary contributions. These phonons have wavelengths which are on the order of the Thomas Fermi wavevector. Thus, the long wavelength is not valid in estimating the screening, and the above arguments must be modified to consider finite $\vec{q}$.

At finite $\vec{q}$, the symmetry arguments can be applied only along certain high symmetry directions. For $\vec{q}$ along the [100] , [110] and [111] directions, the phonons divide into totally transverse and longitudinal modes. In these directions application of simple group theoretical arguments [17] leads to the conclusion that there is no contribution to the potential in Eq. (2.18) from the transverse modes. Hence, for these high symmetry directions there is no screening of the transverse modes. However, for arbitrary $\vec{q}$ the modes

cannot be divided into transverse and longitudinal modes and all the modes are screened.

III. DAMPING OF LOW VELOCITY DROPLETS

Once the effective carriers scattering matrix elements are known, the damping of the droplet motion can be calculated from transport theory. In the low velocity limit, the damping should be linear. The well-known resistivity theory for metal can be applied [14]. The calculations of damping coefficient are outlined in this section.

The damping coefficient is defined by the equation

$$\frac{dv_i}{dt} = - \sum_j \gamma_{ij} v_j \tag{3.1}$$

where v_i is the i^{th} component of the velocity of the droplet. In general γ_{ij} is a second rank tensor. However, in cubic crystals of interest here γ_{ij} can be reduced to a scalar;

$$\gamma_{ij} = \gamma \delta_{ij} \tag{3.2}$$

where δ_{ij} is the Kronecher delta.

To determine γ, we calculate the rate of entropy production [14]. The electrons in the EHD are characterized by a carrier distribution function $f_n(\vec{k})$ with n labelling the various conduction band minimum. The deviation

of each of these distribution functions as given by a function $\phi_n(k)$,

$$f_n(\vec{k}) = f_n^o(\vec{k}) - \phi_n(k) \frac{\partial f_n^o(\vec{k})}{\partial E_n^e(\vec{k})} \tag{3.3}$$

where f_n^o is the equilibrium distribution function. Similar equations hold for the holes. Throughout this discussion we consider for simplicity only the electron part of each expression.

The entropy production rate corresponding to the distribution function in Eq. (3.3) is given by [14]

$$\frac{dS}{dt} = \frac{1}{2k_B T^2} \iint \{\phi(\vec{k}) - \phi(\vec{k}')\}^2 \, p(\vec{k}',\vec{k}) \, d\vec{k} d\vec{k}' \tag{3.4}$$

where k_B is the Boltzmann constant; T is the temperature of the EHD; and $p(\vec{k}',\vec{k})$ is the equilibrium transition probability for carriers from $\vec{k}$ to $\vec{k}'$. For lattice phonon scattering, $p(\vec{k},\vec{k}')$ can be calculated by calculating scattering matrix for the effective carrier-phonon interaction in Eqs. (2.13) and (2.14) using Fermi's golden rule and averaging the matrix over the thermal equilibrium distribution function for carriers and phonons. The $\phi_n(\vec{k})$ is determined by a variational calculation in which the entropy production rate given in Eq. (3.3) is maximized. The total entropy production rate, $(\frac{dS}{dt})_{\text{total}}$, is the sum of Eq. (3.3) over each conduction band valley and each valence band.

The macroscopic rate of energy dissipation for a droplet of total mass M and velocity v is given by $\gamma M v^2$. Equating the product of the temperature

and the entropy production rate in Eq. (3.4) we obtain an expression for γ

$$\gamma = \frac{T}{Mv^2}\left(\frac{dS}{dt}\right)_{total} \tag{3.5}$$

The macroscopic velocity $\vec{v}$ is given by

$$\vec{v} = -\int \vec{v}_n(\vec{k})\,\phi_n(\vec{k})\,\frac{\partial f_n^o(\vec{k})}{\partial E_n^e(\vec{k})}\,d^3k \Big/ \int f^o(\vec{k})\,d^3k \quad , \tag{3.6}$$

where $\vec{v}_n(\vec{k})$ is the group velocity for an electron in valley n with wave vector $\vec{k}$. The value of $\vec{v}$ is required to be independent of the valley and valence band over which the computation in Eq. (3.6) is evaluated. The interial mass M is made up of a sum of terms of the form

$$-\int \frac{\hbar\vec{k}\,\phi_n(\vec{k})\frac{\partial f_n^o}{\partial E_n(\vec{k})}\,d^3k}{\vec{v}} \quad ;$$

the sum runs over the conduction band minimum with $\vec{k}$ measured from the conduction band minimum and the various valence bands.

For our purpose here, we will take $\phi(k)$ simply of the form

$$\phi_n(\vec{k}) = \alpha_n\vec{k}\cdot\vec{u} \tag{3.7}$$

where $\vec{k}$ is measured from the conduction band minimum, $\vec{u}$ is a unit vector in the

direction of the velocity and α_n is a parameter. The value of α_n for each valence band and conduction valley may be different. They are constrained to produce the same velocity of the drops. If the scattering function is very anisotropic, we might have to consider a more complicated trial function[14,18,19].

Collecting the various results, we obtain finally for $\hat{u}$ along [100] direction

$$\gamma = \frac{1}{16\pi^5\hbar^2 kT} \left\{ 2 \sum_{n=1}^{\nu} \sum_{\lambda=1}^{3} \int \frac{(\vec{q}\cdot\hat{u})^2 \omega(\vec{q},\lambda) |M_n^e(\vec{k}',\vec{k},\lambda)|^2}{(1-e^{-\hbar\omega(\vec{q},\lambda)/kT})(e^{\hbar\omega(\vec{q},\lambda)/kT}-1)} \frac{dG_n^e}{v_n^e(\vec{k})} \frac{dG_n^{e'}}{v_n^e(\vec{k}')} \right.$$

$$\left. + \sum_{nn'=1}^{4} \sum_{\lambda=1}^{3} \int \frac{[\hat{u}\cdot(\alpha_n \vec{k}_n^h - \alpha_{n'} \vec{k}_{n'}^h)]^2 \omega(\vec{q},\lambda) |M_{n',n}^h(\vec{k}',\vec{k},\lambda)|^2}{(1-e^{-\hbar\omega(\vec{q},\lambda)/kT})(e^{\hbar\omega(\vec{q},\lambda)/kT}-1)} \frac{dG_n^h}{v_n^h(\vec{k})} \frac{dG_{n'}^h}{v_{n'}^h(\vec{k}')} \right\} \Bigg/$$

$$\left\{ \left[-2 \sum_{n=1}^{\nu} \int \hbar\vec{k}_n^e(\vec{k}_n^e\cdot\hat{u}) \frac{\partial f_n^o(\vec{k})}{\partial E_n^e(\vec{k})} \frac{d^3k_{nn}^e}{(2\pi)^3} - \sum_n \alpha_n \int \hbar\vec{k}_n^h(\vec{k}_n^h\cdot\hat{u}) \frac{\partial f_n^o(\vec{k})}{\partial E_n^h(\vec{k})} \frac{d^3k_n^h}{(2\pi)^3} \right] \cdot \vec{v} \right\} , \tag{3.8}$$

with $\vec{q} = \vec{k}' - \vec{k}$ (3.9)

where $\omega(\vec{q},\lambda)$ is the angular frequency of a phonon with wave vector $\vec{q}$ and polarization λ, and G_n is the surface area of the Fermi surface and $\vec{v}_n(\vec{k})$ is

the group velocity on the Fermi surface; $\vec{v}$ in the denominator of Eq. (3.8) is the velocity of droplet determined by Eq. (3.6) and (3.7) using $\alpha = 1$ for a conduction valley. The α_n's in Eq. (3.8) are constants for the n^{th} valence bands; they are determined from Eq. (3.6) and (3.7) by requiring that electrons and holes in EHD have the same velocity.

IV. THE PHONON DAMPING OF LOW VELOCITY DROPLET MOTION IN Ge

The results for γ given in Eq. (3.8) may be evaluated using the measured deformation potentials [19-24], phonon dispersion curves as computed from elastic constants [19], the well-known band structure for Ge [25], and the properties of EHD [26]. This calculation would require extensive numerical work, particularly for the valence bands. For our purposes here, we want to examine the role of screening and to make simplifying approximations which will result in answers which should give a reasonable estimate of the magnitude of the damping.

A. Model for Electrons

Herring and Vogt [19] have studied the expressions for the relaxation times appropriate to the mobility of electrons in Ge. They find their results are equivalent to a simplified model in which the anistropic scattering rates, variations in sound velocity and contribution from all three phonon modes are replaced by a single phonon mode, the longitudinal mode, a single deformation potential constant and a spherically symmetric effective mass. The single deformation potential which is obtained by comparing their exact results with the simple model is [19]

$$\Xi_e^2 = 0.75\ \Xi_d^2\ [1.31 + 1.61\ \Xi_u/\Xi_d + 1.01(\Xi_u/\Xi_d)^2] \quad . \qquad (4.1)$$

where Ξ_u and Ξ_d are the deformation potentials constant as defined by Herring[18]. The effective mass is taken to be the density of states effective mass.

The results of Herring and Vogt are not directly extendable to the case being treated here since we are dealing with a Fermi degenerate distribution of electrons and the temperatures are low enough that equipartition is not valid for the phonons of interest. However, numerical estimates of the terms in Eq. (3.8) for the electrons show that this model provides a good estimate (i.e., within a factor of two) at 2°K. At lower temperatures the differences between transverse and longitudinal sound velocities are sufficiently large that this model can lead to substantial errors.

B. Model for Holes

For the hole contribution, we use an approximation originally introduced by Lawaetz [22] and Wiley [23,27]. The valence band is approximated by one spherical heavy hole band with the spherically averaged effective mass. The light hole band can be neglected since it has very few holes in it. The velocity of sound is taken to be the average longitudinal sound velocity. The deformation potential is taken to be an average value appropriate to the calculation of the hole mobility[23]

$$\Xi_h^2 = 0.29\ [a^2 + 2{,}6(b^2 + d^2/2)] \qquad (4.2)$$

where a, b and d are the deformation potential constants defined by Pikus and Bir [21].

C. Screening

The potential due to the screening charge must be estimated for the models given above. In the formal expression, Eqs. (2.11) and (2.12), $c_\lambda(\vec{q})$ will depend in general on the details of the anistropy, deformation potentials, and matrix elements in Eq. (2.7) and (2.8). The value of $c_\lambda(\vec{q})$ is sensitive to the relative sign of the electron and hole contributions. Hence, to estimate the role of screening using our model parameters, we must make some judicious choice of the sign of the parameters. To make this determination, we compare the relative phases of the diagonal matrix elements of deformation potential for holes with the deformation potential for electrons.

For electrons in [111] valley [19]

$$D^e = (\Xi_d + \frac{1}{3}\Xi_u)(\varepsilon_{xx} + \varepsilon_{yy} + \varepsilon_{zz}) + \frac{1}{3}\Xi_u(\varepsilon_{xy} + \varepsilon_{yz} + \varepsilon_{xz}) \qquad (4.3)$$

where the strain tensors are referred to crystallographic axis along the [100] directions. The matrix elements for other valleys can be obtained from a symmetry transformation and the dilational parts are in variants. For heavy hole band [20,21]

$$D^h(\vec{k},\vec{k}) = \left[a + \frac{Bb(3\hat{k}_x^2-1)}{2\sqrt{B^2 + C^2(\hat{k}_x^2\hat{k}_y^2 + \text{c.p.})}}\right]\varepsilon_{xx}$$

$$+ \frac{Dd\hat{k}_x\hat{k}_y}{\sqrt{B^2 + C^2(\hat{k}_x^2\hat{k}_y^2 + \text{c.p.})}}\,\varepsilon_{xy} + \text{c.p.} \qquad (4.4)$$

where c.p. stands for cyclic permutations of x, y, and z; B, C, and D are effective mass parameters for hole bands, [20] and $\hat{k}_x$ are unit vectors.

For longitudinal mode, since the dilational part dominates and both $\Xi_d + \frac{1}{3}\Xi_u$ and a in Eqs. (4.3) and (4.4) are negative in Ge (see Table I for parameters), we may regard the deformation potential constants for electrons and holes have the same sign for longitudinal modes. For the transverse modes, the relative signs of D^e and D^h are determined by the shear components. They depend on the direction of $\vec{k}$ of the valence bands and on the valleys of the conduction band. We know from symmetry that the transverse phonons along [100], [110], [111] directions are not screened, as shown in section II. We also know, for example, that the [111] transverse phonons do not scatter electrons in the [111] valley from symmetry, and have little effect for other valleys. However, for most of the phonons propagating in arbitrary directions, the transverse phonon cannot be exactly defined, and it is not obvious that the screening is vanishingly small in general. For simplicity, we adopt the approximation that half of the transverse scattering has D^e and D^h to be of the same sign and half has the opposite sign. Assuming each mode contributes the same weight in scattering, the signs of Ξ_e and Ξ_h are determined as follows: Two-thirds of the total scattering events are assumed to have Ξ_e and Ξ_h of the same sign, and one-third is of the opposite sign. What is important is that Ξ_e and Ξ_h have the same sign for most of the scattering. This corresponds to the bands' edges moving in opposite directions as a result of the phonon perturbations.

This approximation probably overestimates the effect of screening since we are allowing the transverse phonons to be screened in part. However, as will be shown by the results later, the screening effect is small even in

this approximation (reducing the damping by less than a factor of two). Therefore, the errors caused by our approximation for screening of transverse mode is less than a factor of two. Other approximations in our model may introduce errors of comparable size.

The matrix element defined in Eq. (2.4) may be computed using the two band approximations introduced by Kane [28]. In this approximation we consider only the single heavy hole band and $O_{\vec{k}+\vec{q}n,\ \vec{k}n'}$ in Eq. (2.4) turns out to be independent of $\vec{k}$. The result may be written as:

$$O(q) = \frac{1}{2}\,(1 + 3\cos^2\gamma)^{1/2} \tag{4.5}$$

where γ is the angle between $\vec{k}$ and $\vec{k}+\vec{q}$ on the Fermi surface. This addition is found to make a small correction to our final results.

Hence, finally we have for the screened carrier phonon interaction in Eqs. (2.15) and (2.16)

$$M^e(\vec{k}+\vec{q},\vec{k}) = \sqrt{\frac{\hbar}{2\rho\omega}}\, q(\Xi_e + V\pm(q)) \quad , \tag{4.6}$$

and

$$M^h(\vec{k}+\vec{q},\vec{k}) = \sqrt{\frac{\hbar}{2\rho\omega}}\, q(\Xi_h - V\pm(q)O(q)) \quad , \tag{4.7}$$

where $V\pm(q)$ are calculated by Eq. (2.11) and represent potentials arising for

polarization of EHD; the plus and minus subscripts in $V_{\pm}$ denote the two values of V(q) obtained by assuming Ξ_e and Ξ_h are of the same signs and opposite signs as discussed above. The density of the crystal is given by ρ.

D. Calculation for the Damping Coefficient

Using the matrix elements in Eqs. (4.6) and (4.7), one can carry out integrations in Eq. (3.8) for the damping rate γ in our model. The damping coefficient obtained is of the same form as Keldysh's formula[11,12]

$$\gamma = \frac{1}{12\pi^3} \frac{q_{th}^5}{\hbar^2(m_e + m_h)\rho U n} (\nu m_e^2 D_e^2 K_e + m_h^2 D_h^2 K_h) \quad , \qquad (4.8)$$

where

$$q_{th} = \frac{kT}{\hbar U} \quad . \qquad (4.9)$$

In the formula, m_e and m_h are the mass for electrons and holes defined in our model; ν is the number of equivalent valleys ($\nu = 4$ in Ge); the T, ρ, and U are the temperature, density and longitudinal sound velocity of the crystal; n is the carrier pair density in EHD. The K_e and K_h are integrals reduced from Eq. (3.8). They are calculated by assuming that two-thirds of the scattering events use V_+ and one-third use V_- as described in Sec. IVC.

$$K_h = \frac{2}{3}\int_0^{\zeta_h} \frac{\zeta^5(1-V+(\zeta)O(\zeta)/|D_h|)^2}{(e^{\zeta}-1)(1-e^{-\zeta})}\,d\zeta \qquad (4.10)$$

$$+ \frac{1}{3}\int_0^{\zeta_{h_5}} \frac{\zeta^5(1+V-(\zeta)O(\zeta)/|D_h|)^2}{(e^{\zeta}-1)(1-e^{-\zeta})}\,d\zeta$$

where

$$\zeta_h = \frac{2k_{Fh}}{q_{th}} \qquad (4.11)$$

and k_{Fh} is the Fermi wave vector for holes. The overlap integral $O(\zeta)$ can be obtained from Eq. (4.5)

$$O(\zeta) = \frac{1}{2}\left[1+3(1-2\ (\zeta/\zeta_h)^2\right]^{1/2} \qquad (4.12)$$

The two functions V+ (ζ) and V-(ζ) are given by

$$V+(\zeta) = \frac{8\pi e^2 n}{\kappa q_{th}^2 \varepsilon(\zeta)\zeta^2}\left(\frac{|\Xi_h|}{W_h(\zeta)} - \frac{|\Xi_e|}{W_e(\zeta)}\right) \qquad (4.13)$$

$$V-(\zeta) = \frac{8\pi e^2 n}{\kappa q_{th}^2 \varepsilon(\zeta)\zeta^2}\left(\frac{|\Xi_h|}{W_h(\zeta)} - \frac{|\Xi_e|}{W_e(\zeta)}\right) \qquad (4.14)$$

The $W_h(\zeta)$, $W_e(\zeta)$ result from the two summations in Eq. (2.12). For spherical band structure, they are given by

$$\frac{1}{W_e(\zeta)} = \frac{3}{4E_{Fe}} \left(\frac{1}{2} + \frac{\zeta_e^2 - \zeta^2}{4\zeta_e \zeta} \ln \left| \frac{\zeta_e + \zeta}{\zeta_e - \zeta} \right| \right) \tag{4.15}$$

and

$$\frac{1}{W_h(\zeta)} = \frac{3}{4E_{Fh}} \left(\frac{1}{2} + \frac{\zeta_n^2 - \zeta^2}{4\zeta_h \zeta} \ln \left| \frac{\zeta_h + \zeta}{\zeta_h - \zeta} \right| \right) \tag{4.16}$$

where E_{Fe} and E_{Fh} are the Fermi energies for electrons and holes, respectively. Neglecting the small overlap integral effect, the dielectric function in Eq. (2.12) can be reduced to

$$\varepsilon(\zeta) = 1 + \frac{8\pi e^2 n}{\kappa q_{th}^2} \left[\frac{1}{W_e(\zeta)} + \frac{1}{W_h(\zeta)} \right] . \tag{4.17}$$

The same equations hold for K_e; the function $O(q)$ is absent in Eq. (4.10) and the appropriate electron parameters are substituted.

V. DAMPING OF HIGH VELOCITY DROPLETS

When the drift velocity is larger than the sound velocity and comparable to the EHD Fermi velocity, the previous linear calculation is not valid. To treat the damping in this case, we calculate the momentum loss rate due to phonon scattering. The distribution functions for electrons and holes are taken to be drifted Fermi distribution functions both shifted to produce the same average velocity. The carrier-carrier scattering is assumed to maintain a distribution function which is simply a drifted Fermi distribution and to keep the electrons and holes moving at the same velocity. The momentum loss rate for the holes and electrons will be computed independently and simply added together.

Since screening of the carrier-phonon interaction in Ge will modify the result of calculation by only a factor of two or less, and other approximations introduce uncertainties of comparable size, we will use the much simpler "bare" interaction in the high velocity calculation. The same model for band structure of Ge in Sec. IV is used here. The square of matrix elements of $V_{e\text{-}ph}$ in Eq. (2.7) for an electron scattered from $\vec{k}$ to $\vec{k}+\vec{q}$ by phonon absorption averaged over thermal phonon occupation probability may be written as

$$|\langle N_q-1;\ \vec{k}+\vec{q}|\ V_{e\text{-}ph}|\ \vec{k};\ N_{\vec{q}}\rangle|^2$$

$$= \frac{\equiv^2 e^2 \hbar q}{2\rho U} \quad \frac{1}{e^{\hbar Uq/kT}-1} \tag{5.1}$$

where Ξ_e is given by Eq. (4.1), ρ, U is the density and longitudinal sound velocity of the crystal, and volume of crystal is assumed to be unity. Similarly for phonon emission, we have

$$|\langle N_q+1;\ \vec{k}+\vec{q}|V_{e\text{-}ph}|\vec{k};\ N_{\vec{q}}\rangle|^2$$

$$= \frac{\Xi_e^2 \hbar q}{2\rho U} \left(\frac{1}{e^{\hbar Uq/kT}-1} + 1 \right) \tag{5.2}$$

The rate of momentum loss by the electrons in the EHD in one conduction valley can be written down using the usual result of time dependent perturbation theory:

$$\frac{d\vec{P}_e}{dt} = \frac{2\pi}{\hbar} \sum_{\vec{k},\vec{q}} \hbar\vec{q} \{ |\langle N_{\vec{q}}-1;\ \vec{k}+\vec{q}|V_{e\text{-}ph}|\vec{k};\ N_{\vec{q}}\rangle|^2$$

$$\delta(E(\vec{k}) - E(\vec{k}+\vec{q}) + \hbar Uq) + |\langle N_{\vec{q}}+1;\ \vec{k}+\vec{q}|V_{e\text{-}ph}|\vec{k};\ N_{\vec{q}}\rangle|^2$$

$$\delta(E(\vec{k}) - E(\vec{k}+\vec{q}) - \hbar Uq)\} f(\vec{k})\ (1 - f(\vec{k}+\vec{q})) \tag{5.3}$$

where $f(\vec{k})$ is the shifted Fermi distribution function. The shift is taken to be $m_e v/h$ and v is the drift velocity of the drops. Similar equations can be written down for holes with the hole parameters replacing the electron parameters.

The rate of momentum loss by the carriers in the EHD is balanced by the damping of the EHD velocity.

$$\frac{dP_e}{dt} + \frac{dP_h}{dt} = (m_e + m_h)\, n\Omega \frac{dv}{dt} \quad , \tag{5.4}$$

where Ω denotes the volume of the droplet. To determine the damping of the EHD, we must compute the rate of momentum loss by the carriers from Eq. (5.3). The rate of momentum loss by the carriers is a nonlinear function of v.

The integrations involved in the evaluation of the rate of momentum loss in Eq. (5.3) are complicated for arbitrary values of the drift velocity limits. In the low velocity case, this approach gives linear damping with the same value obtained in Sec. IV.

In the high velocity limit, the shift of the Fermi function is larger than the thermal broadening, and we can simplify the calculation by neglecting the thermal broadening of the shifted carrier distribution function. In addition, we neglect the phonon energy compared with electronic energies which is a reasonable approximation when the drift velocity is considerably larger than sound velocity. The details of our estimate of the integrals are given in the Appendix. We only give the results here.

The rate of momentum loss for electrons is given by

$$\frac{d\vec{P}_e}{dt} = -C_e(F_1(S) + F_2(S))\, \hat{v} \quad , \tag{5.5}$$

where the dimensional constant C_e is given by

$$C_e = \frac{16\nu k_{Fe}^6 \Xi_e^2 m_e \Omega}{(2\pi)^3 \hbar \rho U} \quad , \tag{5.6}$$

where ν is the number of equivalent valleys (4 in Ge). The unit vector $\hat{v}$ is in the direction of the drift velocity. The parameter S is defined to be

$$S = \frac{v}{v_{Fe}} \quad , \tag{5.7}$$

where v_{Fe} is the Fermi velocity for electrons. The functions F_1 and F_2 are defined in the Appendix.

The same expressions hold for the momentum loss rate for holes in droplets, except parameters for holes are used. The integrals in Eq. (5.5) and the analogous equation for the hole contribution may be carried out numerically to give the rate of momentum loss in Eq. (5.4).

VI. RESULTS AND DISCUSSION

A. Low Velocity

The values of parameters used in the calculation are given in Table I. The one-dimensional integrals in the expressions for K_e and K_h were calculated numerically. The result of the calculation of the damping coefficient in pure Ge, as a function of temperature, is plotted in Fig. 1. For comparison, the result of damping coefficient without including screening is also indicated by dashed line. Experimental results by Alekseev, et al [2,3], using 160 MHz ultrasonic absorption; by Alekseev, et al [5], using droplet motion in a nonuniform stressed crystal; and by Etienne, et al [4], using 1.5 GHz ultrasonic absorption are shown in Fig. 1 for comparison.

First of all, we see that screening of carrier-phonon interaction in the EHD has reduced the damping by only about a factor of two. The screening effect is rather small in Ge, because the valence and conduction bands tend to move in opposite directions when Ge is subjected to an arbitrary deformation. Thus, the two types of carriers tend to move in the same direction in response to a deformation and the net induced charge is small.

Second, we see that the results of calculation are in reasonable agreement with the values of the damping rate determined by ultrasonic absorption experiments and droplet motion in an inhomogeneous deformation. In our model, we used the averaged deformation potential constants in Eqs. (4.1) and (4.2). The averaging involved in them is slightly different from the "averaging" prescribed in Eq. (3.8). This

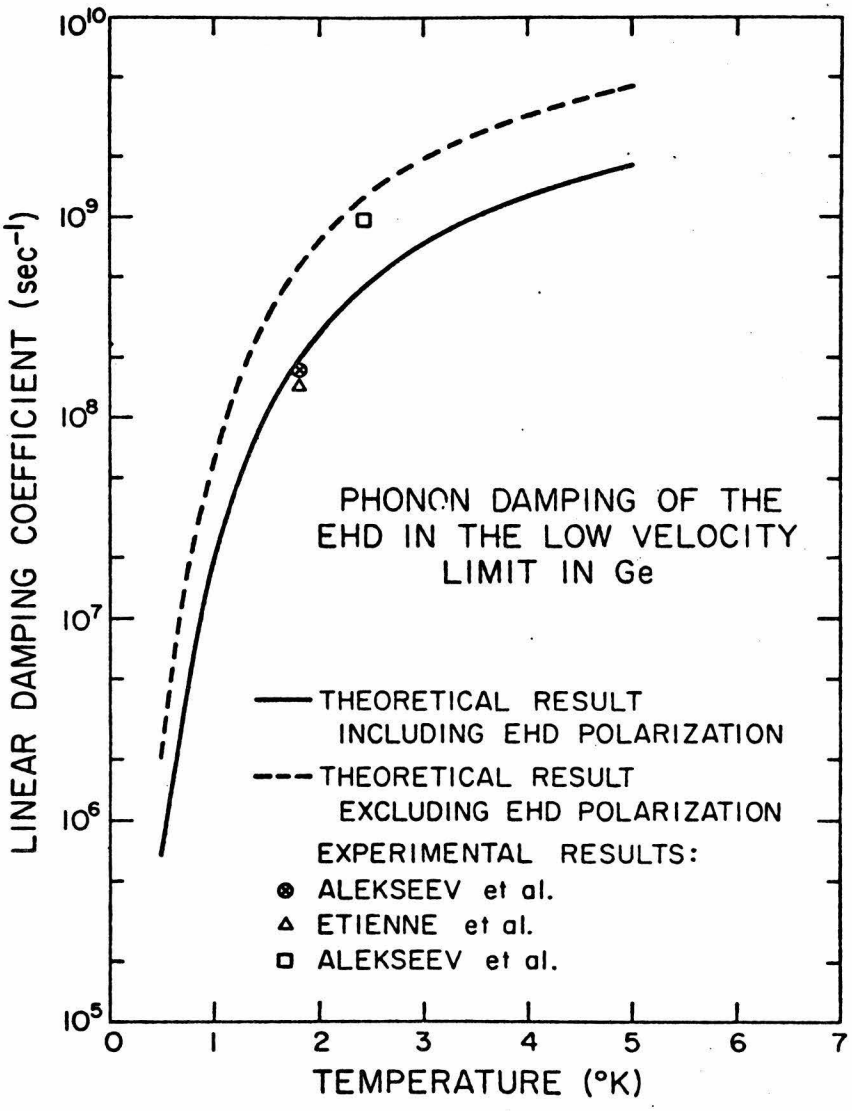


Fig. 1. The phonon damping coefficient for EHD motion in Ge vs temperature in the low drift velocity limit. The dashed curve is the result for the "bare" carrier-phonon interaction; the solid curve is the result when screening of the carrier-phonon interaction by the carriers in the EHD is included. The experimental points are from ⊗ Ref. 2, △ Ref. 7, and □ Ref. 5.

TABLE I. List of Parameters Used in Calculation

ε_f^e	ε_F^h	n	m_e	m_h	U
2.5 meV[a]	3.9 meV[a]	2.4×10^{17} cm^{-3}[a]	0.22m[b]	0.30 m[b]	5×10^{5} cm/sec[c]

ρ	κ	Ξ_d	Ξ_u	a	b	d
5.3 g/cm^3[d]	15.36[e]	-8.5ev[f]	19 ev[f]	-2.0 ev[g]	2.2 ev[g]	4.4 ev[g]

a Ref. 26

b Ref. 32

c Ref. 19

d Ref. 33

e Ref. 34

f Ref. 24

g Ref. 23

approximation is still reasonable for temperatures around and above 2°K. In the low temperature limit (below 1°K), one may expect the transverse modes of phonons will dominate because the smaller value of transverse sound velocity (about 3.5×10^5 cm/sec in Ge).

The calculated damping coefficient is approximately three orders of magnitude larger than that obtained if the junction noise experiments [8] and Doppler shifted light scattering experiments [9] are interpreted in terms of damped motion without a driving force. Hence, we conclude the droplet motion in those experiments were pushed by an external force, most likely the force from the interaction of a stream of nonequilibrium phonon-the phonon wind [6]. This effect has been investigated recently. In the junction noise experiments. since pulsed (10 nsec) excitation is used, it is most likely that the phonon wind produced in nonradiative recombination of electrons and holes in the nonuniform distribution of EHD pushes the droplets a distance of about 0.3 mm. A rough estimate using Keldysh phonon wind theory [5] gives results in qualitative agreement with the experimental observations. Worlock [30] have estimated the role of phonon wind in the Doppler shifted light scattering experiments and finds qualitative agreement with the experimental observations.

B. High Velocity

Evaluating the results stated in Sec. V for the parameters in Table I, we obtain the results shown in Fig. 2. Since we find that spontaneous emission dominates the damping, we expect the results to be almost independent of temperature. Hence, while the results in Fig.

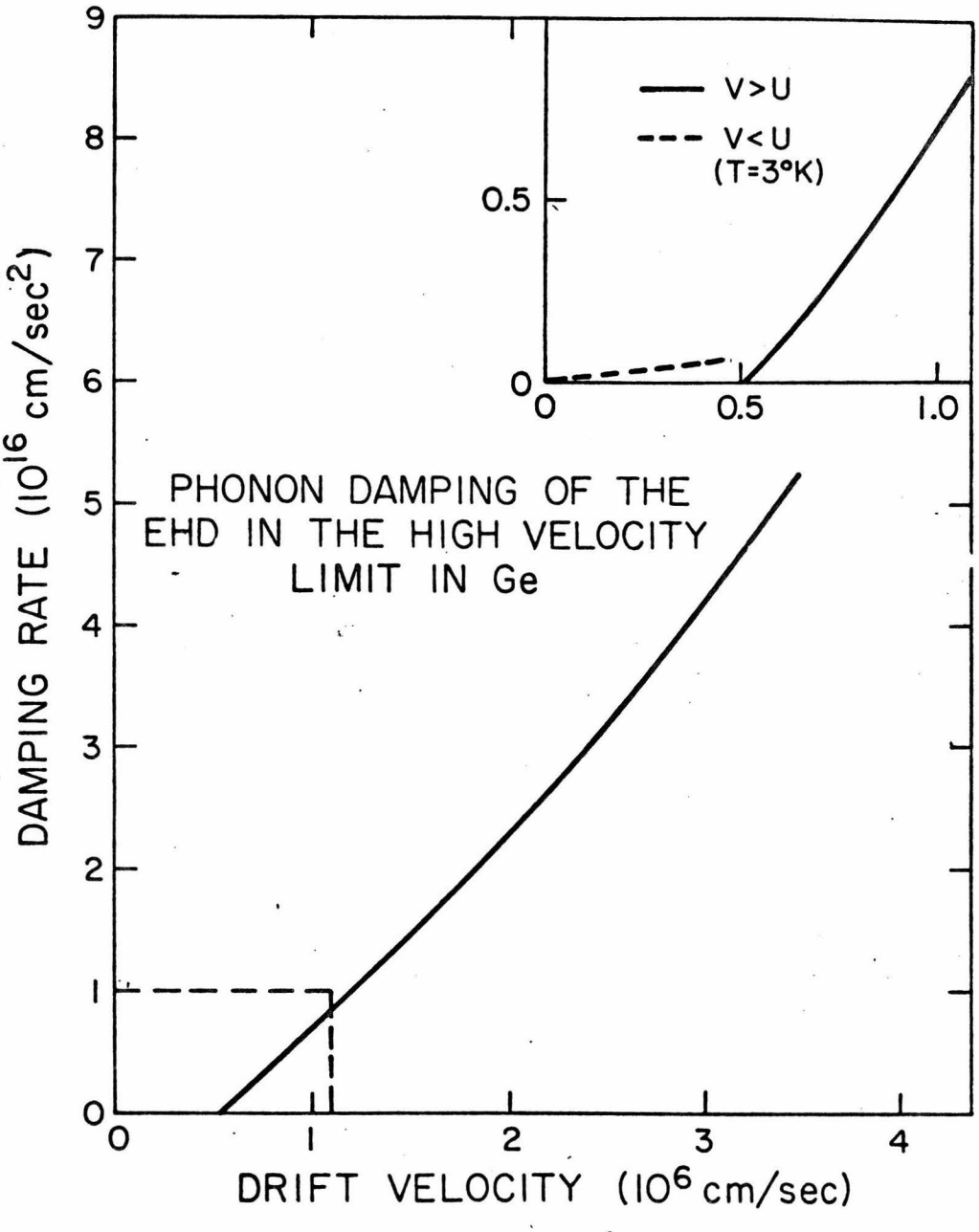


Fig. 2. The damping rate for EHD motion in Ge vs drift velocity in the high velocity limit ($V_d > U$). The calculation was done for zero temperature, but the damping rate is insensitive to temperature when $V_d >> U$. There is no phonon damping of the EHD motion at zero degrees when $V_d < U$. The insert compares the low velocity damping rate at T = 3°K curve with that at high drift velocities.

2 are obtained for 0°K, they are in fact valid for the temperature range where EHD occur, $T \lesssim 7$°K. At zero degrees, there is no damping of EHD motion for $v_d < U$. For comparison, we show the low velocity result for T = 3°K in the insert of Fig. 2.

The main point of this figure is that the damping rate increases very rapidly when the droplet velocity exceeds the sound velocity. This sudden increase is due to the large number of phonon emission processes which become kinematically possible when v is greater than U. If a droplet were moving at velocities greater than the sound velocity, its motion should be very rapidly damped.

Comparing with the experiment [10], we find the damping observed in Ref. [10] is smaller than our theoretical phonon damping by at least two orders of magnitude. Therefore, the experimental results cannot be explained without assuming an external force, most likely from phonon wind [6].

Based on our results, we believe that the initial drift velocities, larger than the sound velocity, reported in Ref. [10] should be reinterpreted. They are obtained by fitting the data and extrapolating to the initial time of droplets motion. The phonon wind cannot push the droplet to a velocity exceeding the sound velocity in the crystal. Even if some other forces, for instance, the pressure from a highly degenerate electron-hole plasma, imparts the droplet with an initial velocity exceeding the sound velocity, the droplet should quickly relax to sound velocity in about 0.1 nsec for the damping obtained here. Therefore, the extrapolation to obtain the initial velocity in Ref. [10] is not valid.

Further, the subsequent motion of the drops described in Ref. 10 may be explained by the force provided by phonon wind generated from the nonradiative recombinations of carriers inside the other droplets which distributed nonuniformly. The phonon wind generated during the thermalization of excited nonequilibrium carriers should not have a significant role in determining the subsequent motion of drops, because the phonon wind produced by this process lasts only about .3 μsec and drop motion is observed for a period of several microseconds. To give a rough estimate of this phonon wind effect, we can make use of the results of Bagaev, et al [6]. In that experiment[6] they find that the phonon wind can push the drops to a distance of about 1 mm with phonons produced by a continuous laser with power of about 40 mw. In the experiment in Ref. 10, the drops are pushed to a distance of about 2 mm when the carrier is generated by a Nd:YAG laser with a pump power of 20 W. The total number of carriers generated by this pump pulse is about 3×10^{13}. The recombination lifetime of drops in Ge is about 40 μsec, a significant contribution of which is due to nonradiative process [31]. The phonon generated from the nonradiative recombination of all drops created by the pump pulse of 20W is estimated to be between 40 mw and 80 mw. Since the powers going to phonon generation are about the same in the two experiments, we would expect the distances the EHD would be pushed would be comparable. This observation is in agreement with the experimental results.

C. Summary

We have calculated the phonon damping in the low and high velocity limit. We find that the theoretical value of the damping in the low velocity agrees with that observed in ultrasonic absorption and stress induced droplet motion experiments. We find that the screening changes the damping by about a factor of two.

For high velocities our calculations show that damping is very rapid if the droplet gives faster than sound velocity. Spontaneous phonon emission dominates the damping. Our damping is sufficiently large that we think it unlikely droplet velocities greater than sound velocity will be observed.

APPENDIX: Evaluation of Integrals for the Momentum Loss Rate

In this appendix, we evaluate the rate of momentum loss by electrons in the EHD given by Eq. (5.3) in the high velocity case. Similar results hold for the momentum loss rate by the holes.

It is convenient to divide the sums in Eq. (5.3) into two terms and to rewrite Eq. (5.3) as

$$\frac{dP_e}{dt} = I_1 + I_2 \quad . \quad . \qquad \text{(A1)}$$

Here I_1 includes all the phonon absorption and stimulated phonon emission process. Since the square of stimulated phonon emission matrix element equals that of phonon absorption, I_1 is given by

$$I_1 = \frac{2\pi}{\hbar} \sum_{\vec{k},\vec{q}} (\hbar\vec{q}) \; (|\langle N_{\vec{q}}-1; \vec{k}+\vec{q}|V_{e\text{-}ph}|\vec{k}, N_{\vec{q}}\rangle|)^2$$

$$\{\delta(E(\vec{k}) - E(\vec{k}+\vec{q}) + \hbar Uq) + \delta(E(\vec{k}) - E(\vec{k}+\vec{q}) - \hbar Uq)\}$$

$$f(\vec{k}) \; (1-f(\vec{k}+\vec{q})) \quad . \qquad \text{(A2)}$$

The term I_2 includes all the "spontaneous" phonon emission process. The square of matrix elements for these processes is the difference of the values in Eq. (5.1) and Eq. (5.2). We can write I_2 as

$$I_2 = \frac{2\pi}{\hbar} \sum_{\vec{k},\vec{q}} (\hbar\vec{q})\left(\frac{\equiv^2 \hbar q}{e^{2\rho U}}\right) \delta(E(\vec{k}) - E(\vec{k}+\vec{q}) - \hbar U q)$$

$$f(\vec{k})\ (1 - f(\vec{k}+\vec{q})) \quad , \tag{A3}$$

where the parameters are defined in Eq. (6.2). In the high velocity limit, I_2 makes a larger contribution to the momentum relaxation than I_1. However, we will estimate I_1 before I_2 because some of the results for I_1 can be used in evaluating I_2.

The sum of the terms in I_1 which contain the product $f(\vec{k})\ f(\vec{k}+\vec{q})$ is identically zero. In the high velocity limit, the small thermal spreading of the electron distribution function is unimportant, and we replace this distribution function with its zero temperature value. The integral I_1 then becomes

$$I_1 \simeq \frac{2\pi}{\hbar} \sum_{\vec{k},\vec{q}} (\hbar\vec{q})\ (|\langle N_{\vec{q}}-1;\vec{k}+\vec{q}|V_{e\text{-}ph}|\vec{k};\ N_{\vec{q}}\rangle$$

$$\{\delta(E(\vec{k}) - E(\vec{k}+\vec{q}) - \hbar U q) + \delta(E(\vec{k}) - E(\vec{k}+\vec{q}) + \hbar U q)\}$$

$$\theta\left(k_{Fe} - \left|\vec{k} - \frac{m_e \vec{v}}{\hbar}\right|\right) \quad , \tag{A4}$$

where the θ function is the heavyside function defined in the usual way: $\theta(x) = 0$ for $x < 0$, $\theta(x) = 1$ for $x \geq 0$.

This integral in Eq. (A4) can be carried out straightforwardly. Applying the standard approximation of neglecting phonon energy [35], the result is simply

$$I_1 = - C_e F_1(S) \hat{v} \quad , \tag{A5}$$

where the dimensional constant C_e is given in Eq. (5.6) and the dimensionless integral $F_1(S)$ is given by

$$F_1(S) = \int_{1-S}^{1+S} R_e(y)\, A(y,S)\, dy \quad , \tag{A6}$$

where the variable y is the wavevector of electrons measured in units of Fermi wavevector k_{Fe}, i.e., $y = k/k_{Fe}$; S is defined in Eq. (5.7). The function A(y,S) is given by

$$A(y,S) = 1 - \left(\frac{y^2+S^2-1}{2yS}\right)^2 \quad . \tag{A7}$$

The function $R_e(y)$ is an integral given by

$$R_e = \frac{1}{(\zeta_e)^5} \int_0^{y\zeta_e} \frac{Z^4}{(e^Z-1)}\, dZ \quad , \tag{A8}$$

where ζ_e is defined in Eq. (4.11).

The summation of the $\int(\vec{k}) \int(\vec{k}+\vec{q})$ product terms doesnot vanish for

I_2. In the high velocity limit, we can neglect the small temperature spreading of the electron distribution function in I_2, and also neglect the phonon energies. The sum of the $(\vec{k})$ $(\vec{k}+\vec{q})$ product terms vanishes in this approximation; and the integral I_2 can be put into the same form as in Eq. (A4)

$$I_2 = \frac{2\pi}{\hbar} \sum_{\vec{k},\vec{q}} (\hbar\vec{q})\left(\frac{\equiv^2 \hbar q}{2\rho U}\right) \delta(E(\vec{k}) - E(\vec{k}+\vec{q})$$

$$\theta(k_{Fe} - |\vec{k} - \frac{m_e \vec{v}}{\hbar}|) \quad . \tag{A9}$$

The result of the integration of Eq. (A9) is

$$I_2 = -C_e E(S)\hat{v} \quad , \tag{A10}$$

where the integral E(S) is given by

$$E(S) = \int_{1-S}^{1+S} Q_e(y)\, A(y,S)\, dy \tag{A11}$$

The function $Q_e(y)$ is given by

$$Q_e(y) = \frac{1}{10} y^5 \quad . \tag{A12}$$

The above results are valid for drift velocities considerably larger than the sound velocity. For the case when the drift velocity nearly equals the sound velocity, approximation of neglecting the finite phonon energy for I_1 is still valid. The limits of integration on two contributions (phonon absorption and spontaneous phonon emission) to I_1 are such that the first order terms in the ratio of sound velocity to Fermi velocity vanishes. However, for I_2, this approximation is not valid. For the spontaneous phonon emission process, the effect of finite phonon energy is important when the droplet velocities are comparable with the sound velocity.

We can obtain a qualitative interpolation of the results for I_2 between low velocity limit and high velocity limit. The arguments are as follows:

The dominant contribution for the momentum loss rate comes from carrier scatterings from the direction of drift velocity to the opposite of that direction. For a Fermi sphere shifted by S; $S=v/v_{Fe}$ as defined in Eq. (5.7), those carriers in the states with $\vec{k}$ in the direction of the velocity $\hat{v}$ can scatter into a vacant state in the opposite direction. Carriers undergoing this scattering must have a momentum larger than a minimum value Z (measured in the units of Fermi momentum), where Z is determined by the energy conservation equation

$$\frac{\hbar^2 k_{Fe}^2}{2m_e}(1-S)^2 + 2\hbar U k_{Fe} = \frac{\hbar^2 k_{Fe}^2}{2m_e} Z^2 \qquad \text{(A13)}$$

To express Z in terms of S, we have

$$Z = \sqrt{(1-S)^2 + 4U/v_{Fe}} \qquad \text{(A14)}$$

Therefore, the carriers with momentum less than $\hbar Zk_F$ should not make significant contribution to the momentum loss rate. Because of the finite phonon energy, it is a much better approximation to exclude that contribution than to include it with the negligence of phonon energy. An improved approximation for Eq. (A11) is therefore to replace E(S) by $F_2(S)$ such that

$$F_2(S) = \int_Z^{1+S} Q_e(y)\, A(y,S)\, dy \qquad \text{(A15)}$$

This replacement of the lower limit of integration from 1-S to Z provides a reasonable interpolation between the results from the calculations of low velocity limit and high velocity limit.

REFERENCES

1. See, for example, Ya. Pokrovskii, Phys. Status Solidi(a) 11, 385 (1972), and V. S. Bagaev, Springer Tracts in Modern Phys. 73, 72 (1975).
2. A. S. Alekseev, T. I. Galkina, V. M. Maslennikov, R. G. Khakomov, and E. E. Shchebnev, Pis'ma Zh Eksp. Teor. Fiz. 21, 578 (1975) [Sov. Phys. JETP Lett. 21, 271 (1975)].
3. A. S. Alekseev, T. I. Galkina, Fiz. Tverd. Tela. 18, 2005 (1976) [Sov. Phys. Solid State 18, 1167 (1976)].
4. B. Etienne, L. M. Sander, C. Benoit à la Guillaume, M. Voos, and J. Y. Prisur, Phys. Rev. Lett. 37, 1299 (1976).
5. A. S. Alekseev, V. S. Bagaev, and T. I. Galkina, Zh Eksp. Teor. Fiz. 63, 1020 (1972) [Sov. Phys. JETP 36, 536 (1973)].
6. V. S. Bagaev, L. V. Keldysh, N. N. Sibel'din, and V. A. Tsvetkov, Zh. Eksp. Teor. Fiz. 70, 702 (1976) [Sov. Phys. JETP 43, 362 (1976)].
7. V. B. Fuks, Pis'ma Zh. Eksp. Teor. Fiz. 20, 33 (1974) [JETP Lett. 20, 14 (1974)].
8. J. M. Hvam, and I. Balslev, Phys. Rev. B11, 5053 (1975).
9. J. Doehler, J. C. V. Mattos, and J. M. Worlock, Phys. Rev. Lett. 38, 726 (1977).
10. T. C. Damen, and J. M. Worlock, in the Proceedings of the Third International Conference on Light Scattering in Solids, edited by M. Balkanski, R. C. Leute, and S. P. Porto (Flammarion, 1976), p. 183-188.

11. L. V. Keldysh, and S. G. Tikhodeev, Pis'ma Zh Eksp. Teor. Fiz. 21, 582 (1975) [Sov. Phys. JETP Lett. 21, 273 (1975)].

12. L. V. Keldysh, in Excitons in Semiconductors, Nauka (1974) p. 5-19.

13. J. Bardeen, Phys. Rev. 52, 688 (1937).

14. See, for example, J. M. Ziman, Electrons and Phonons,(Oxford University Press, London , 1963).

15. In principle κ would depend on q. But for our purpose here since we will be dealing with small q, we can neglect this variation.

16. See, for example, D. Pines and P. Noziers, The Theory of Quantum Liquids I (Benjamin, New York, 1966).

17. See, for example, M. Lax, Symmetry Principles in Solid State and Molecular Physics, (John Wiley & Sons, New York, 1974).

18. C. Herring, Bell System Tech. J. 34, 237 (1955).

19. C. Herring and E. Vogt, Phys. Rev. 101, 944 (1956).

20. G. L. Bir and G. E. Pikus, Fiz. Tverd. Tela 2, 2287 (1960) [English transl: Soviet Phys. Solid State 2, 2039 (1961)]. A similar theory was worked out independently by M. Tiersten, IBM J. Res. Develop. 5, 122 (1961).

21. G. E. Pikus and G. L. Bir, Fiz. Tverd. Tela 1, 1642 (1959) [English transl: Soviet Physics - Solid State 1, 1502 (1960)].

22. P. Lawaetz, Phys. Rev. 174, 867 (1968).

23. J. D. Wiley, Solid State Comm. 8, 1865 (1970).

24. M. Costato, S. Fontanesi and L. Reggiam, J. Phys. Chem. Solids,

34, 547 (1973).

25. G. Dresselhaus, A. F. Kip, and C. Kittel, Phys. Rev. 98, 368 (1955).

26. G. A. Thomas, T. G. Phillips, T. M. Rice, and J. C. Hensel, Phys. Rev. Lett. 31, 386 (1973).

27. J. D. Wiley, Phys. Rev. 4, 2485 (1971).

28. E. O. Kane, J. Phys. Chem. Solids 1, 249 (1957).

29. See, for example, L. I. Shiff, Quantum Mechanics,(McGraw-Hill, New York, 1949).

30. J. M. Worlock, J. Doehler, and J. C. V. Mattos, Bull. Am. Phys. Soc. 22, 349 (1977).

31. C. Benoit à la Guillaume, M. Voos and F. Salvan, Phys. Rev. Lett. 27, 1214 (1971).

32. M. Combescot and P. Nozieres, J. Phys. C, 5, 2369 (1972).

33. S. M. Sze, Physics of Semiconductor Devices (Wiley, New York, 1969), p. 57.

34. W. F. Brinkman and T. M. Rice, Phys. Rev. B7, 1508 (1973).

35. See, for example, E. M. Conwell, High Field Transport in Semiconductors, in Solid State Physics, Supplement Vol. 9 (Academic Press, New York, 1967), Chap. III.

CHAPTER 3

DAMPING OF THE DROPLET MOTION: II.

IMPURITY AND PIEZOELECTRIC SCATTERING

I. Introduction

The damping of electron-hole droplets is of great interest recently[1]. In Chapter 1, we have investigated the phonon damping of droplet motion due to the deformation potential coupling. That work is motivated by the fact that most of the experiments that have been done are only for rather pure Ge, where the observed damping is due to the deformation potential coupling between phonons and carriers inside the droplet. However, recently there have been reports of electron-hole droplet formation in polar materials, CdS[2], GaAs[3], GaP[4]. Also, there are recent interests in the properties of droplets in doped Ge and Si[5-8]. The questions naturally arise then as to what are the important damping mechanisms for the droplet motion in polar and doped materials.

In doped material, obviously the impurity scattering will be an important damping mechanism one has to consider. Mobilities due to ionized[9] and neutral impurities[10] in doped semiconductors have been investigated by many authors. In the case of scattering by impurities inside the droplet, the impurities will be ionized[11] and the potential of the ionized impurity should be screened by the carriers inside the droplet. We calculated the screening[12] in the random phase approximation (RPA). The damping coefficient may be calculated by evaluating the entropy production rate due to impurity scattering as in Chapter 1. In Section II, the damping coefficients are calculated in simple models, taking Ge and GaP as examples. For the impurity scattering, we find the damping is essentially temperature independent.

For polar semiconductors, it is known that the mobilities due to piezoelectric scattering[13] depend only weakly on temperature ($\mu \sim T^{-1/2}$). This implies that piezoelectric scattering should dominate deformation potential scattering ($\mu \sim T^{-3/2}$) at low enough temperatures in crystals having the piezoelectric effect. Some estimates[14] show that the piezoelectric mobility for GaAs is less than the deformation potential mobility for temperatures less than 100^{0}K. Therefore, it is very important to consider the piezoelectric scattering mechanism for the damping of droplet in polar semiconductors. In the calculation of piezoelectric mobilities[13,14], screening effects due to free carriers are usually neglected since the carriers' densities are very small. However, for the piezoelectric scattering of carriers inside droplets which causes damping, the screening due to carriers inside droplets may play an important role. Since the piezoelectric scattering is electrostatic in nature, the screening can be accounted for by the dielectric function of the two components droplet. We use the dielectric function for droplets in the random phase approximation calculated in Chapter 1. The damping coefficient due to piezoelectric scattering is calculated in Section III by taking GaP as an example. We find that, due to the screening effect, the piezoelectric damping has a T^{7} temperature dependence in the low temperature limit; whereas, the deformation potential damping usually has a T^{5} dependence. Therefore, deformation potential scattering will dominate the damping of droplets at low temperatures for pure polar semiconductors.

In Section II, the calculation for the impurity damping is pre-

sented. The calculation for the piezoelectric damping is presented in Section III. Our results and conclusions are given in Section IV.

II. Impurity Damping

We consider the case that impurities which play a role in the damping of droplet are shallow enough to be ionized inside the droplets. The surface effects of the droplet are assumed to be negligible. Then the matrix element for the impurity scattering can be approximated by that for the screened Coulomb interaction. For electrons scattered from $\vec{k}$ to $\vec{k}+\vec{q}$ in the n^{TH} valley, the matrix element may be written down as

$$M_n^e(\vec{k}+\vec{q},\vec{k}) = \frac{4\pi e^2}{\kappa q^2 \varepsilon(q)} \quad , \tag{2.1}$$

where e is electronic charge, κ is the static dielectric constant of the material. $\varepsilon(q)$ is the RPA dielectric function of droplets as given by Eq. (2.12) of Chapter 1. Neglecting the overlap integral effect[15], the matrix element for holes has the same form as Eq. (2.1).

The damping coefficient can be calculated by evaluating for each band the entropy production rate given in Eq. (3.4) in Chapter 1. For impurity scattering, the entropy production rate in Eq. (3.4) in Chapter 1 can be reduced to integrations over the Fermi surface of the carriers. Following the procedures in Section III of Chapter 1, we obtain formally the damping coefficient due to impurity scattering as follows:

$$\gamma = \frac{1}{32\pi^5\hbar^3} \left\{ 2 \sum_{h=1}^{\nu} [\hat{u}\cdot(\vec{k}'-\vec{k})]^2 |M^e_n(\vec{k}',\vec{k})|^2 \frac{dG^e_n}{v^e_n(\vec{k})} \frac{dG^e_{n'}}{v^e_n(\vec{k}')} \right.$$

$$\left. + \sum_{hh'=1}^{4} \int [\hat{u}\cdot(\alpha_n\vec{k}^k_n - \alpha_{n'}\vec{k}^{h'}_{n'})]^2 |M^h_{n'n}(\vec{k}',\vec{k})|^2 \frac{dG^h_n}{v^h_n(\vec{k})} \frac{dG^h_{n'}}{v^h_{n'}(\vec{k}')} \right\} \Bigg/$$

$$\left\{ \left[-2 \sum_{n=1}^{\nu} \int \hbar\vec{k}^e_n(\vec{k}^e_n\cdot\hat{u}) \frac{\partial f^o_n(\vec{k})}{\partial E^e_n(\vec{k})} \frac{d^3k^e_n}{(2\pi)^3} \right.\right.$$

$$\left.\left. \sum_{n} \alpha_n \int \hbar\vec{k}^h_n(\vec{k}^h_n\cdot\hat{u}) \frac{\partial f^o_n(\vec{k})}{\partial E^h_n(\vec{k})} \frac{d^3k^h_n}{(2\pi)^3} \right] \cdot \vec{v} \right\} , \qquad (2.2)$$

where G_n is the surface area of the Fermi surface and $v_n(k)$ is the group velocity on the Fermi surface; $\hat{u}$ is a unit vector in the direction of drift velocity; ν is the number of valleys in the conduction band. The $f^o_n(\vec{k})$ is the Fermi distribution for carriers at temperature T. As long as the thermal energy kT is rather smaller than the Fermi energy, the result is independent of temperature. $\vec{v}$ and α_n in the denominator of Eq. (2.2) are defined in the same way as in Section III of Chapter 1.

The results for γ given in Eq. (2.2) may be evaluated using the known band structure for a given semiconductor and the properties of the droplet. This calculation would require extensive numerical work. For our purpose here, we want to make some simplifying approximations which will give a reasonable estimate of the magnitude of damping. We

take the same simple model for the band structures of conduction and valence band edges as in Section IV of Chapter 1. Therefore, the conduction band edges are represented by ν equivalent spherical valleys using density of states effective mass, and the valence band edges are represented by one spherical heavy hole band. Then Eq. (2.2) reduces to

$$\gamma_{im} = \frac{2e^4 N_I}{3\pi k^2 \hbar^3 n_o (m_e+m_h)} [\nu m_e^2 G_e + m_h^2 G_h] \quad , \tag{2.3}$$

where N_I denotes impurity concentration, G_e and G_h are integrals given by

$$G_e = \int_0^{2k_{Fe}} \frac{1}{q\varepsilon^2(q)} dq \tag{2.4a}$$

$$G_h = \int_0^{2k_{Fh}} \frac{1}{q\varepsilon^2(q)} dq \tag{2.4b}$$

where k_{Fe} (k_{Fh}) is Fermi wave vector for the electrons (holes) in our model; the dielectric function $\varepsilon(q)$ here is the RPA dielectric function as evaluated in Eqs. (4.15) - (4.17) in Chapter 1.

III. Piezoelectric Damping

For crystals with zinc blende symmetry, there is only one indepen-

dent piezoelectric constant[16]. For simplicity, we neglect the elastic anisotropies. The model "bare" piezoelectric coupling[17] frequently used in transport theory may be written down for electrons in the form as Eq. (2.7):

$$V_{e\text{-}ph} = \sum_{\vec{k}q\lambda} \sqrt{\frac{\hbar}{2\rho U q}} \frac{e e_{pz} 4\pi}{\kappa} a^{\dagger}_{\vec{k}+\vec{q}n} a_{\vec{k}n} (A_{\vec{q}\lambda} + A^{\dagger}_{-\vec{q}\lambda}) \quad , \tag{3.1}$$

where ρ, U, κ are the density, sound velocity, and static dielectric constant of the crystal, respectively, q the magnitude of the wave vector of the phonon, e is electronic charge, e_{pz} is the piezoelectric constant. The operator $a^{\dagger}_{\vec{k}n}$ creates an electron in the state with wave vector $\vec{k}$ in the n^{TH} valley and $A^{+}_{q\lambda}$ creates a phonon with wave vector $\vec{q}$ and polarization λ. A similar expression can be written down for holes.

For carrier inside the droplet, the modification due to screening of carriers inside EHD is to divide Eq. (3.1) by the dielectric function of the droplet, i.e.,

$$V^{S}_{e\text{-}ph} = \sum_{\vec{k}\ \vec{q}\ \lambda} \sqrt{\frac{\hbar}{2\rho U q}} \frac{e\, e_{pz} 4\pi}{\varepsilon(\vec{q})\kappa} a^{\dagger}_{\vec{k}+\vec{q}n} a^{\dagger}_{\vec{k}n} (A_{\vec{q}\lambda} + A^{\dagger}_{-\vec{q}\lambda}) \quad , \tag{3.2}$$

where the dielectric function $\varepsilon(\vec{q})$ is given by Eq. (2.12) in Chapter 1.

From the matrix element in Eq. (3.2), we can calculate the piezoelectric damping coefficient by using Eq. (3.8) of Chapter 1. Again,

we will take a similar model, as in Chapter 1, Section IV, to evaluate the damping coefficient. To be specific, we will take the indirect polar material GaP[4] as an example to calculate the piezoelectric damping. The conduction band structure is taken to be three equivalent spherical valleys[18] using density of states effective mass[19] $m_e = 0.40$. The valence band structure is taken to be two light-hole spherical bands with mass parameter $m_{\ell h} = 0.13$[20] and two heavy-hole spherical bands with mass parameter $m_{hh} = 0.55$[20]. Neglecting elastic anisotropy, the averaged sound velocity[21] ($= 4.76 \times 10^5$ cm/sec) is used here. Then the damping coefficient in Chapter 1, Eq. (3.8) can be evaluated in a straightforward manner anologous to the previous calculation. The final results may be put in the form

$$\gamma_{pz} = \frac{4 e^2 e_{pz}^2}{3\pi \hbar^2 \rho U m^{*} h_K^2} \left(\frac{kT}{\hbar U}\right)^3 \left\{ 3m_e^2 G_e + m_{\ell h}^2 G_{\ell h} + m_{hh}^2 G_{hh} \right\} , \tag{3.3}$$

where m^* is the inertial mass per pair of electron and hole for the droplet in GaP. It is determined by

$$m^* = m_e + \left(\frac{m_{\ell h}^{5/2} + m_{hh}^{5/2}}{m_{\ell h}^{3/2} + m_{hh}^{3/2}} \right) , \tag{3.4}$$

The G_e in Eq. (3.3) is an integral for electrons in droplet given by

$$G_e = \int_0^{\zeta_e} \frac{\zeta^3 e^{\zeta}}{[\varepsilon(\zeta)(e^{\zeta}-1)]^2} \, d\zeta \quad , \tag{3.5a}$$

where the dimensionless parameter ζ_e is twice the ratio of electron Fermi momentum to the momentum of thermal phonons with energy kT. The ζ_e is determined by the formula

$$\zeta_e = 2(\pi^2 n)^{1/3} \hbar U/kT \tag{3.5b}$$

where n is the density of electron-hole pairs in the droplet $\sim 6 \times 10^{18}$ in GaP[4]. The $G_{\ell h}$ and G_{hh} are integrals for the contribution from light and heavy hole bands, respectively. They are given by the same formula as Eq. (3.5a) except ζ_e are replaced by $\zeta_{\ell h}$ and ζ_{hh}. The $\zeta_{\ell h}$ and ζ_{hh} are given by

$$\zeta_{\ell h} = 2\left(\frac{3\pi^2 \, m_{\ell h}^{3/2} \, n}{m_{\ell h}^{3/2} + m_{hh}^{2/2}}\right)^{1/3} \hbar U/kT \tag{3.6a}$$

$$\zeta_{hh} = 2\left(\frac{3\pi^2 \, m_{hh}^{3/2} \, n}{m_{\ell h}^{3/2} + m_{hh}^{3/2}}\right)^{1/3} \hbar U/kT \tag{3.6b}$$

The RPA dielectric function $\varepsilon(q)$ for the droplet in GaP may be calculated from Eq. (2.12). The result is

$$\varepsilon(q) = 1 + \frac{6\pi e^2 n}{\kappa E_{Fe} q^2}\left\{F_e(\zeta) + \frac{m_{\ell h}^{3/2}}{3^{2/3}(m_{hh}^{3/2} + m_{\ell h}^{3/2})^{1/3} m_e} F_{\ell h}(\zeta) + \frac{m_{hh}^{3/2}}{3^{2/3}(m_{hh}^{3/2} + m_{\ell h}^{3/2})^{1/2} m_e} F_{hh}(\zeta)\right\} \tag{3.7a}$$

where E_{Fe} is the Fermi energy of electrons calculated in using spherical valleys:

$$E_{Fe} = \frac{\hbar^2(\pi^2 n)^{2/3}}{2m_e} \tag{3.7b}$$

The function $F_e(\zeta)$ is given by

$$F_e(\zeta) = \frac{1}{2} + \frac{\zeta_e^2 - \zeta^2}{4\zeta_e \zeta} \ell n\left|\frac{\zeta_e + \zeta}{\zeta_e - \zeta}\right| \quad . \tag{3.7c}$$

The functions $F_{\ell h}(\zeta)$ and $F_{hh}(\zeta)$ are given by the same formula as Eq. (3.7c) with the only change being that ζ_e is replaced by $\zeta_{\ell h}$ and ζ_{hh} in Eqs. (3.6a) and (3.6b), respectively.

For low enough temperature (less than 5^oK for GaP), the long wavelength phonons (much longer than Fermi wavelength of carriers in droplet)

will dominate the damping. In this case the RPA dielectric function in Eqs. (3.7a) - (3.7c) can be effectively replaced by the much simpler Thomas Fermi function $\varepsilon_{TF}(q)$ given by[22]

$$\varepsilon_{TF}(q) = 1 + q_{TF}^2/q^2 \quad , \tag{3.8a}$$

where the Thomas Fermi screening wave vector q_{TF} is [22]

$$q_{TF}^2 = \frac{6\pi e^2 n}{\kappa}\left(\frac{1}{\varepsilon_{Fe}} + \frac{1}{\varepsilon_{Fh}}\right) \tag{3.8b}$$

where E_{Fe} is the Fermi energy of electron given in Eq. (3.7b), and E_{Fh} is hole Fermi energy determined by

$$E_{Fh} = \frac{\hbar^2(3\pi^2 n)^{2/3}}{2(m_{hh}^{3/2}+m_{\ell h}^{3/2})^{2/3}} \tag{3.8c}$$

Substituting Eq. (3.3a) into Eq. (3.3), the damping coefficient in this low temperature limit may be approximated by

$$\gamma_{pz} = \frac{4e^2e_{pz}^2(3m_e^2+m_{\ell h}^2+m_{hh}^2)}{3\pi\hbar^2\rho U m^* n q_{TF}^4}\left(\frac{kT}{\hbar U}\right)^7 \int_0^\infty \frac{\zeta^7 e^\zeta}{(e^\zeta-1)^2}\, d\zeta \quad , \tag{3.9}$$

where all the upper limits for integrals G_e, $G_{\ell h}$, G_{hh} are replaced by

infinity because the integrand falls off exponentially as ζ goes to infinity.

IV. Results and Discussions

A. Impurity Damping

We calculate the impurity damping coefficient in Eq. (2.3) by taking Ge and GaP as examples. The values of parameters used in the calculation are listed in Table I. The one dimensional integrals in the expressions for G_e and G_h in Eqs. (2.4a) and 2.4b) were evaluated numerically. The results of the calculation of the impurity damping coefficient for Ge and GaP are

$$\gamma_{im} = 2.87\times10^{-6}N_I \qquad \text{(for Ge)} \quad , \tag{4.1}$$

$$\gamma_{im} = 0.60\times10^{-6}N_I \qquad \text{(for GaP)} \quad , \tag{4.2}$$

where N_I is the impurity concentration; both γ_{im} and N_I are measured in CGS units.

As usual, the impurity scattering is independent of temperature. Since the phonon scattering always decreases as the temperature is lowered, the impurity scattering is the mechanism to determine the damping of the droplet at low enough temperature. For Ge, as an example, the impurity damping will dominate the phonon damping at temperatures $T \lesssim 2^{o}K$, for impurity concentrations $N_I \gtrsim 10^{15}cm^{-3}$.

B. Piezoelectric Damping in GaP

Evaluating the results in Eq. (3.3) for parameters in Table I, we

TABLE I. List of Parameters Used in Calculation

	n	m_e	$m_{\ell h}$	m_{hh}	U
Ge[a]	$2.4\times10^{17}cm^{-3}$	0.22m	0.04m	0.30m	5×10^{5}cm/sec
GaP	$6\times10^{18}cm^{-3}$ [b]	0.40m[c]	0.13m[d]	0.55m[d]	4.8×10^{5}cm/sec[e]

	ρ	κ	e_{14}
Ge	$5.3g/cm^3$	15.36	0
GaP	$4.13g/cm^3$[f]	10 [g]	$-3\times10^{4}esu/cm^2$[h]

a. Table I in Chapter 1

b. Ref. 4

c. Ref. 19

d. Ref. 20

e. Ref. 21

f. Ref. 23

g. Ref. 24

h. Ref. 25

obtained the results shown in Fig. 1. For comparison, we also show the results of piezoelectric damping without including the screening effect in dashed line in Fig. 1.

We see that screening of the piezoelectric carrier-phonon coupling has reduced the damping by orders of magnitude, especially at low temperature. In fact, the screening effect has changed the temperature dependence of the piezoelectric damping from T^3 to T^7 for temperatures less than about 10^oK. Since the deformation potential damping coefficient usually has a T^5 temperature dependence as a result of Chapter 1, we expect the deformation potential coupling will dominate the damping of droplets in rather pure dislocation-free polar materials at low temperatures. The deformation potential damping in GaP will not be substantially different from that in Ge. By comparing the deformation potential damping calculated for Ge in Chapter 1, we expect the deformation potential coupling will dominate the piezoelectric coupling in GaP at temperatures below 10^oK. This is in contrast to the case that mobilities in pure dislocation-free polar materials are determined by the piezoelectric coupling at low temperatures[13,14].

Fig. 1. The piezoelectric damping coefficient for EHD motion in GaP vs temperature. The dashed curve is the result for the "bare" carrier-phonon interaction; the solid curve is the result when screening of the carrier-phonon interaction by carriers in the EHD is included. The solid curve has a T^7 dependence for T <5°K.

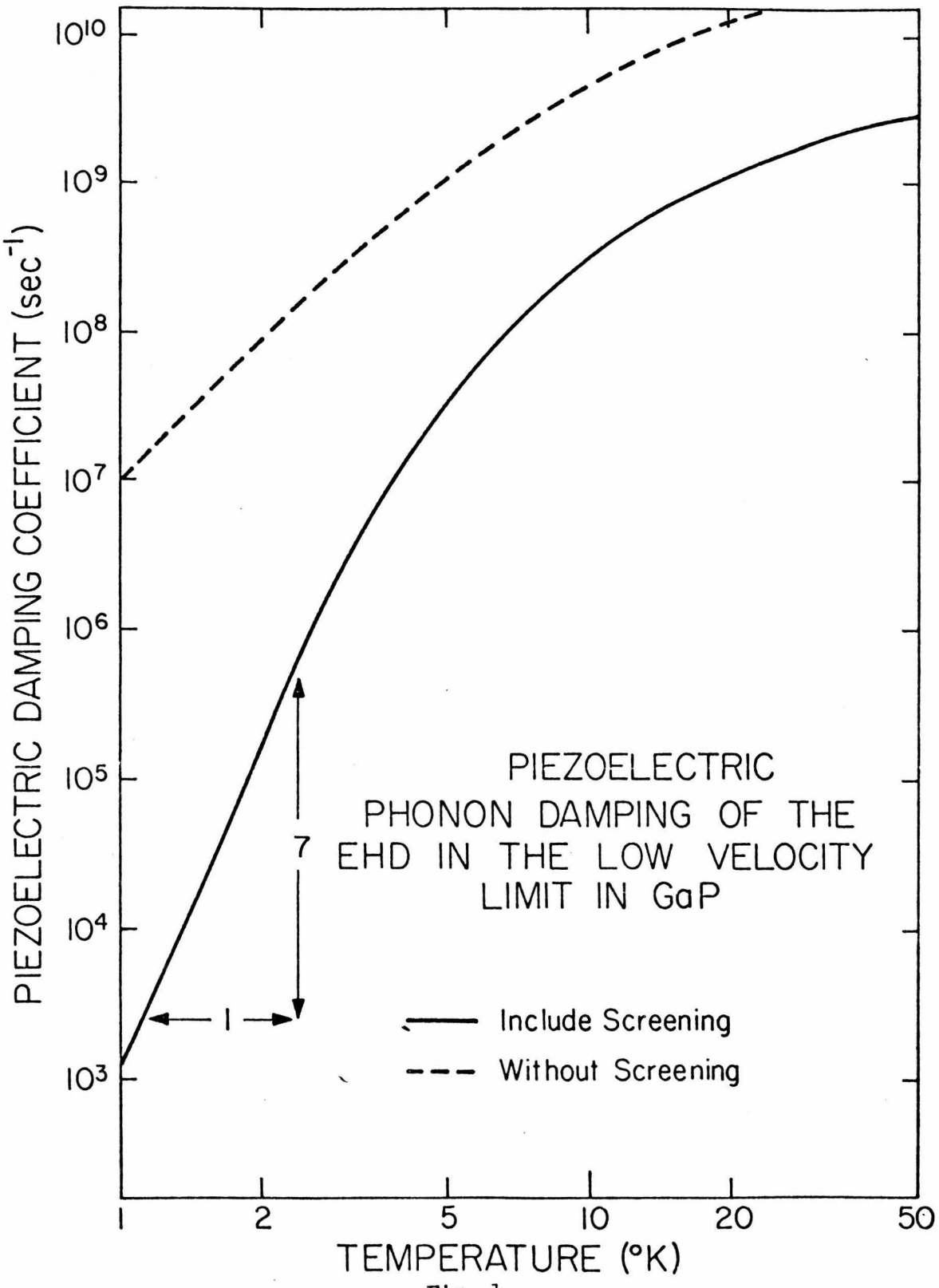

PIEZOELECTRIC DAMPING COEFFICIENT (sec^{-1})
10^{10}
10^{9}
10^{8}
10^{7}
10^{6}
10^{5}
10^{4}
10^{3}
1
2
5
10
20
50
TEMPERATURE (°K)
PIEZOELECTRIC
PHONON DAMPING OF THE
EHD IN THE LOW VELOCITY
LIMIT IN GaP
7
1
Include Screening
Without Screening

Fig. 1

REFERENCES

1. See Chapter 1, and references therein.
2. R. F. Leheny and Jagdeep Shah, Phys. Rev. Lett. 37, 871 (1976).
3. O. Hildebrand, B. O. Faltermeier and M. H. Pilkuhn, Solid State Comm. 19, 841 (1976).
4. Jagdeep Shah, R. F. Leheny, W. R. Harding, and D. R. Wight, Phys. Rev. Lett. 38, 1164 (1977).
5. J. M. Hvam and O. Christensen, Solid State Commun. 15, 929 (1974).
6. D. L. Smith, Solid State Commun. 18, 637 (1976).
7. G. Mahler and J. L. Birman, Phys. Rev. B12, 3221 (1975).
8. M. Chen, D. L. Smith, and T. C. McGill, Phys. Rev. 15, 4983 (1977).
9. H. Brooks, Phys. Rev. 83, 879 (1951); and C. Herring, unpublished, E. Conwell and V. F. Weisskopf, Phys. Rev. 77, 388 (1950).
10. C. Ekgrinsoy, Phys. Rev. 79, 1013 (1950), T. C. McGill and R. Baron, Phys. Rev. B11, 5208 (1975).
11. This is true for shallow impurities, See Ref. 6
12. It is easy to show that for scatterings which are electrostatic in nature the bare interaction should be screened by the dielectric function in Eq. (2.12) of Chapter 1.
13. H. J. G. Meijer and D. Polder, Physica 19, 255 (1953).
14. C. M. Wolfe, G. E. Stillman, and W. T. Lindley, J. Appl. Phys. 41, 3088 (1970).
15. The calculations in Section IV.D of Chapter 1 include the overlap integral effect. It turns out this effect is negligible.

16. See, for example, W. P. Mason, Piezoelectric Crystals and Their Application to Ultrasonics (D. Van Nostrand, New York, 1950) p. 40.

17. See, for example, E. M. Conwell, Solid State Physics, Suppl. (Academic, New York, 1967), Vol. 9, p. 111.

18. There are uncertainties for the conduction band minima. The minima are either at the three equivalent points x of the Brillouin zone, or close to the x point [in this case, the number of minima is doubled, with an inverted camelback structure. See P. Lawaetz, Solid State Commun. 16, 65 (1975)]. However, our calculation of the damping coefficient is insensitive to these uncertainties.

19. A. Onton, Phys. Rev. 186, 786 (1969).

20. M. Cardona, J. Phys. Chem. Solids 24, 1543 (1963).

21. J. D. Wiley and M. DiDomenico, Jr., Phys. Rev. B2, 427 (1970).

22. See, for example, D. Pines and P. Noziers, The Theory of Quantum Liquids I (Benjamin, New York, 1966) p. 150.

23. Handbook of Chemistry and Physics, edited by R. C. Weast, published by The Chemical Rubber Co., 51st edition, p. E-106.

24. J. I. Pankove, in Optical Processes in Semiconductors, (Dover, New York, 1971), p. 412.

25. D. F. Nelson and E. H. Turner, J. Appl. Phys. 39, 3337 (1968).

CHAPTER 4

BINDING OF AN EXCITON TO A NEUTRAL ACCEPTOR

(I) INTRODUCTION

The optical spectrum due to recombination of excitons bound to impurity centers in semiconductors has been extensively studied. Haynes[1] first studied the photoluminescence of Si of known donor and acceptor concentration and identified some of the lines observed in the luminescence as arising from the recombination of an electron-hole pair bound to a neutral acceptor or donor. He found that the ratio of the dissociation energy of the exciton-neutral-dopant-complex, E_D, to the ionization energy for the neutral dopant, E_i, was about 0.1 for a number of different donor and acceptor dopants. Following this work, radiative recombination due to bound excitons has been studied in a number of elemental and compound semiconductors[2,3,4]. Experimentally, the ratio E_D/E_i was found to cluster near 0.1 with some scatter between 0.08 and 0.12 for acceptor. On the other hand, for an exciton bound to a neutral donor, the ratio E_D/E_i is scattered between 0.1 and 0.25 [1,2] for different semiconductors.

The calculation of the bound exciton to a neutral acceptor is a non-reducible three-particle problem. Hopfield[5] first made an approximate estimate of the bound exciton dissociation energy. Later, Sharma and Rodriguez[6,7] have calculated rather accurately the binding energies of excitons bound to ionized donors, ionized acceptors and neutral donors. Their variational calculation for the exciton-neutral-donor complex made use of a trial wavefunction in which the hole's mass is assumed to be much larger than the electron's mass[7]. While this approach is physically correct for the exciton-neutral-

donor complex, it is not valid for the exciton-neutral-acceptor complex as pointed out by Sharma and Rodriguez[7].

The purpose of this chapter is to investigate the structure of a bound exciton-neutral acceptor complex and to explain why the relation, $E_D \approx 0.1E_i$, usually called Haynes' rule, holds for acceptors in different semiconductors. The binding of an exciton to a neutral acceptor is calculated for a model in which the semiconductor consists of a single valence band and a single conduction band with isotropic effective masses, m_h and m_e, respectively. The dielectric response of the semiconductor is included via the dielectric constant, ε. We find that the structure of the bound exciton-neutral impurity complex is more analogous to atoms than molecules. The correlation interaction is very important for the existence of a stable structure of the complex. The dissociation energy in units of the acceptor Rydberg $\left(\frac{m_h e^4}{2\varepsilon^2\hbar^2}\right)$ is calculated as a function of the electron to hole mass ratio σ. For a variation of σ between 0.1 and 1.0, the calculated E_D/E_i is found to vary between 0.075 and 0.13 in agreement with experimentally observed values. Therefore, the Haynes' rule is explained.

Our calculations are presented in Section II. In Section III we give the results and discussion.

(II) CALCULATION OF GROUND STATE BINDING ENERGY

For the exciton-neutral-acceptor complex, we have two relatively massive holes which are attracted to the negative acceptor center forming a "core" and a single relatively light electron which is repelled by the negative acceptor center. Hence, we choose a central-field model. However, because we have both positive and negative charge particles in a central Coulomb field, correlation energy is more important than in atomic physics. In fact, we find that there is no stable bound state in the Hartree-Fock approximation when the electron to hole mass ratio is of order one. A rigorous treatment of correlation energy is very difficult. Our claculation for correlation correction is based on the assumption that we can divide the correlation correction energy into two separate parts: hole-hole correlation and correlation of the hole core with the electron. The hole-hole core correlation energy correction is obtained using a remarkable fact observed for the correlation energy in helium and helium-like ions[8]. The correlation energy due to the interaction of the electron with the holes is taken into account by an effective "core polarization" potential[9].

A suitable trial wavefunction for the three particles is chosen to simplify both the Hartree-Fock and the correlation-correction calculations. For the two holes making up the "core", 1s hydrogenic type wavefunctions are a good approximation for the Hartree-Fock states.

$$\Psi_h(r_{1h},r_{2h}) = e^{-r_{1h}/\alpha_e}e^{-r_{2h}/\alpha}$$

where α is a variational parameter, and r_{1h} and r_{2h} are the radial coordinates of the two holes as measured with respect to the acceptor center. The spin wave function is a singlet so that the total wave function is antisymmetric. Both the hole-hole correlation energy and electron-hole correlation energy can be easily found for this type of hole orbits. The wavefunction for the electron is chosen as

$$\chi_e(r_e) = (1 + r_e + \frac{r_e^2}{2})e^{-r_e/\beta} \qquad (2)$$

where β is a variational parameter and r_e is the radial coordinate of the electron measured with respect to the acceptor center. The polynomial factor is chosen so that the wavefunction possesses the correct behavior near the origin where the electron is forced away from the negatively charged coulombic center.

To illustrate the quality of these analytic forms of the wavefunction, we have made comparisons of these analytic wavefunctions with more accurate wavefunctions for the case when $m_e=m_h$. The results of this comparison are presented in Fig. 1. In the case of the electron wavefunction, we compare Eq. (2) with the wavefunction obtained by a numerical solution of the Hartree-Fock Hamiltonian for the electron. As shown in Fig. 1, the size of the orbit for the numerical solution is about 5% smaller than that found from Eq. (2). Numerical solution of the Hartree-Fock Hamiltonian resulted in a 1% increase in the binding energy for the electron. The hole charge density given by Eq. (1) is compared with that obtained for electrons in the negative

hydrogen ion using Hylleraas-type wavefunctions[10]. The electron charge density in H^- should provide a valid comparison with the hole charge density here since the probability of finding the electron inside the core formed by the two holes is quite small (see Fig. 1). As illustrated in Fig. 1, the radial charge density is almost the same as that obtained for H^-.

The variational calculations were carried out for a number of different mass ratios. The variational parameter α was found to vary between 1.30 acceptor bohr $(\frac{\hbar^2\varepsilon}{m_h e^2})$ and 1.45 acceptor bohr for a variation of the mass ratio $\sigma(=m_e/m_h)$ between 0.125 and 1.0. For the same range of σ, the variational parameter β is found to vary between 1.30 acceptor bohr and 4.25 acceptor bohr, and the dissociation energy between -0.18 acceptor Ry and -0.09 acceptor Ry.(The states are not bound.) These energies and wavefunctions provided the zeroth order basis upon which the correlation corrections were made.

The hole-hole core correlation energy correction is estimated in the following way. For the helium atom and helium-like ions (H^-, Li^+, Be^{++}), variational calculations based on a trial wavefunction like that given in Eq. (1) are found to produce energies which require correlation corrections of 0.11 Ry. The correlation energy is found to be largely independent of the size of the orbit which is produced for different nuclear charges[8]. From He to H^-, the size of orbit changes from 0.37 bohr to 1.45 bohr, and the correlation energy only changes from 0.110 Ry to 0.112 Ry as shown in Table (I). In our case, we use exactly the same form of trial wavefunction for the holes. For a variation of the mass ratio from zero to one, the size of the orbit

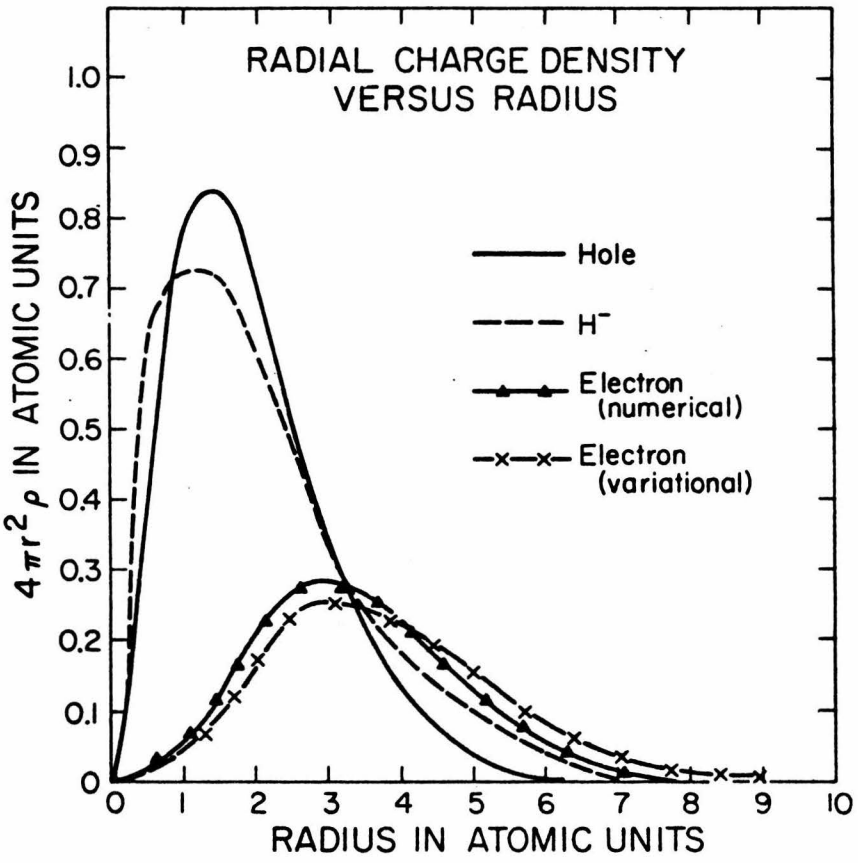


Fig. 1. The radial charge distribution for an exciton-neutral acceptor complex plotted against radial distance R when the electron to hole mass ratio equals one. The solid curve and the curve marked by crosses are the charge distributions for two holes, one electron, respectively, calculated from wavefunctions (1) and (2). The curve marked by the triangle is the electron charge distribution obtained by solving the Hartree-Fock equation for the electron numerically. The dashed curve is the electron charge distribution in H^- by using accurate Hylleraas-type wavefunctions (after Ref. 10).

TABLE I. Correlation energy[a] for helium and helium-like ions.

	H^-	H_e	L_i^+	B_e^{++}
Without correlation[b]	-0.055	1.695	5.445	11.195
With correlation	+0.055	1.807	5.560	11.312
Difference	0.110	0.112	0.115	0.117

a See, for example, H. A. Bethe, and E. E. Salpeter, Quantum Mechanics of One and Two Electron Atoms, p. 155 (Academic, New York, 1957).

b The binding energies here are calculated by using the hydrogenic orbitals for the two electrons.

of the holes varies between 1.45 and 1.30 acceptor bohr. Most of the time the electron is outside the two-hole core. The small penetration effect of the electron may be represented by introducing an effective charge which is reflected in the two holes wavefunction by the parameter α. Therefore, the two-hole core is very similar to a system of two particles in an effective Coulomb center. Hence, using the relative independence of the correlation energy from the calculation for atoms and ions, we take the correlation correction for the two holes to be 0.11 acceptor Ry over the entire range of mass ratio between zero and one.

Finally, we consider the correlation energy due to the two holes and the single electron. From the above-discussed Hartree-Fock calculations, we know that the electron is most likely to be found outside the two-hole core (see Fig. 1), we approximate the electron-holes correlation correction using a core polarization potential[9,11,12]. The potential we use here is from the work of Bethe[9] and Callaway[12]. The dipole polarization potential V_d for the electron from the two 1s holes orbits is

$$V_d = -9\left[1 - \frac{1}{3}e^{-2x}(1 + 2x + 6x^2 + \frac{20}{3}x^3 + \frac{4}{3}x^4) - \frac{2}{3}e^{-4x}(1+x)^4\right]/x^4 \qquad (3)$$

where $x = r_e/\alpha$. The parameter α characterizes the size of the hole orbit (see Eq. (11)). The energy unit is the acceptor Rydberg. The quadrupole polarization potential V_q is[12]

$$V_q = -30\left[1 - e^{-2x}\left(1 + 2x + 2x^2 + \frac{4}{3}x^3 + \frac{2}{3}x^4 + \frac{4}{15}x^5 + \frac{4}{45}x^6 + \frac{4}{255}x^7\right)\right]/x^6 \quad (4).$$

We add these two potentials to the Hartree-Fock potential of the electron from the two 1s holes and negative coulomb center which is

$$V_{HF} = -\frac{2}{r_e} + e^{-2r_e/\alpha}\left(\frac{4}{r_e} + \frac{4}{\alpha}\right) \quad . \quad (5)$$

Then we solve the Schrodinger equation for the electron numerically. In this way we include the electron-holes correlation energy. When the effective mass of electron and hole are equal, the correction due to quadrupole polarization potential is found to be 20% of that due to dipole polarization potential. For an electron mass which is half that for the hole, the correction is about 10%. The convergence of the multipole-polarization expansion is rapid whenever the overlap between the electron wavefunction and hole wavefunction is small. Hence, we expect this procedure for estimating the correction to the energy to become better as the mass ratio σ decreases.

(III) RESULTS AND DISCUSSION

The final results for the dissociation energy, E_D, of the exciton-neutral-acceptor complex are presented in Fig. 2. In this figure, we have plotted E_D in units of the acceptor Ry versus the mass ratio along with the results of Sharma and Rodriguez[7] for the exciton-neutral-donor complex in units of the donor Ry. Such a comparison is for the convenience of displaying the results over the entire mass ratio range;

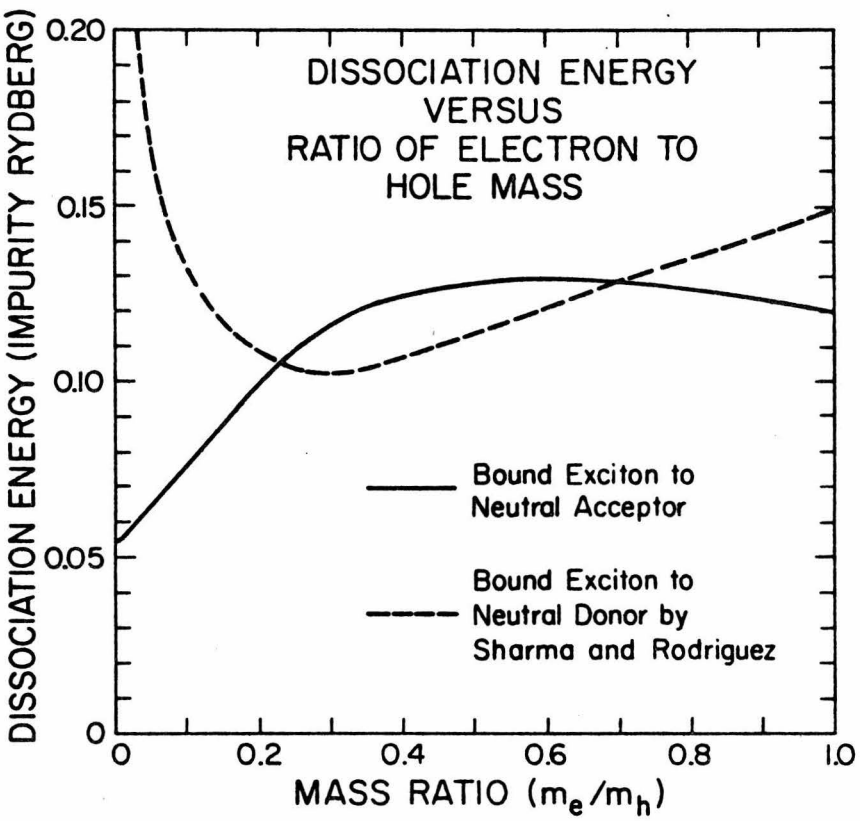


Fig. 2. Dissociation energy of an exciton-neutral acceptor complex as a function of electron to hole mass ratio. The dashed line is Sharma and Rodriguez's result (after Ref. 7) for exciton-neutral donor complex for comparison. If $\sigma = m_e/m_h$ is replaced by its reciprocal, Sharma and Rodriguez's result can be interpreted as representing the acceptor case with an electron to hole mass ratio greater than unity.

if $\sigma = m_e/m_h$ is replaced by its reciprocal, Sharma and Rodriguez's result can be interpreted as representing the acceptor case with an electron to hole mass ratio greater than unity. Fig. 2 shows that our results for the exciton-neutral-acceptor complex give a variation of E_D bounded by 0.055 and 0.13 acceptor Ry for a variation in mass ratio of between zero and one. Hence, we find that the dissociation energy is relatively independent of mass ratio. Comparing our results with those of Sharma and Rodriguez[7], we see that for a mass ratio of one their results are approximately 25% larger than ours. Since Sharma and Rodriguez's calculation is a variational calculation, we expect their results to be a lower bound for the dissociation energy. Our results are somewhat less than theirs. The discrepancy comes about because of the rather slow convergence of the multipole expansion for the core polarization potential when the mass ratio is one[12]. However, as noted above, we expect the core polarization approximation used here to become better as the mass ratio decreases.

These calculations are for a rather simplified model in which the details of the band structure and central cell corrections have not been included[13]. Hence, we find on detailed comparison between theory and experiment that the fluctuation in the experimental values of E_D/E_i for a single semiconductor are nearly as large as the variation of the theoretical values of E_D/E_i with mass ratio. Further, in many cases, the levels are quite deep (for example, In in Si[1]) where we would not expect the simple effective mass theory to apply. On the other hand, our calculations show that the ratio of E_D to E_i is approximately 0.1

and approximately independent of the mass ratio. Hence, the calculations provide at least a qualitative explanation of the observation that $E_D/E_i \approx 0.1$ for a number of semiconductors with rather different mass ratios[1-4].

REFERENCES

1. Haynes, J. R., Phys. Rev. Lett. 4, 361 (1960).
2. Halsted, R. E., and Aven M., Phys. REv. Lett. 14, 64 (1965).
3. Gross, E. F., Novikov, B. V. and Sokolov, N. S., Soviet Physics-Solid State, 14, 368 (1972).
4. Bogardus, E. H. and Bebb, H. B., Phys. Rev., 176, 993 (1968).
5. Hopfield, J. J., in Proceedings of the Seventh International Conference on the Physics of Semiconductors (Edited by Hulin M.) p. 725 ff, Dunod, Paris (1964).
6. Sharma, R. R. and Rodriguez, S., Phys. Rev. 153, 823 (1967).
7. Sharma, R. R. and Rodriguez, S., Phys. Rev. 159, 649 (1967).
8. Bethe, H. A. and Salpeter, E. E., Quantum Mechanics of One and Two Electron Atoms, p. 148, Academic Press Inc., New York (1957).
9. Bethe, H.A., in Handbook der Physik Vol. 24, part 1, pp 339 ff, Edward Brothers, Ann ARbor, Michigan (1943).
10. Bethe, H. A. and Salpeter, E. E., Quantum Mechanics of One and Two Electron Atoms, p. 155, Academic Press, Inc., New York (1957).
11. Hartree, D. R., Repts. Progr. Phys. Kyoto 11, 113 (1946).
12. Callaway, J., Phys. Rev. 106, 868 (1957).
13. Baldereschi, A., in Proceedings of the Twelfth International Conference on the Physics of Semiconductors (Edited Pilkuhn, M. H.) p. 345, B. G. Teubner, Stuttgart (1974); and the references contained therein.

CHAPTER 5

IMPURITY BANDING OF BOUND EXCITON STATES

(I) INTRODUCTION

The luminescence and absorption spectrum of a bound exciton (BE) have been studied in many experiments[1]. The lines are found to be very sharp [2] which is a result of the localization of the electron-hole pair. As the impurity concentration increases, a single exciton should interact with more than one impurity. One would expect, in analogy with the impurity band [3], banding of the bound exciton states. The question arises then as to how fast the banding occurs when one increases the impurity concentration. No theoretical work has been done for this problem.

The purpose of this work is to investigate theoretically the banding of the bound exciton state in a simple model. We consider the situation where exciton concentration is much smaller than the impurity concentration. Therefore, the interactions between excitons are neglected. Due to the interaction of an exciton with many impurities, the bound exciton hops between neutral impurities. We assume that impurities form a lattice, as is often postulated in the impurity band problem [3]. Then the banding problem is simply equivalent to a calculation of the hopping matrix element of the bound exciton between two neutral impurities. The hopping matrix element is calculated in a tight binding approximation by taking a simple model for the bound exciton. The mechanism of transferring excitons among impurities by the direct hopping process assumes excitons have infinite lifetimes. Another possible mechanism is also considered: the bound exciton recombines at one impurity site and subsequently excites a neighboring impurity site. This mechanism

turns out to be negligible for indirect semiconductors. We find that BE hopping is even less likely than hopping due to the carriers on impurities. Physically, this result is because the hopping of a bound exciton involves simultaneous changing of two orbitals for an oppositely charged pair. (Although, the size of the bound exciton wave function is larger than that of a bound carrier). Thus, we expect impurity banding to occur before BE banding becomes important.

The effect from the random distribution of impurities would change our estimate of banding (assuming impurity lattice) substantially only if the diagonal matrix elements are substantially larger than the hopping matrix element. To check this,we have calculated the first order diagonal matrix element; and we also have estimated the Van Der Waals interaction energy (corresponding to second order diagonal matrix element.) It turns out both are of comparable magnitude with the bound exciton hopping matrix element. Therefore, our results should be a reasonable estimate of the banding of bound exciton states.

Historically, the absorption experiment by Dean, et al [4] reported a BE line broadening of about 1 meV for Si doped with 3.6×10^{17} boron/cm^3. This broadening is about two orders of magnitude larger than our estimated value 0.005 meV. We believe that the data cannot be accounted for by impurity concentration effect. The smallness of our estimate of bound exciton banding is in agreement with recent experiments by Parsons[5] and by Elliot[6].

In Section II, we investigate the off-diagonal and diagonal matrix element for the interaction between a bound exciton complex and a neutral

$$= \left(\frac{-2}{|\vec{r}_{e1}-\vec{r}_{h3}|} + \frac{2}{|\vec{r}_{h2}-\vec{R}|} \right) + \left(\frac{2}{|\vec{r}_{h1}-\vec{r}_{h3}|} - \frac{2}{|\vec{r}_{h1}-\vec{R}|} \right)$$

$$+ \left(\frac{2}{|\vec{r}_{h2}-\vec{r}_{h3}|} - \frac{2}{|\vec{r}_{h2}-\vec{R}|} \right) + \left(\frac{-2}{|\vec{r}_{h3}+\vec{R}|} + \frac{2}{R} \right) \qquad (2b)$$

where r_{e1}, r_{h1}, r_{h2}, r_{h3} are the position coordinates of the electron and three holes of the system. The atomic units are used throughout this calculation. Energy is measured in impurity rydberg. Distance is measured in the impurity bohr radius.

Physically, E1 (H1) corresponds to the interaction of the electron (hole) in the bound exciton with the neighboring neutral impurity. H2 + I is the interaction between two neutral impurities. Since the three holes are identical particles, the subscripts for holes in our grouping in Eq. (2b) can be exchanged. However, the physical meaning of the four terms in Eq. (2a) remains unchanged.

Neglecting correlation effect, we approximate the two resonant eigenstates of H_{ro} by products of spin orbitals:

$$\psi_o(o) = \phi_e{}^{\uparrow}(\vec{r}_e) A \phi_h{}^{\uparrow}(\vec{r}_{h1}) \phi_h{}^{\downarrow}(\vec{r}_{h2}) \psi_{im}{}^{\uparrow}(\vec{r}_{h3}-\vec{R}) \qquad (3)$$

$$\psi_o(\vec{R}) = \phi_e{}^{\uparrow}(\vec{r}_e-\vec{R}) A \phi_h{}^{\uparrow}(\vec{r}_{h1}-\vec{R}) \phi_h{}^{\downarrow}(\vec{r}_{h2}-\vec{R}) \psi_{im}{}^{\uparrow}(\vec{r}_{h3}) \qquad (4)$$

where $\phi_e\uparrow$, $\phi_h\downarrow$, $\phi_h\uparrow$ are the spin orbitals for the electron and two holes in a bound exciton-neutral acceptor complex. $\psi_{im}\uparrow$ are the spin orbitals for the bound hole in the neutral acceptor. A is the antisymmetrization operator for holes.

The correlation effect is very important [7] for establishing a stable bound exciton state. However, for hopping matrix element, one may obtain a valid estimate without considering it explicitly.

To calculate the matrix element of H_{rI} in Eq. (2) for shallow impurities, we need only the envelope function of the spin orbitals. Assuming simple band structures for conduction and valence band, all the integrals involved in the calculation can be carried out analytically if all the envelope functions are approximated by the hydrogenic 1s type wave functions. Therefore, we take the envelope function to be the following form

$$\psi_{im}(r) = \sqrt{\frac{1}{\pi}}\, e^{-r} \tag{5a}$$

$$\phi_e(r) = \sqrt{\frac{\beta^3}{\pi}}\, e^{-\beta r} \tag{5b}$$

$$\phi_h(r) = \sqrt{\frac{\alpha^3}{\pi}}\, e^{-\alpha r} \tag{5c}$$

where α,β are the parameters measuring the sizes of the BE orbitals.

For bound exciton, this approximation for hole is reasonably good [7].

For electrons, the proper threshold behavior of the wave function at the origin is not included. However, we expect the hopping matrix element is determined essentially by the part of wave function at large distance from the origin. The values for the parameters α,β will be estimated from the result of a previous work [7] studying the structure of BE-neutral acceptor complex. Both α and β depend on the electron to hole mass ratio m_e/m_h. For a variation of the mass ratio from zero to one, α changes from 0.7 to 0.8 [7]. The electron orbit depends strongly on mass ratio. The accuracy of our hydrogenic approximation for electron orbit improves quickly when the mass ratio m_e/m_h decreases. To be specific, we will calculate matrix elements by choosing the case $m_e/m_h = 1/3$. In this case, using the results of previous calculation [7], a good approximation for BE wave functions is obtained by taking $\alpha = 0.75$ and $\beta = 0.33$.

A. The Bound Exciton Hopping Matrix Element

The off-diagonal matrix element of the interaction Hamiltonian in Eq. (2) may be written as:

$$\gamma_o^{BE}(R) = \langle \psi_o(o)|H_{rI}|\psi_o(R)\rangle \ . \qquad (6)$$

Physically, the matrix element is the hopping amplitude for the bound excitons between two neutral acceptors. Using wave functions in Eqs. (5a) - (5c), the matrix element $\gamma_o^{BE}(R)$ in Eq. (6) may be simplified as

$$\gamma_o^{BE}(R) = \langle \phi_e^{\uparrow}(\vec{r}_{e1})\ \phi_h^{\uparrow}(\vec{r}_{h1})\ \phi_h^{\downarrow}(\vec{r}_{h2})\psi_{im}^{\downarrow}(\vec{r}_{h3}) |H_{rI}|$$

$$\phi_e^{\uparrow}(\vec{r}_{e1}-\vec{R})\ \phi_h^{\uparrow}(\vec{r}_{h1}-\vec{R})\psi_{im}^{\downarrow}(\vec{r}_{h2})\phi_h^{\downarrow}(\vec{r}_{h3}-\vec{R})\rangle \qquad (7)$$

In the above formula, an exchange term has been dropped. That term corresponds to the changing of four spin orbitals and should be negligible except at very small impurity distance. We divide the matrix element into four terms produced by the grouping of the Hamiltonian shown explicitly by parentheses in Eq. (2).

$$\gamma_o^{BE} = \gamma_{E1} + \gamma_{h1} + \gamma_{H2} + \gamma_I \qquad (8)$$

Using Eqs. (5a), (5b), and (5c), the integrals in Eq. (7) can be evaluated analytically. The final expressions for γ_{E1} and γ_{H1} are rather tedious.

$$\gamma_{E1} = \frac{\alpha^3}{(\alpha')^6} e^{-\alpha R} \left(1+\alpha R+\frac{1}{3}\alpha^2 R^2\right) \{F(\alpha,\beta,R)$$

$$+ \beta e^{-\beta R} (2+2\beta R)\} \quad , \qquad (9)$$

where α,β are parameters in Eqs. (5b) and (5c); and α' is given by

$$\alpha' = (\alpha+1)/2 \qquad (10)$$

The function $F(\alpha,\beta,R)$ is given by the formula

$$F(\alpha,\beta,R) = -\beta^3R^2 \left\{e^{-\beta R}\left[\frac{2}{\beta R} + \left(\frac{2}{\gamma} - \frac{3}{(\gamma+1)} - \frac{1}{(\gamma+1)^2}\right)\frac{1}{(\alpha R)^2}\right.\right.$$

$$\left. + \left(\frac{2}{(\gamma+1)} - \frac{1}{(\gamma+1)^2} - \frac{1}{(\gamma+1)^3}\right)\frac{1}{(\alpha' R)^3}\right] + e^{-(\beta+2\alpha')R}$$

$$\left.\left[\left(\frac{1}{(\gamma+1)^2} - \frac{1}{(\gamma+1)}\right)\frac{1}{(\alpha' R)^2} + \left(\frac{1}{(\gamma+1)^2} - \frac{2}{(\gamma+1)} + \frac{1}{(\gamma+1)^3}\right)\frac{1}{(\alpha' R)^3}\right]\right\} \tag{11}$$

where $\gamma = \beta/\alpha'$, (12)

The expression for γ_{H1} is similar

$$\gamma_{H1} = -\frac{\alpha^3}{(\alpha')^6}\, e^{-\beta R\left(1+\beta R+\frac{1}{3}\beta^2R^2\right)}\left\{F(\beta,\alpha,R) + \alpha e^{-\alpha R}(2+2\alpha R)\right\} \tag{13}$$

The contribution of γ_{E1} (γ_{H1}) to the hopping matrix elements comes from the interaction of the electron (hole) in the bound exciton orbitals with the neighboring neutral impurity. γ_{E1} and γ_{H1} have opposite signs due to opposite charges on electron and hole. Their net contributions to γ_o^{BE} tend to cancel each other.

The values of γ_{H2} and γ_I are given by

$$\gamma_{H2} + \gamma_I = \frac{\alpha^3}{(\alpha')^5} e^{-(\alpha+\beta+2\alpha')R}(1+\alpha R+\frac{1}{3}\alpha^2R^2)$$

$$(1+\beta R+\frac{1}{3}\beta^2R^2)\left[\frac{5}{4} + \frac{2}{R\alpha'} - \frac{3}{2}\alpha' R - \frac{1}{3}(\alpha' R)^2\right] \qquad (14)$$

Physically, $\gamma_{H2} + \gamma_I$ comes from the interaction between two neutral impurities. At large impurity separations the terms γ_{E1} and γ_{H1} make the largest contribution to γ_o^{BE}. At small impurity distances all the terms must be included.

B. The Bound Exciton Diagonal Matrix Element

The diagonal matrix element of the interaction H_{rI} in Eq. (2) is defined as

$$\gamma_D^{BE}(R) = \langle \psi_o(o)|H_{rI}|\psi_o(o)\rangle \qquad (15)$$

This matrix element can be evaluated in the same fashion as the off-diagonal matrix element. The final expression for $\gamma_D^{BE}(R)$ may be written as

$$\gamma_D^{BE}(R) = \left[G(\beta) - e^{-2\beta R}\left(2\beta + \frac{2}{R}\right)\right] - 2\left[G(\alpha) - e^{-2\alpha R}\left(2\alpha + \frac{2}{R}\right)\right] \quad (16a)$$

The function $G(\beta)$ in Eq. (16a) is determined by

$$G(\beta) = \frac{e^{-CR^2}}{2C}\left\{\left(\frac{2}{D} - \frac{2\beta R}{D^2}\right)\left[\frac{e^{D} - e^{-D}}{D} - (e^{D} + e^{-D})\right] + \frac{(e^{D} - e^{-D})}{D}\right.$$

$$\left.\left[2 + \frac{2}{C} + \frac{2\beta R}{C} + \frac{2\beta R}{C^2}\right]\right\} \quad , \quad (16b)$$

where C and D are constants given by

$$C = (1 + \beta)R \quad , \quad (16c)$$

$$D = (1 - \beta)R \quad . \quad (16d)$$

The function $G(\alpha)$ has exactly the same expression as $G(\beta)$, except the parameter β is replaced by parameter α.

C. Matrix Element for Single Carrier Impurity Band

For comparison, we have also estimated the relevant diagonal and off-diagonal matrix elements for the simpler case of neutral acceptors

banding. The relevant hopping matrix element for the banding of neutral acceptors is determined by the hole hopping between two ionized acceptors. Physically, this case corresponds to a situation in which a hole is absent from a filled neutral acceptor band. This hole hopping matrix element can be easily calculated using hydrogenic wave functions in Eq. (5a). The result may be written as

$$\gamma_o^h(R) = e^{-R}(\frac{2}{R} - \frac{4}{3}R) \quad . \tag{17a}$$

Similarly, one can calculate the diagonal matrix element. The result is given by

$$\gamma_D^h(R) = e^{-2R}(2 + \frac{2}{R}) \quad . \tag{17b}$$

Note that the diagonal matrix element falls off exponentially twice as fast as the off-diagonal one. Therefore, it is negligible compared with the off-diagonal matrix element at fairly large distance.

III, SECOND ORDER INTERACTIONS

In Section II, the interactions between the bound exciton complex and a neutral acceptor are studied in the perturbation theory to first order. However, it is well known that the "long-range" interaction (van der Waals interaction) between two neutral atoms is a second order

effect in terms of perturbation theory. Therefore, we will estimate the interaction between a bound exciton complex and a neutral acceptor to second order in this section.

The second-order interaction energy between a bound exciton complex and a neutral acceptor at fairly large distance is given by[8]:

$$W_{BE}(R) = \sum_n \frac{|\langle \psi_o(o)|H'|\psi_n(o)\rangle|^2}{E_o - E_n} \tag{18}$$

where the index n refers to all excited states in the system of the bound exciton complex and neutral acceptor. The interaction Hamiltonian H' in Eq. (18) is simplified by expanding H_{rI} in Eq. (2b) in powers of 1/R and keeping the lowest terms.

Following the well-known argument to obtain an estimate of van der Waals interaction[8], Eq. (18) can be approximated[9] by

$$W_{BE}(R) \simeq \frac{\langle \psi_o(o)|H'^2|\psi_o(o)\rangle}{E_o - E_n^*} \tag{19}$$

where E_n^* is the energy of the lowest excited state for which $\langle o|H'|n^*\rangle$ is different from zero.

Since the electron in the bound exciton-neutral acceptor complex is much more polarizable than the two-holes core, we will neglect the polarization of the two-hole core. The state n^* should be that: (1) the neutral impurity is excited to a state of principle quantum

number 2; and (ii) the electron orbitals in the bound exciton complex should also be changed. The energy required to excite this electron is approximated by the ionization energy of the electron E_I. (The first excited state of bound exciton should be near the continuum states). The ionization energy may be calculated from the dissociation energy of bound exciton, D_{BE}; the exciton binding energy E_x; and the affinity energy of adding a hole to a neutral acceptor, A. The E_I is determined by

$$E_I = D_{BE} + E_x - A \tag{21}$$

From experimental measurements, we may determine that D_{BE}=0.1; E_x=0.22; A=0.06; all energies are measured in acceptor rydberg. The excitation energy for the neutral acceptor is about 0.75 acceptor rydberg. Therefore, we obtain

$$E_n^* - E_o = E_I + 0.75 \cong 1 \text{ acceptor rydberg} \tag{22}$$

The matrix element in Eq. (19) may be easily evaluated by using wave functions in Eqs. (5a) - (5c). The final results for the van der Waals interaction between a bound exciton complex and a neutral acceptor is given by

$$W_{BE}(R) = - \frac{24}{R^6 \beta^2} \tag{23}$$

where β is the parameter measuring the size of electron orbit in Eq. (5b).

The van der Waal interaction between two neutral acceptors may be written as[8]

$$W_s(R) = -\frac{16}{R^6} \tag{24}$$

The van der Waals interaction for the bound exciton complex in Eq. (23) is larger than that for the neutral impurity in Eq. (24). Physically, this is because a bound exciton complex is more polarizable than a neutral impurity.

We have also considered another second order process to transfer bound excitons among neutral impurities: the bound excitons may recombine at one impurity site and subsequently excites a neighboring impurity. This process has been studied in detail in the problem of "sensitized luminescence"[10] in solids. The hopping matrix element for this process may be written in terms of the bound exciton absorption cross section. For indirect material, it turns out to be small. Since the direct hopping decreases exponentially at large distance, the new mechanism, which is basically dipole-dipole interaction, may be dominant at large distance. However, an estimate[11] for impurity concentration $\sim 2\times10^{16}cm^{-3}$ in Si shows the value of the matrix element is about 10^{-6} meV. It is much smaller than the natural width of the usual atomic spectra ($\sim10^{-4}$meV). We believe this

mechanism is unimportant for indirect material.

IV. RESULTS AND DISCUSSION

The result of the bound exciton hopping matrix element in Eq. (8) is calculated for $\alpha = 0.75$, $\beta = 0.33$ as a function of distance between two impurities. This choice of values of α and β is suitable for the case that $m_e/m_h = 1/3$. The magnitudes of the matrix element $|\gamma_o^{BE}(R)|$ are plotted in Fig. 1 as a function of the distance between two impurities. As shown in Fig. 1, the values of γ_o^{BE} increase rapidly as the distance R between impurities decreases. It reaches a local maximum around R = 4.5 and begins decreasing as R decreases further. In our calculation, this variation of γ_o^{BE} is due to the interference between the hopping of the electron and hole in the exciton, namely, the interference of the γ_{E1} and γ_{H1}. They are opposite in sign. γ_{E1} is larger than γ_{H1} in magnitude at large distance; whereas, γ_{H1} is larger at short distance. At a distance around R = 3.5, the matrix elements γ_o^{BE} change sign and the magnitudes increase rapidly as the distance decreases further. For comparison, we also show in Fig. 1 the hopping matrix element in Eq. (17a) of a single hole between two ionized impurities. We find that the hopping matrix element for a bound exciton is much smaller than that of a bound carrier. Physically, the reasons are twofold: the bound exciton is a neutral entity and the hopping of it involves the changing of two orbitals.

In addition, we have calculated the diagonal matrix element $\gamma_D^{BE}(R)$ in Eq. (16a) for $\alpha = 0.75$, $\beta = 0.33$. The results are plotted in Fig. 2.

Fig. 1. The magnitudes of hopping matrix elements vs impurity distance. The solid line is the result for the hopping of a bound exciton between two neutral impurities. The dashed line is the result for the hopping of a carrier between two ionized impurities.

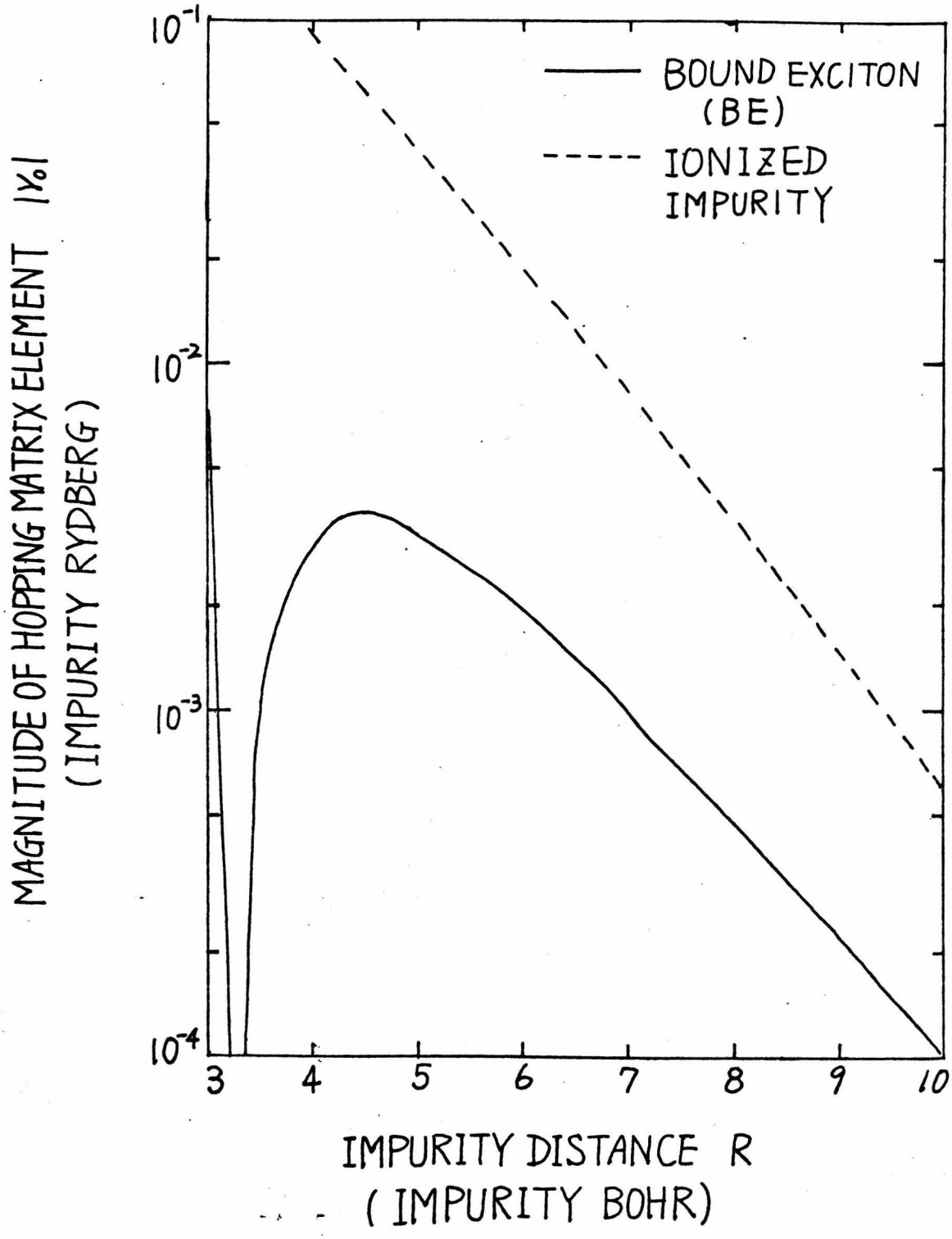

BOUND EXCITON
(BE)
IONIZED
IMPURITY
MAGNITUDE OF HOPPING MATRIX ELEMENT |V|
(IMPURITY RYDBERG)
10^{-1}
10^{-2}
10^{-3}
10^{-4}
3
4
5
6
7
8
9
10
IMPURITY DISTANCE R
(IMPURITY BOHR)

Figure 1.

Fig. 2. The magnitudes of the diagonal matrix elements vs impurity distance. The solid line is the result for the interaction between a bound exciton (BE) complex and a neutral impurity. The dashed line is the van der Waals interaction energy between a bound exciton complex and a neutral impurity. The dashed line marked by dots is the result for the interaction between a neutral impurity and a ionized impurity. The dashed line marked by triangles is the result for the van der Waals interaction energy between two neutral impurities.

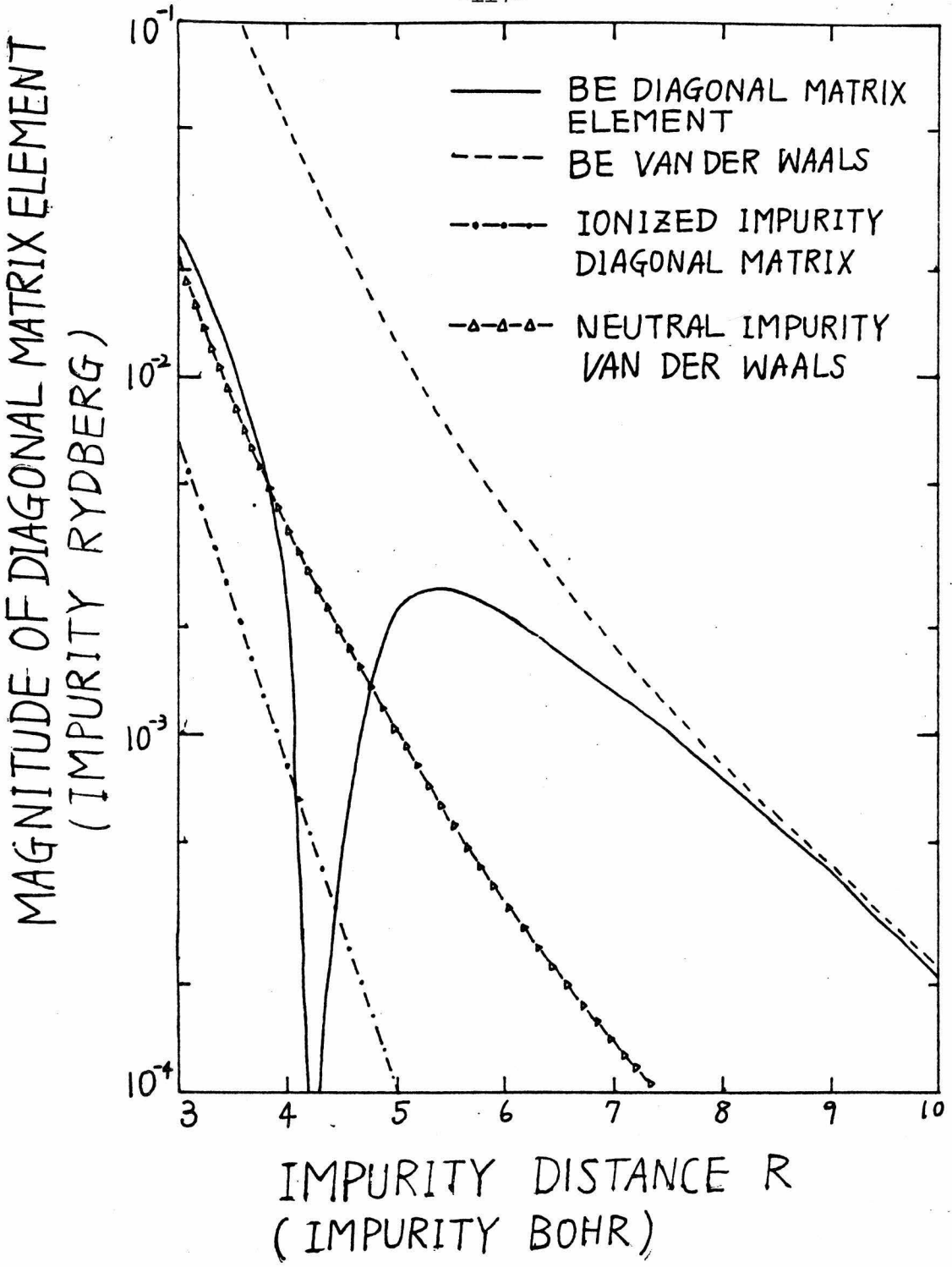

MAGNITUDE OF DIAGONAL MATRIX ELEMENT
(IMPURITY RYDBERG)
10^{-1}
10^{-2}
10^{-3}
10^{-4}
3
4
5
6
7
8
9
10
IMPURITY DISTANCE R
(IMPURITY BOHR)
BE DIAGONAL MATRIX ELEMENT
BE VAN DER WAALS
IONIZED IMPURITY DIAGONAL MATRIX
NEUTRAL IMPURITY VAN DER WAALS

Figure 2

The functional dependence of $\gamma_D^{BE}(R)$ is quite analogous to the hopping matrix elements $\gamma_o^{BE}(R)$ in Fig. 1; and they are of comparable magnitudes. The van der Waals interaction energy between the bound exciton complex and a neutral acceptor as shown in Eq. (23) is also plotted in Fig. 2 for $\beta = 0.33$. This second order interaction energy is of the same magnitude as the diagonal matrix element $\gamma_o^{BE}(R)$ for impurity distances between 6 and 11 as shown in Fig. 2. At distances smaller than 6, the van der Waals interaction increases monotonically; whereas, the $\gamma_D^{BE}(R)$ shows interference effect as already discussed for $\gamma_o^{BE}(R)$. For comparison in Fig. 2, we also show the diagonal matrix element for a single hole between two ionized impurities and the van der Waals interaction between two neutral impurities. In this case they are both smaller than the matrix elements for the bound excitons.

From our results, first of all, because the hopping matrix elements for a single hole $\gamma_o^h(R)$, are larger than all the relevant matrix elements for the banding of bound excitons, we expect the usual impurity banding to occur before the banding of a bound exciton state becomes important. Second, since the off-diagonal matrix element for the interaction between a neutral acceptor and a bound exciton complex is not substantially smaller than the diagonal matrix element and the van der Waals interaction energy, it is reasonable to estimate the banding of bound exciton states by assuming the impurities form a lattice.

We assume that the impurities form a simple cubic lattice. Then the bound exciton band should have a bandwidth of 12 γ_o^{BE}. Applying our result to, for example, Si doped with 4×10^{17} boron/cm^3, the estimated

bandwidth is about 0.005 meV. In this estimate, the impurity bohr radius is given by $a = (m/m_h)\kappa a_H$, where κ is static dielectric constant and a_H is the hydrogen bohr radius. The effective mass for hole m_h/m is taken to be 0.45. This value of m_h is determined by requiring that the hydrogenic formula yield agreement with the observed boron ground state energy 46 meV[12]. The optical mass[13] for electron in Si is about 0.26. The electron to hole mass ratio is about 0.5. Our result in Fig. 1 is calculated for simple conduction and valence band with mass ratio 0.33. The obtained estimate 0.005 meV is believed to have the right order of magnitude for Si, and probably contains a small overestimate. The point we want to make here is that the banding for bound exciton is very small compared with the usual impurity band. The earlier absorption experiment by Dean, et al reported[4] a BE line broadening of about 1 meV for Si doped with 3.6×10^{17} boron/cm^3. This broadening is about two orders of magnitude larger than our estimated value 0.005 meV. The random distribution of impurities should not modify our banding-width estimate by orders of magnitude. We conclude that the data cannot be accounted for by impurity concentration effect. Recent experiment[5] by Parsons reported the width at half-maximum height of the bound exciton is about 0.05 meV for 10^{15} p/cm^3 in Si. He believes the broadening is due to dislocations. Another recent absorption measurement by Elliot[6] shows that no BE line broadening was observed in 0.1 meV resolution limit on concentrations as high as 1.3×10^{17} Ga/cm^3 in Si. Both experimental observations are consistent with our results of small banding of BE.

In conclusion, we have presented a simple model in which to investi-

gate the banding of bound excitons in doped semiconductor. The adopted model of bound exciton complex is more suitable for acceptors. The banding mechanism is the direct hopping of bound excitons among impurities. We find that BE hopping is small for the impurity concentrations up to where impurity banding already plays an important role and will modify the model. Despite the larger radius of the bound exciton complex than that of a bound carrier, this result is due to two reasons: the bound exciton is a neutral entity and the hopping of it involves changing of two orbitals simultaneously. The smallness of our estimate of the bound exciton banding is in agreement with recent experimental results[5,6]. The model discussed here is only valid for exciton concentration considerably smaller than the impurity doping concentration.

REFERENCES

1. Haynes, J. R., Phys. REv. Lett. 4, 361 (1960).
   Thewalt, M. L. W., Kirczennow G., Parsons, R. R., and Barrie, R., Can. J. Phys. 54, 1728 (1976) and references contained therein.
2. The no phonon (NP) bound exciton luminescence lines was reported to be less than 0.05 meV by Sauer, R., Phys. Rev. Lett. 31, 376 (1973).
3. Fistul', V. I., Heavily Doped Semiconductors, (Plenum Press, New York,1969), pp. 24-34 and references contained therein.
4. Dean, P.J., Flood, W. F., Kaminsky, G., Phys. Rev. 163, 721 (1967).
5. Parsons, R. R., Solid State Comm., 22, 671 (1977).
6. Elliot, K., private communication.
7. Pan, D. S., Smith, D. L., McGill, T. C., Solid State Comm. 18, 1557 (1976).
8. See, for example, L. I. Schiff, Quantum Mechanics, Third Edition (McGraw-Hill, New York, 1949) p. 259.
9. This approximation is valid for hydrogen atom about 20%. See, for example, L. Pauling and E. B. Wilson, Jr., Introduction to Quantum Mechanics, Sec. 47a (McGraw-Hill, New York, 1935).
10. Dexter, D. L., J. Chem. Phys. 21, 836 (1953).
11. Using the absorption cross section from the experimental results in Ref. 4.
12. Burstein, E., Picus, G. S., Henvis, B. and Wallis, R., J. Phys. Chem. Solids, 1, 65 (1956).
13. W. F. Brinkman and T. M. Rice, Phys. Rev. 1, 1508 (1973).

CHAPTER 6

IMPACT IONIZATION OF EXCITONS IN Ge AND Si

I. INTRODUCTION

An exciton in a semiconductor can be ionized by a number of processes: phonon absorption, collision with an impurity, collision with a free carrier etc. In pure materials with relatively low carrier concentrations in thermal equilibrium, phonon absorption is the dominant ionization process.[1] In thermal equilibrium each ionization process is balanced by a corresponding formation process; corresponding ionization and formation rates are related by the principle of detailed balance. If the exciton lifetime (recombination of electron and hole) is much longer than the total ionization time, the law of mass action is satisfied.

The application of an external electric field will change the balance between ionization and formation processes and can, therefore, modify the relative concentration of excitons and free carriers. Impact ionization by free carriers is especially sensitive to electric fields; even quite small fields can greatly increase the rate of this process. A critical field is reached when the impact ionization process first dominates both exciton recombination and ionization by phonon absorption. Exciton concentration will plunge if fields larger than the critical field are applied.

Impact ionization of excitons has been observed in low temperature photoconductivity experiments in Ge.[2-4] Gurnee, Glicksman and Yu[2] have observed finite photoconductivity in Ge at low temperature (~ 2K°) and low photoexcitation levels

when the mass action law predicts electrons and holes should combine to form excitons and electron-hole droplets with overwhelming probability. Impact ionization of excitons and electron-hole droplets by field excited free carriers could account for this observation. Asnin, Rogachev and Ryvkin[3] have measured photocurrent as a function of applied electric field at constant temperature (~ 2.5°K) in Ge. They observed a large (about two orders of magnitude) increase in photocurrent when the field is increased from about 3 V/cm to about 7 V/cm and attributed this observation to impact ionization of excitons. More recently Yao, Inagaki and Maekawa[4] have repeated this experiment at 4.2°K; they also observed a large increase in photocurrent, but their measured critical fields are somewhat lower (~ 0.6 V/cm) and depend on the photoexcitation level. Impact ionization should also be important in double injection devices at low temperatures[5,6] and preliminary measurements[7] indicate that the relative concentration of excitons and free carriers is field dependent and not given by the law of mass action. The purpose of this paper is to investigate theoretically the effect of an external electric field on exciton concentration at different temperatures.

Section II contains a qualitative discussion of the effect of impact ionization on exciton concentration. Quantitative calculations are presented in Section III. Our results are summarized and compared with experiment in Section IV.

II. QUALITATIVE PHYSICS

Only those free carriers whose energy is greater than the exciton binding energy can impact ionize an exciton. At low temperatures ($kT << \varepsilon_B$) few free carriers are this energetic and the impact ionization rate is very small. An external electric field accelerates free carriers and increases the number of carriers which are sufficiently energetic to impact ionize. This carrier heating greatly increases the impact ionization rate. Whereas, the impact ionization rate is greatly increased by an electric field, exciton ionization by phonon absorption (the dominant ionization process at thermal equilibrium) is not signifcantly affected by an electric field. So long as the impact ionization rate is slower than the phonon absorption rate, the applied field will have little affect on the excition concentration; but once the field becomes large enough that the impact ionization rate exceeds both the phonon absorption and exciton annihilation rates, the exciton concentration will drop sharply with increasing field.

The rate of change of the exciton concentration is controlled by the rate of exciton recombination and the thermal (phonon absorption) and impact ionization and formation rates.

Assuming spatial uniformity (i.e., no exciton diffusion), the rate of change of exciton concentration is described by the rate equation

$$\frac{dn_{Ex}}{dt} = A_T n_e n_h + A_e n_e^2 n_h + A_h n_e n_h^2 - \frac{n_{Ex}}{\tau} - B_T n_{Ex} - B_e n_{Ex} n_e - B_h n_{Ex} n_h \qquad (1)$$

where n_{Ex}, n_e and n_h are respectively, the exciton concentration, the electron and hole concentrations; $A_T(B_T)$, $A_e(B_e)$ and $A_h(B_h)$ are respectively the coefficients for thermal, electron impact and hole impact formation (ionization); and τ is the exciton lifetime. Assuming equal concentrations of electrons and holes ($n_e = n_h \equiv n$; this will be the case in intrinsic materials and double injection devices), the steady state exciton concentration is given by

$$n_{Ex} = \frac{[A_T + (A_e + A_h)n]n^2}{[B_T + \frac{1}{\tau} + (B_e + B_h)n]} \qquad (2)$$

In a state of thermal equilibrium (no external field), the ionization and formation coefficients are related by the principle of detailed balance,

$$A_i/B_i = K \qquad (3a)$$

$$K = \left(\frac{2\pi m^* kT}{h}\right)^{-3/2} e^{\varepsilon_B/kT} \qquad (3b)$$

$$m^* = \frac{m_t^{2/3} m_\ell^{1/3} m_h}{(m_t + m_h)^{2/3} (m_\ell + m_h)^{1/3}} \qquad (3c)$$

Here K is the equilibrium constant, m_t, m_ℓ and m_h are respectively the transverse electron, longitudinal electron and hole (density of states) effective masses, and ε_B is the exciton binding energy. If the exciton lifetime (electron-hole recombination) is long compared to ionization times, the exciton concentration is given by the law of mass action

$$n_{Ex} = Kn^2 \qquad . \qquad (4)$$

In any exciton ionization process, some particle (free carrier, phonon, exciton) must have an energy greater than the exciton binding energy. In thermal equilibrium, the number of such energetic particles decreases exponentially with temperatures (for $kT << \varepsilon_B$); therefore, the exciton ionziation rate decreases approximately exponentially with temperature. At sufficiently low temperature ($T \lesssim 5°K$ in Ge, $T \lesssim 17°K$ in Si) the exciton ionization rate will become longer than the exciton lifetime and the mass action law (Eq. 4) will not be satisfied. In Figure 1, we plot exciton density versus temperature in Ge for infinite exciton lifetime (mass action law) and for the experimental lifetime. There is a significant deviation at low temperature. At these low temperatures, the rate of exciton loss (in Eq. 1) is governed by the temperature independent exciton lifetime; the rate of exciton gain is a slowly varying function of temperature and therefore the exciton

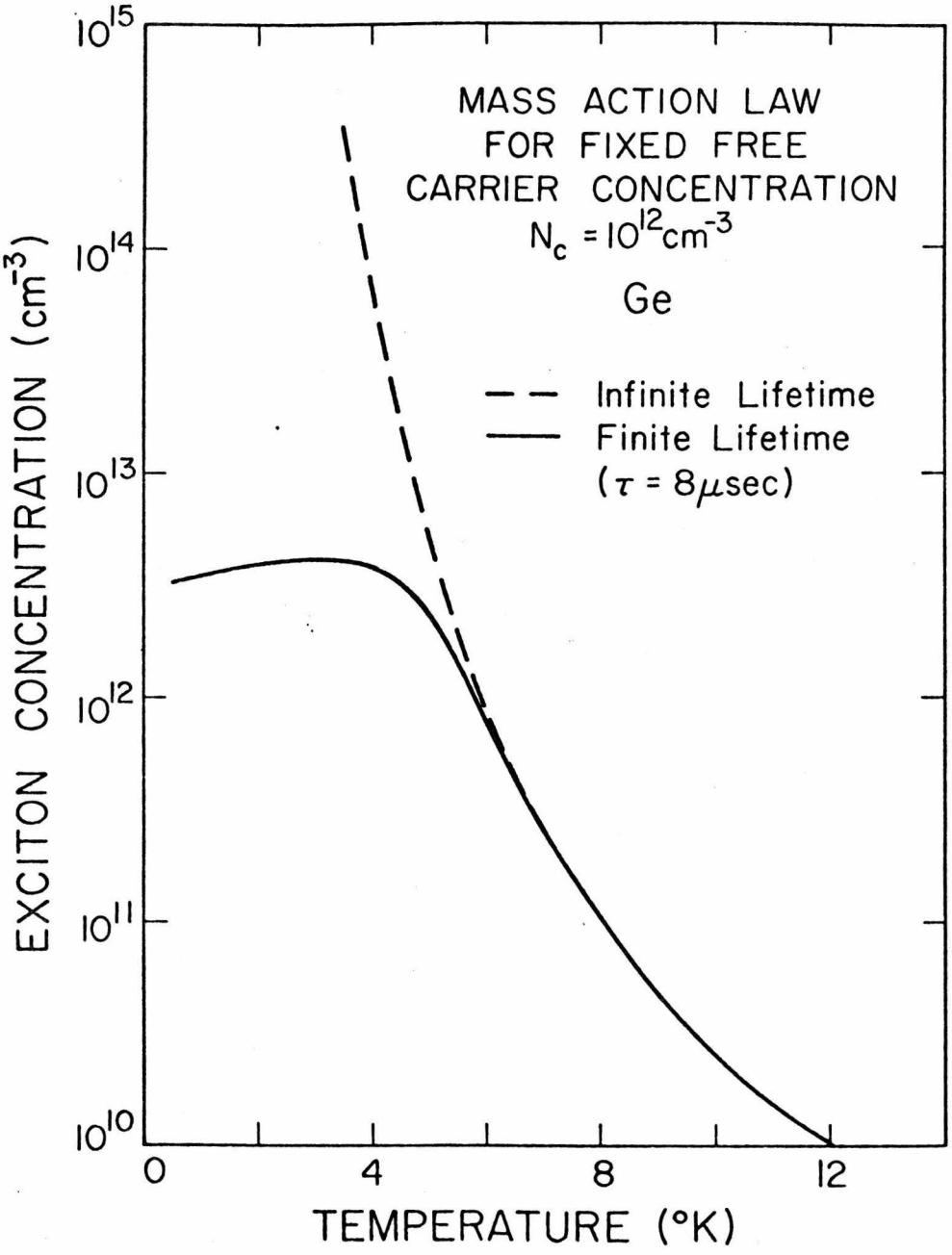


Figure 1. Exciton density versus temperature for Ge in thermal equilibrium computed using Equation 2; dashed line for infinite exciton lifetime, solid line for an exciton lifetime of 8 μsec. The concentration of electrons and of holes was taken to be 10^{12} cm^{-3}.

concentration varies slowly with temperature in this low temperature region.

The cross sections for thermal ionization and formation and impact formation are smoothly varying functions of carrier energy: therefore, the coefficients A_T, B_T, A_e and A_h are slowly varying functions of the external electric field. The impact ionization cross section, however, contains a threshold (the exciton binding energy); therefore, as the field excites carriers to states with energy greater than the exciton binding energy the impact ionization coefficients B_e and B_h will increase sharply. In Figure 2, we show the electron distribution function at several values of applied field and the impact ionization cross section as a function of electron energy. At zero field, a very small fraction of the electrons are sufficiently energetic to impact ionize an exciton; as an external field is applied, the fraction of electrons capable of impact ionization is greatly increased. The effect this carrier heating has on the impact ionization rate is shown in Figure 3. The sudden increase in the impact ionization coefficient depends only on the existence of a threshold in the impact ionization cross section. Because the impact ionization coefficient increases very rapidly with field strength, small uncertainties in the thermal ionization coefficient (which is not affected by the field) will have very little effect on the predicted behavior of the exciton concentration. The effect of the field will be especially dramatic at low temperatures where few carriers in thermal equilibrium would be energetic enough to impact ionize, the thermal ionization rate is low and mobilities are high (so carriers are easily excited).

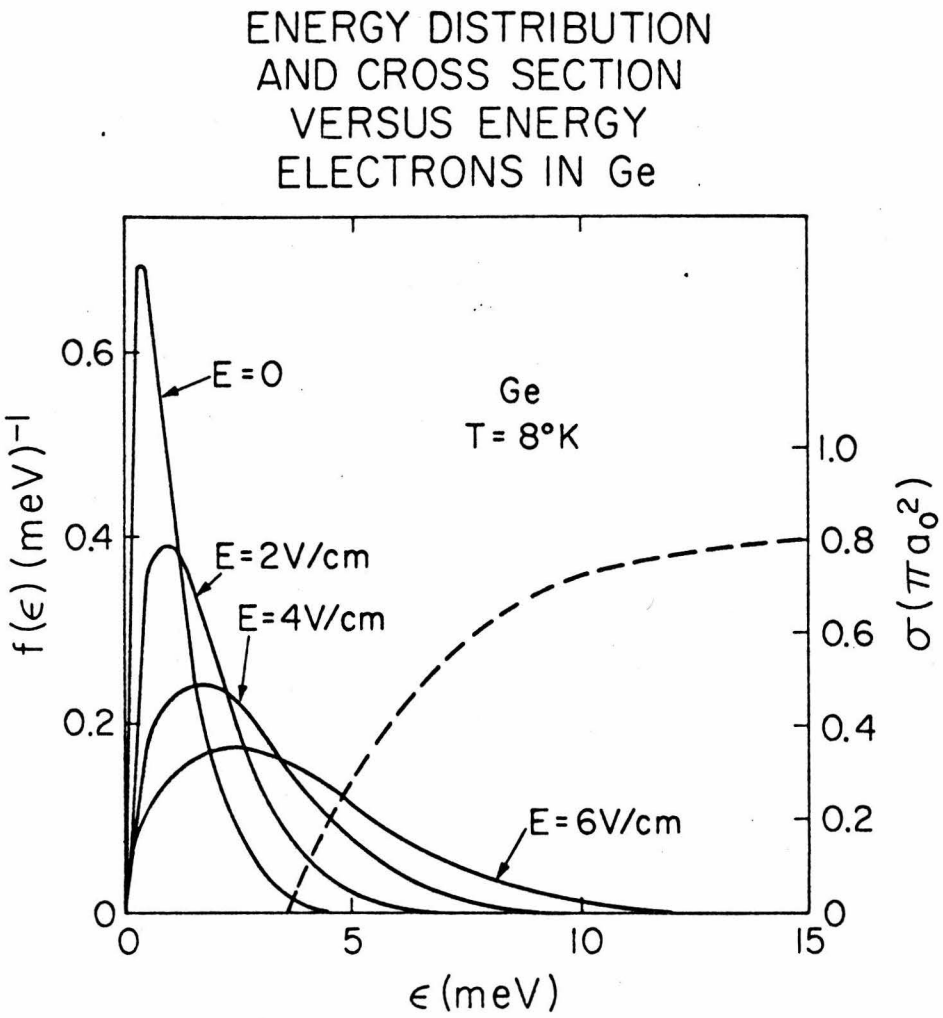


Figure 2. Electron energy distribution at several applied electric fields (solid lines) and exciton impact ionization cross section (dashed line) measured in units of the geometrical cross section versus electron energy in Ge at 8°K. The threshold in the impact ionization cross section is the exciton binding energy (3.6 meV). At zero applied field, a very small fraction of the electrons are sufficiently energetic to impact ionize an exciton; as an external field is applied, the number of electrons capable of impact ionization is greatly increased.

III. CALCULATION OF EXCITON CONCENTRATION

In order to determine the steady state exciton concentration from Eq. 2, it is necessary to compute the kinetic coefficients A_T, A_e, A_h, B_T, B_e and B_h (the exciton lifetime is known experimentally). We first consider the thermal formation coefficient,

$$A_T = \sum_{\underset{\sim}{k}_e, \underset{\sim}{k}_h} \sigma_T(\varepsilon_e, \varepsilon_h) |\underset{\sim}{v}_e - \underset{\sim}{v}_h| f_e(\underset{\sim}{k}_e) f_h(\underset{\sim}{k}_h) \tag{5a}$$

$$\sum_{\underset{\sim}{k}} f(\underset{\sim}{k}) = 1 \quad , \tag{5b}$$

where σ_T is the cross section for exciton formation, V is the carrier velocity and f is the distribution function. The cross section σ_T has been calculated by Lipnik[1]; he found that it was essentially independent of the carrier energies and of the order of 10^{-13} cm^2 for both Ge and Si. The external field increases the average carrier velocity and therefore the rate at which electrons and holes collide; since the probability for forming an exciton in an electron-hole collision is roughly independent of carrier energy, the thermal formation coefficient A_T is a slowly increasing function of field.

The thermal ionization coefficient is not affected by a small external electric field and can therefore be determined from the thermal formation coefficient at zero field using the principle of detailed balance,

$$B_T = \frac{A_T(E = o)}{K} \quad . \tag{6}$$

The impact ionization coefficient is taken to be

$$B_e = \sum_{\underset{\sim}{k}} \sigma_I(\varepsilon) |\underset{\sim}{v}| f_e(\underset{\sim}{k}) \qquad (7)$$

where σ_I is the impact ionization cross section. To estimate σ_I, we use Percival's emperical formula for the electron impact ionization cross section of the hydrogen atom[8], scaled by effective masses and the dielectric function

$$\sigma_I(\varepsilon) = \pi a_o^2 (1.19 \ln x + 5.26)(x - 1)[x^2 + 1.67x + 3.57]^{-1} x\theta(x - 1) \qquad (8a)$$

$$x = \varepsilon/\varepsilon_B \quad , \qquad (8b)$$

where a_o is the exciton radius. Because of the threshold in the impact ionization cross section, $A_{e(h)}$ is a rapidly increasing function of electric field.

In this calculation of B_e, exciton motion has been ignored; this approximation introduces two sources of error, both of which are small and which affect the result in opposite directions. First, part of the energy necessary to ionize the exciton can be supplied by the exciton kinetic energy so that impact ionization can occur in a collision with a free carrier whose energy is less than the exciton binding energy. From this point of view, the impact ionization coefficient should be larger than that computed using Equation 7. With an applied external field, however, the free carrier energies will be statistically larger than exciton kinetic energies (which are

Figure 3. Impact ionization rate ($B_e + B_h$) vs applied electric field at several temperatures in pure Ge. As the field strength is increased, the fraction of carriers energetic enough to impact ionize rises rapidly and the impact ionization rate is greatly increased. The effect is especially large at low temperature where the fraction of thermal carriers (zero applied field) sufficiently energetic to impact ionize is very small and carrier mobilities are high so that they are easily excited by an electric field.

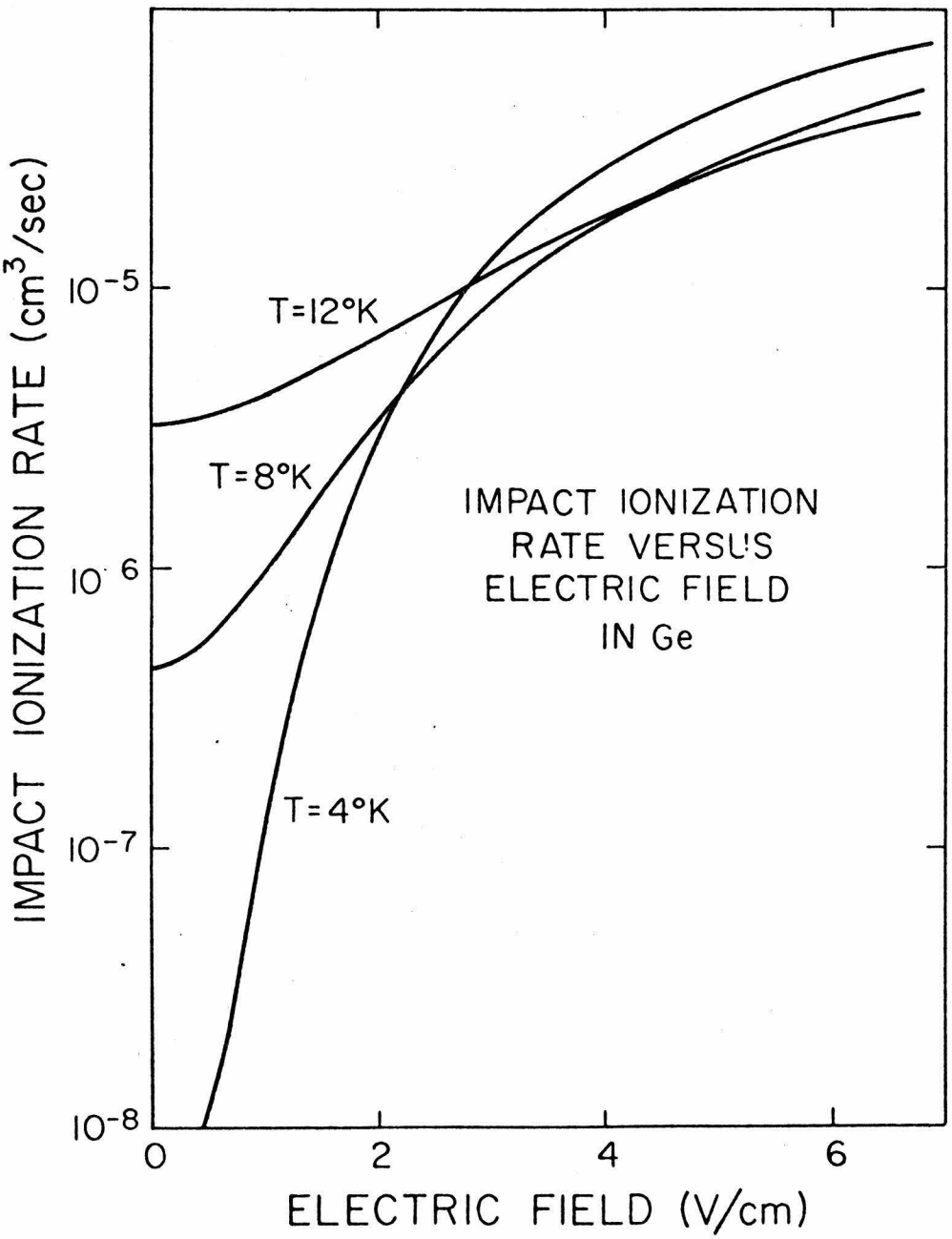

IMPACT IONIZATION RATE (cm^3/sec)
10^{-5}
10^{-6}
10^{-7}
10^{-8}
T=12°K
T=8°K
T=4°K
IMPACT IONIZATION
RATE VERSUS
ELECTRIC FIELD
IN Ge
0
2
4
6
ELECTRIC FIELD (V/cm)

Fig. 3

not changed by the field) and, therefore, we expect this effect to be small. Second, the exciton (ionized) will recoil following collision with the carrier so as to conserve total crystal momentum. Therefore, a carrier colliding with a stationary exciton must have energy somewhat greater than the exciton binding energy in order for ionization to occur. From this point of view, the impact ionization coefficient should be somewhat lower than that computed using Eq. 7. This recoil effect is small for ionization due to impact with the light carrier. In particular, for an electron moving in the light mass (transverse) direction (the direction in which an electron is most easily accelerated) this recoil effect is quite small. While these considerations should be included in a detailed, very accurate treatment of the ionization process, they have no effect on the qualitative results presented here.

The impact formation coefficient is a slowly varying function of field; at zero field it can be determined from the impact ionization coefficient and the principle of detailed balance. To determine this coefficient at finite fields, the energy dependence of the three body recombination cross section must be known. Sclar and Burstein[9] have considered this problem for shallow impurities and we use their result here

$$A_{e(h)} = \frac{B_{e(h)}}{K} \left(\frac{\sum_{\tilde{k}} \frac{f(\tilde{k})}{\varepsilon(\tilde{k})}}{\sum_{\tilde{k}} \frac{f_B(\tilde{k})}{\varepsilon(\tilde{k})}} \right)^2 \qquad (9)$$

where f_B is the Boltzmann distribution for zero field. The impact formation coefficient decreases with increasing

field strength. For the carrier concentrations we will consider, the impact formation rate will be slower than thermal formation.

In pure Ge and Si at low temperature, intravalley acoustic phonon scattering is the most important carrier scattering mechanism. In the temperature range we are considering, optical phonons and acoustic phonons with wavevector large enough to cause intervalley scattering are too energetic to be thermally excited and carriers in a thermal distribution are not energetic enough to emit these phonons. An external electric field heats the carriers, but impact ionization of excitons become important before optical or intervalley phonon scattering because the exciton binding energy is smaller than both the optical phonon energy and the lowest energy phonon with momentum large enough for intervalley scattering (TA mode). In pure Ge and Si (less than about 10^{13} impurities/cm^3), acoustic intravalley phonon scattering is more important than neutral impurity scattering for temperatures greater than about one Kelvin.[10,11] Therefore, for temperatures and fields where impact ionization begins to become important, intravalley acoustic phonon scattering is the important scattering mechanism.

An analytic expression for the distribution function may be found assuming longitudinal acoustic intravalley scattering, Boltzmann statistics, that the mean energy loss per collision is small and that equipartition holds for the phonons,[12]

$$f(\varepsilon) = N\left(\frac{\varepsilon}{kT} + y\right)^{y} e^{-\varepsilon/kT} \qquad (10a)$$

$$y = (E/E_o)^2 \tag{10b}$$

$$E_o = (6\ ms^2 kT)^{1/2}/e\ell \tag{10c}$$

$$N = \frac{\sqrt{\pi}}{4\left(\frac{2\pi mkT}{h}\right)^{3/2} \int_o^\infty (x+y)^y \sqrt{\pi}\ e^{-x} dx} \quad . \tag{10d}$$

Here s is the velocity of sound, m is the carrier density of states effective mass and ℓ is the carrier mean free path. The mean free path due to acoustic phonon scattering is inversely proportional to the temperature; we set

$$E_o = CT^{3/2} \tag{11}$$

and determine the parameter C by comparing computed with measured electron drift velocities.[13] In Figure 4 we show the result of this comparison in Ge; a good fit is possible for fields less than about 25 V/cm. In the case of Si, it was possible to fit the measured drift velocities for fields less than about 100 V/cm. We set the hole distribution function equal to the electron distribution function. (We expect electron impact ionization to be somewhat more important than hole impact ionization due to slightly higher electron mobilities; therefore, this approximation to the hole distribution function can introduce at most a factor of two error in the kinetic coefficients. However, our estimates of the cross sections are no more accurate than a factor of two.) Comparison of the simple distribution function with detailed Monte Carlo calculations[14] for electrons in Si show good agreement for fields less than or equal to about 25 V/cm at 20°K. At a field

Figure 4. Electron drift velocity versus applied electric field (applied parallel to <100> direction) in Ge at 8°K. The dashed line was computed using the distribution function given in Eq. 10, and E_o given in Eq. 11; the parameter C was fit to give the best agreement with the experimental drift velocity (solid line) measured by Nava et al (Ref. 13). We see that a good fit is possible for fields less than about 25 V/cm. In the case of Si, it was possible to fit the measured drift velocities (electrons, 20°K, field parallel to <111>, data from Ref. 13, the quality of the fit is comparable to that for Ge) for fields less than about 100 V/cm.

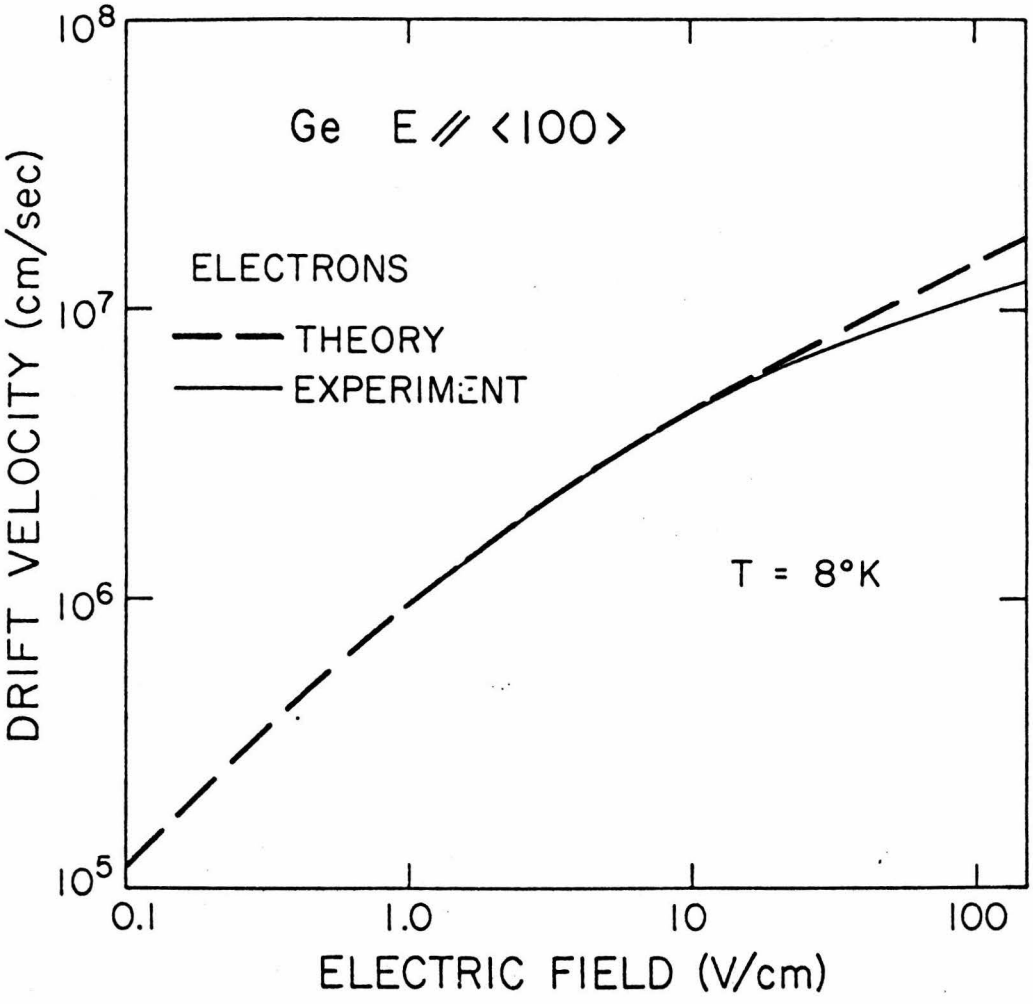

Ge E // <100>
ELECTRONS
THEORY
EXPERIMENT
T = 8°K
DRIFT VELOCITY (cm/sec)
10^8
10^7
10^6
10^5
0.1
1.0
10
100
ELECTRIC FIELD (V/cm)

Fig. 4

of 50 V/cm, the simple distribution function overestimates the effect of the field due to the neglect of intervalley phonon scattering which begins to become important at these higher fields.

After the distribution function and cross sections have been determined, the kinetic coefficients can be computed by a numerical integration. Once the kinetic coefficients are known, the steady state exciton concentration is found from Equation 2; the results for Ge and Si are shown in Figures 5 and 6, respectively. Parameters used in the calculation are summarized in Table I. The carrier concentrations are typical of those appearing in low temperature double injection experiments.[5,6] For both Ge and Si a sharp drop in exciton concentration (due to impact ionization) occurs when fields greater than a temperature dependent critical field are reached. The dependence of critical field on carrier concentration can be found from Figure 3. The critical field is reached when the impact ionization rate first exceeds both the thermal ionization and exciton annihilation rates. If the number of carriers is increased, the impact ionization rate per carrier (plotted in Figure 3) at the critical field is decreased by the same factor. For example, if at $T = 4°K$ and $E_c = 1$ V/cm the carrier concentration is increased by an order of magnitude, the critical field decreases by about a factor of two. The drop in exciton concentration with external field is more dramatic at low temperatures where ionization rates in thermal equilibrium are slow; at higher temperatures ($T \gtrsim 12°K$ in Ge,

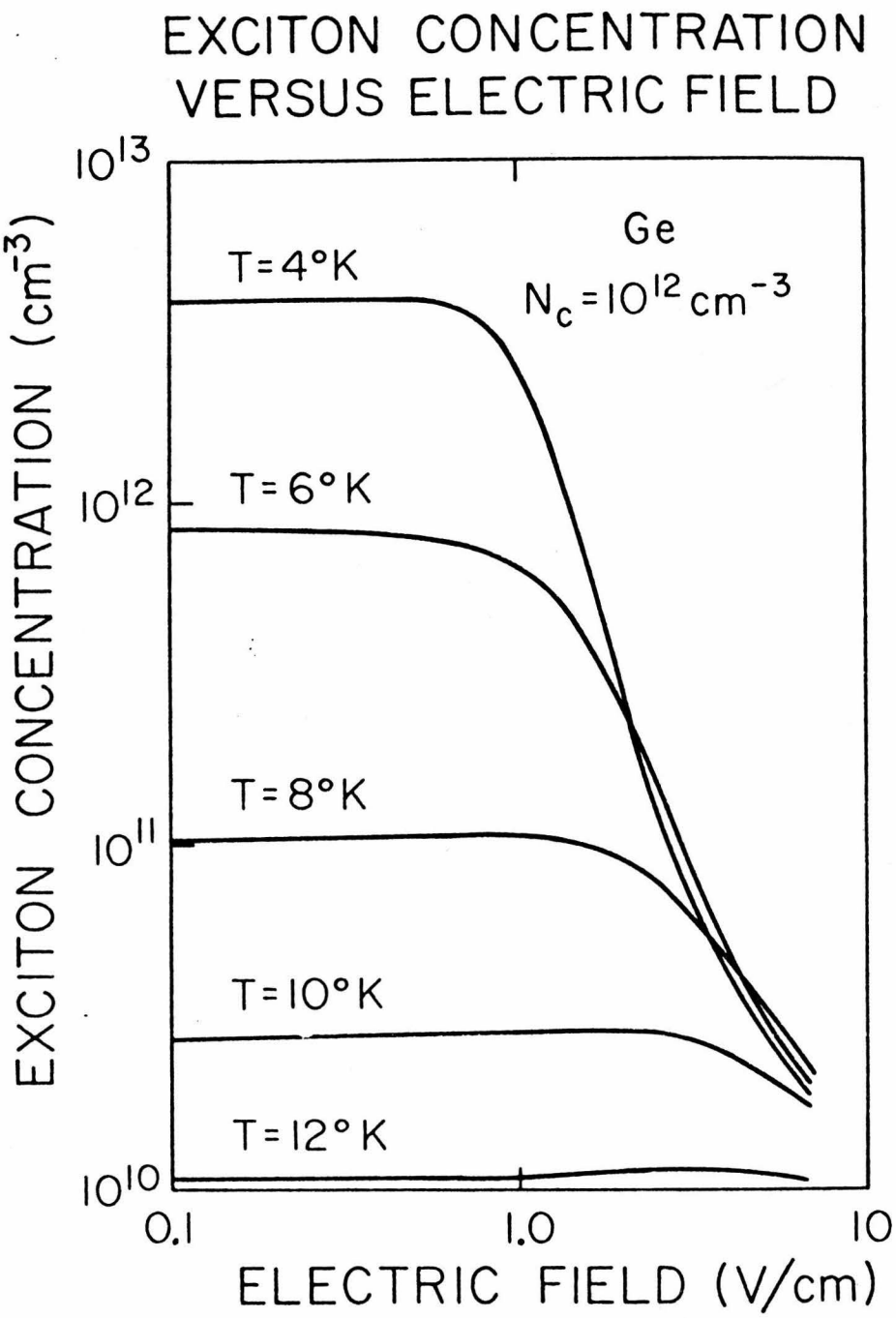


Figure 5. Exciton concentration versus applied electric field in Ge at several temperatures; the concentration of electrons and holes was taken to be 10^{12} cm^{-3}. The sharp drop in exciton concentration when the applied field exceeds a temperature dependent critical field is due to impact ionization by field excited carriers.

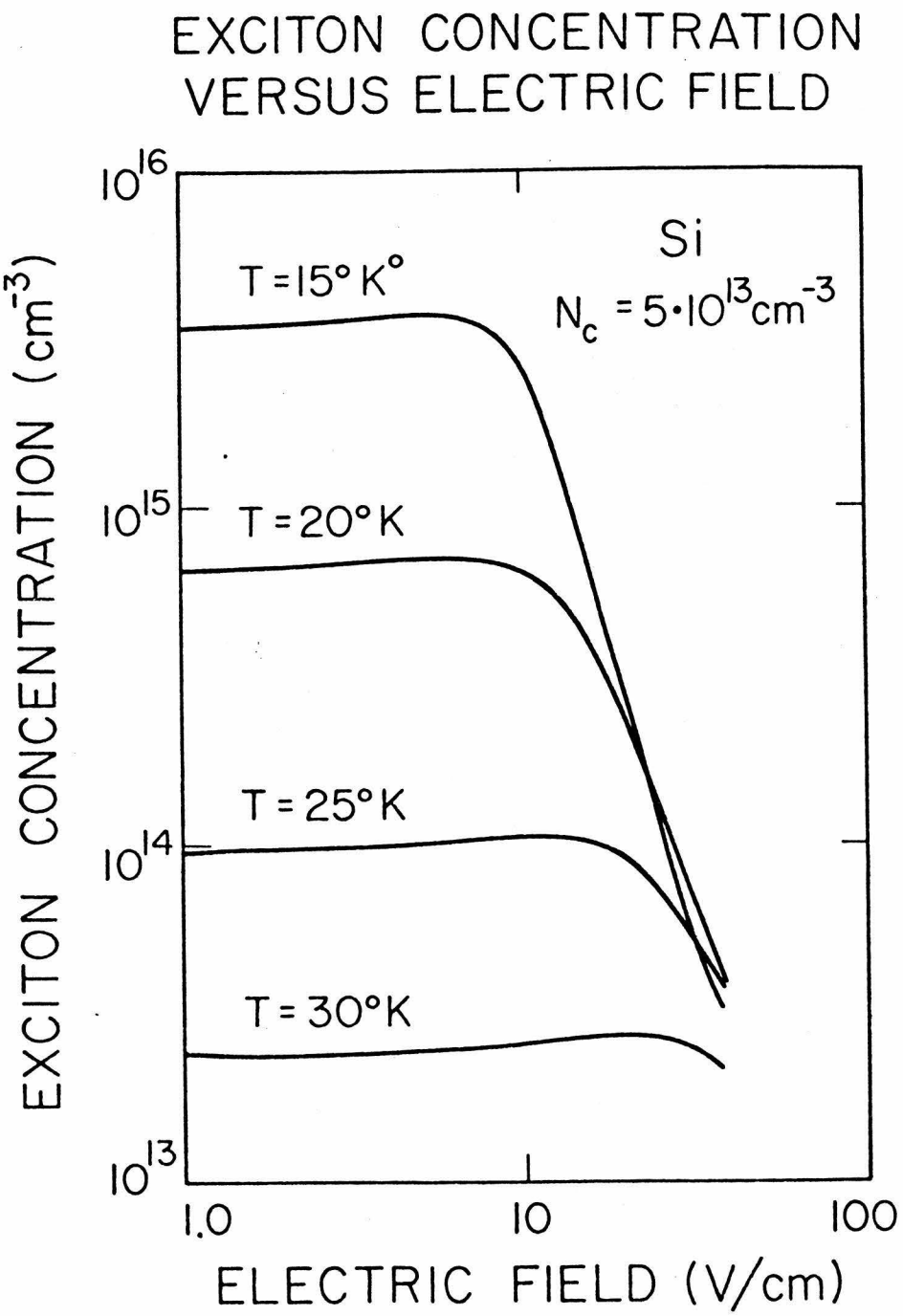


Figure 6. Exciton concentration versus applied electric field in Si at several temperatures; the concentration of electrons and holes was taken to be 5 x 10^{13} cm^{-3}. The sharp drop in exciton concentration when the applied field exceeds a temperature dependent critical field is due to impact ionization by field excited carriers.

TABLE I. Parameters used in the calculations: ε_B, the exciton binding energy; a_o, the exciton radius; τ, the exciton lifetime; σ_T, the thermal recombination cross section; n, the carrier concentration; C, carrier scattering parameter; m_t, electron transverse effective mass; m_ℓ, electron longitudinal effective mass; m_h, hole density of states effective mass.

	Ge	Si
ε_B	3.6 meV[a]	14.7 meV[b]
a_o	180 Å[c]	50 Å[c]
τ	8 μsec[d]	2.6 μsec[e]
σ_T	10^{-13} cm^2[f]	10^{-13} cm^2[f]
n	10^{12} cm^{-3}	5×10^{13} cm^{-3}
C	5.9×10^{-2} V/cm	8.3×10^{-2} V/cm
m_t	0.082 m_o[g]	0.19 m_o[g]
m_ℓ	1.6 m_o[g]	0.97 m_o[g]
m_h	0.3 m_o[g]	0.5 m_o[g]

[a] E.F. Gross, V.I. Safarov, A.N. Titkov and I.S. Shilmak, Pis'ma Zh. Eksp. Teor. Fiz. 13, 332 (1971). See JETP Lett. 13, 235 (1971).

[b] K.L. Shaklee and R.E. Nahory, Phys. Rev. Lett. 24, 942 (1970).

[c] T.P. McLean and R. Loudon, J. Phys. Chem. Solids 13, 1 (1960).

[d] Ya. Pokrovskii, Phys. Stat. Sol. (a) 11, 385 (1972).

[e] J.D. Cuthbert, Phys. Rev. B1, 1552 (1970).

[f] Reference 1.

[g] S.M. Sze, The Physics of Semiconductor Devices (Wiley, New York, 1969).

$T \gtrsim 30°K$ in Si) the thermal ionization rate is fast enough that this process is competitive with impact ionization even with relatively large applied fields. The numerical differences between Ge and Si are due almost entirely to the larger exciton binding energy in Si.

IV. SUMMARY AND DISCUSSION

At low temperatures ($T \lesssim 10°K$ in Ge and $T \lesssim 30°K$ in Si), relatively modest electric fields ($E \sim 2$ V/cm in Ge and $E \sim 20$ V/cm in Si) can excite free carriers to the point that impact ionization of excitons becomes more important than thermal ionization; as a result the exciton concentration drops rapidly with increasing field. The sensitivity of the impact ionization process to external fields is due to the existence of a threshold in the impact ionization cross section. Because of the rapid increase in the impact ionization rate with applied field, small uncertainties (factor of 2) in the magnitude of the impact ionization or thermal ionization cross sections would not significantly affect the results of the calculation.

The results of our calculation appear to be in qualitative agreement with observations of the field dependence of low temperature photoconductivity measurements in Ge; however, the interpretation of these measurements may be complicated by the formation of electron-hole droplets. (The boundary conditions used in the calculation, fixed carrier concentration and spatial uniformity, are really more appropriate to

double injection device experiments where exciton impact ionization is also expected to be important.) Our calculated critical field (about 0.6 V/cm at T = 4°K) is somewhat smaller than that observed by Asnin et al.[3] (about 3 V/cm at T = 2.5°K) but in good agreement with the more recent results of Yao et al.[4] (about 0.6 V/cm at T = 4.2°K) and of Gurnee et al.[2] (about 1 V/cm at T = 2°K). The calculated decrease in exciton concentration between fields of 1 V/cm and 5 V/cm is about two orders of magnitude, in agreement with the increase in photoconducitivity observed by Yao et al. between these two fields and also in agreement with Asnin et al. (for fields of E_c to E_c + 4V/cm). The dependence of critical field on carrier concentration (an order of magnitude increase in carrier concentration decreases the critical field by about a factor of two) agrees with the observation of Yao et al. (Asnin et al. reported that the critical field does not vary with exciting light intensity). Finally, we note that in the experiments of Gurnee et al. and Asnin et al. the excitation levels were probably high enough to form electron-hole droplets which are also sensitive to an applied electric field[15] and may have contributed to the observed increase in photoconductivity in these experiments.

ACKNOWLEDGEMENTS

We thank C. Jacoboni for sending us his unpublished Monte Carlo calculations of the electron distribution function in Si and C. Canali, A. Loria, F. Nava and G. Ottaviani for sending us electron drift velocity measurements in Si and Ge

prior to publication. We thank V. Marrello, R.B. Hammond, M. Chen and J.W. Mayer for valuable conversations on low temperature double injection experiments. We thank the referee for calling our attention to reference 15.

REFERENCES

1. A.A. Lipnik, Fiz. Tverd. Tela. 3, 2322 (1961). See Sov. Phys.-Solid State 3, 1683 (1962).
2. M.N. Gurnee, M. Glicksman and P.W. Yu, Solid State Comm. 11, 11 (1972).
3. V.M. Asnin, A.A. Rogachev and S.M. Ryvkin, Fiz. Tekh. Poluprov. 1, 1740 (1967). See Sov. Phys.-Semiconductors 1, 1445 (1968).
4. T. Yao, K. Inagaki and S. Maekawa, Solid State Comm. 13, 533 (1973).
5. V. Marrello, T.F. Lee, R.N. Silver, T.C. McGill and J.W. Mayer, Phys. Rev. Lett. 31, 593 (1973).
6. R.B. Hammond, V. Marrello, R.N. Silver, T.C. McGill and J.W. Mayer, Solid State Comm. 15, 251 (1974).
7. V. Marrello and M. Chen, private communication.
8. I.C. Percival, Nucl. Fusion 6, 182 (1966).
9. N. Sclar and E. Burstein, J. Phys. Chem. Solids 2, 1 (1957).
10. N. Sclar, Phys. Rev. 104, 1559 (1956).
11. T.C. McGill and R. Baron, Phys. Rev. B11, 5208 (1975).
12. See for example, E.M. Conwell, High Field Transport in Semiconductors, in Solid State Physics, Supplement Vol. 9 (Academic Press, New York, 1967).
13. F. Nava, C. Canali, A. Loriz and G. Ottaviani (unpublished).
14. Carlo Jacoboni, private communication.

15. A. R. Hartman and R. H. Rediker, Proc. 10th Intl. Conf. Phys. Semicond., Cambridge, 1970, p. 202.

APPENDIX:

EFFECTIVE MASS APPROXIMATION

APPENDIX: EFFECTIVE MASS APPROXIMATION

In this Appendix, we give a simple deviation of the "effective mass approximation". Basically, the problem is to find a simple description of the behavior of electrons in solids when some weak non-periodic perturbation is added to the usual periodic field. In the effective mass approximation, one assumes that the electrons move entirely among the states of a single band and the kinetic motion of the electron can be described by an effective mass determined by the band structure. Intuitively, this is reasonable, because a smoothly varying potential may move the electron adiabatically back and forth among states of nearly the same energy, but will not cause real transitions into other bands. There are many sources[1-4] of fairly complete discussions of the effective mass approximation. In this Appendix, we follow the approach used by Kohn[5] for impurity states.

In the absence of non-periodic perturbation potential, the Hamiltonian for a conduction electron is

$$H_o = -\frac{\hbar^2}{2m_o}\nabla^2 + v(\vec{r}) \quad , \tag{A1}$$

in which $v(\vec{r})$ is an effective periodic potential. The eigen-functions are the Bloch waves

$$\psi_{n,\vec{k}}(\vec{r}) = \frac{1}{\sqrt{\Omega}}\, u_{n,\vec{k}}(\vec{r})\, e^{i\vec{k}\cdot\vec{r}} \quad , \tag{A2}$$

which we shall take to be normalized to unity in a large cube of volume $\Omega = L^3$. The $u_{n,\vec{k}}(\vec{r})$ are periodic functions. We denote the energy corresponding to $\psi_{n,\vec{k}}$ by $E_n(\vec{k})$.

The Hamiltonian for an extra electron move in a non-periodic perturbation potential will be

$$H = H_o + U(\vec{r}) \quad , \tag{A3}$$

where $U(\vec{r})$ is a sufficiently slowly varying, non-periodic, perturbation potential.

We consider now the motion of the extra electron as governed by the Hamiltonian H in Eq. (A3). We expand its wave function ψ in terms of the eigen functions $\psi_{n,\vec{k}}$ of the unperturbed Hamiltonian H_o

$$\psi = \sum_{n,\vec{k}} A_n(\vec{k})\, \psi_{n,\vec{k}} \tag{A4}$$

Here $\vec{k}$ runs over all points inside the first Brillouin zone which are consistent with periodic boundary conditions imposed on the surface of our large cube:

$$k_\alpha L = 2\pi\, \ell_\alpha \quad , \tag{A5}$$

ℓ_α being an integer.

Substituting (A4) into the Schroedinger equation

$$(H_o + U)\,\psi = E\psi \tag{A6}$$

and taking the scalar product with $\psi_{n,\vec{k}}$, we obtain

$$(E_n(\vec{k}) - E)\,A_n(\vec{k}) + \sum_{n',\vec{k}'} \langle n\vec{k}|U|n'\vec{k}'\rangle\, A_{n'}(\vec{k}') = 0 \tag{A7}$$

where

$$\langle n\vec{k}|U|n'\vec{k}'\rangle \equiv \int \psi^*_{n,k}\, U(\vec{r})\, \psi_{n',\vec{k}'}\, d^3\vec{r}$$

$$= \frac{1}{\Omega}\int u^*_{n,\vec{k}}\, u_{n',\vec{k}'}\, e^{i(\vec{k}',\vec{k})\cdot\vec{r}}\, U(\vec{r})\, d^3\vec{r} \quad . \tag{A8}$$

We note first that $u^*_{n,\vec{k}}\, U_{n',\vec{k}'}$ is a periodic function and can be written as a Fourier series with the use of the reciprocal lattice vector $\vec{K}_\nu$:

$$u^*_{n,\vec{k}}\, u_{n',\vec{k}'} = \sum_\nu C^\nu_{n\vec{k},n'\vec{k}'}\, e^{i\vec{K}_\nu\cdot\vec{r}} \quad . \tag{A9}$$

For the convenience of discussion, we take the perturbation potential to be of the form of a impurity ion:

$$U(\vec{r}) = -\frac{e^2}{\kappa r} \quad , \tag{A10}$$

where κ being the static dielectric constant, then the matrix element in Eq. (A8) is given by

$$\langle n\vec{k}|U|n'\vec{k}'\rangle = \sum_{\nu} C_{nk,n'k'} \left(\frac{-4\pi e^2}{\Omega\kappa|\vec{K}_{\nu} + \vec{k} - \vec{k}|^2}\right) \tag{A11}$$

From the othonormality of $\psi_{n,\vec{k}}$ we find by integrating Eq. (A9) under the condition $\vec{k} = \vec{k}' = 0$,

$$C^{o}_{n,o;n',o} = \begin{cases} 1 & n = n' \\ 0 & n \neq n' \end{cases} \tag{A12}$$

It is clear that if the attractive force of the impurity ion is imagined to become weaker and weaker, the wave function ψ will be more and more like a Bloch wave near the conduction band minimum. Since the actual Coulomb force is strongly reduced by the dielectric constant, we anticipate that the system of Eq. (A7) will have solutions in which $A_n(\vec{k})$ is negligible unless n=0 and $\vec{k}$ is small. This suggests that in Eq. (A7), we display the terms with n=0 in a prominent way:

$$(E_o(\vec{k}) - E)\, A_o(\vec{k}) + \sum_{\vec{k}'} \langle O_{\vec{k}}|U|O_{\vec{k}'}\rangle\, A_o(\vec{k}')$$

$$+ \sum_{n'\neq 0} \langle O_{\vec{k}}|U|n'\vec{k}'\rangle\, A_{n'}(\vec{k}') = 0 \tag{A13a}$$

$$(E_n(\vec{k}) - E)\, A_n(\vec{k}) + \sum_{\vec{k}'} \langle n_{\vec{k}}|U|O_{\vec{k}'}\rangle\, A_o(\vec{k}')$$

$$+ \sum_{\substack{n'\neq 0 \\ \vec{k}'}} \langle n\vec{k}|U|n'\vec{k}'\rangle\, A_{n'}(\vec{k}') = 0 \quad (n\neq 0) \tag{A13b}$$

As a first approximation let us set $A_n(\vec{k}) = 0$ for $n \neq 0$ and replace $E_o(\vec{k})$ and $\langle O_{\vec{k}}|U|O_{\vec{k}}\rangle$ by their expressions for small $\vec{k}$ and $\vec{k}'$:

$$E_o(\vec{k}) \rightarrow \frac{\hbar^2}{2m^*} k^2 \tag{A14}$$

$$\langle O_{\vec{k}}|U|O_{\vec{k}'}\rangle \rightarrow - \frac{4\pi e^2}{\Omega\kappa|\vec{k}-\vec{k}|^2} \tag{A15}$$

Substituting into Eq. (A13a) we find

$$(\frac{\hbar^2}{2m^*} k^2 - E)\, A_o(\vec{k}) - \frac{4\pi e^2}{\Omega\kappa} \sum_{\vec{k}'} \frac{1}{|\vec{k}-\vec{k}'|^2}\, A_o(\vec{k}) = 0 \tag{A16}$$

This will be recognized as the Schroedinger equation in momentum space of an electron of mass m^* moving in the attractive Coulomb potential $\frac{-e^2}{Kr}$. We note, however, that in Eq. (A16) $\vec{k}$ and $\vec{k}'$ are restricted to lie within the first Brillouin zone. If this restriction is ignored, the solutions of Eq. (A16) are almost zero for $\vec{k}$ outside the first Brillouin zone in any case, so that the restriction is not of great importance. For the time being, therefore, we replace Eq. (A16) by the equation

$$(\frac{\hbar^2}{2m^*} k^2 - E)\, A_o(\vec{k}) - \frac{4\pi e^2}{\Omega\kappa} \sum_{\text{all } \vec{k}'} \frac{1}{|\vec{k}-\vec{k}'|^2}\, A_o(\vec{k}') = 0 \tag{A17}$$

To transform this equation into a Schroedinger equation in coordinate space we introduce the Fourier transform of A_o in the usual way, namely,

$$F_{(r)} = \frac{1}{\sqrt{\Omega}} \sum_{\substack{\text{all} \\ \vec{k}}} A_o(\vec{k})\, e^{i\vec{k}\cdot r} \tag{A18}$$

Multiplying Eq. (A17) by $e^{i\vec{k}\cdot\vec{r}}$ and summing over $\vec{k}$, we obtain

$$\left(-\frac{\hbar^2}{2m^*}\nabla^2 - \frac{e^2}{\kappa r}\right) F(\vec{r}) = EF(\vec{r}) \quad , \tag{A19}$$

A hydrogen-like so-called effective mass equation.

We now want to verify the two presumptions on which our derivation was based, namely, that $A_o(\vec{k})$ extends over only a small fraction of the first Brillouin zone and that the neglected amplitudes $A_n(\vec{k})$, $n\neq 0$ are in fact negligible.

If we invert Eq. (18) and use the hydrogenic solution for F(r) in Eq. (A19), we find

$$A_o(k) = \frac{8\sqrt{\pi}}{\sqrt{\Omega}\, a^{*\,5/2}} \frac{1}{\left[k^2 + (1/a^*)^2\right]^2} \quad , \tag{A20}$$

where a^* is the "effective Bohr radius",

$$a^* = \frac{\hbar^2 \kappa}{m^* e^2} \tag{A21}$$

Therefore, $A_o(\vec{k})$ extends appreciably in momentum space only to value of k less than or equal to

$$\bar{k} \equiv 1/a^* \tag{A22}$$

This must be compared to the mean value of k at the zone boundary, obtained by replacing the first Brillouin zone by a sphere of the same volume

$$k_{ZB} = \sqrt[3]{24\pi^2}/a = 6.2/a \quad , \tag{A23}$$

where a is the lattice parameter. In Si and Ge, for example, a^* has the approximate value 20 and 45A, respectively; whereas a has the values 5.42 and 5.62 A. Therefore,

$$\bar{k}/k_{ZB} \approx \begin{cases} 0.04 \text{ in Si} \\ 0.02 \text{ in Ge} \end{cases} \tag{A24}$$

At the zone boundary, $A_o(\vec{k})$ has dropped to the fraction $(\bar{k}/k_{ZB})^4$ of its maximum value, which is quite negligible for both materials.

An estimate of $A_n(\vec{k})$ for $n \neq 0$ can be made from Eq. (A13b). Treating $A_n(\vec{k})$ as small quantity, we have

$$A_n(\vec{k}) = - \frac{1}{E_n(\vec{k}) - E(k')} \sum_{\vec{k}} \langle n\vec{k}|U|0_{\vec{k}}\rangle A_o(\vec{k}') \tag{A25}$$

which gives, in order of magnitude,

$$|A_n| \sim \frac{E_o}{\Delta E} \frac{a}{a^*} |A_o| \tag{A26}$$

Here E_o and ΔE are the ionization energy and the band gap energy, respectively. Thus, in this case, the ratio $|A_n|/|A_o|$ is a very small quantity, of the order of 10^{-3} to 10^{-2}, in silicon and germanium.

REFERENCES

1. G. H. Wannier, Elements of Solid State Theory, (Cambridge University Press, Cambridge, 1959) Chapter 6.
2. P. W. Anderson, Concepts in Solids, (Benjamin, New York, 1964) Chapter 2C.
3. E. I. Blount, in Solid State Physics, Vol. 13, p. 305, (1962).
4. C. Kittel, Introduction to Solid State Physics, (2nd ed, Wiley, New York, 1953), p. 288.
5. W. Kohn, Solid State Physics, Vol. 5, p. 277, (1957).